FLEXURAL PERFORMANCE OF COLD FORMED STEEL TUBE FILLED WITH OIL PALM CLINKER CONCRETE

MUHAMMAD FAISAL JAVED

FACULTY OF ENGINEERING
UNIVERSITY OF MALAYA
KUALA LUMPUR

2018

FLEXURAL PERFORMANCE OF COLD FORMED STEEL TUBE FILLED WITH OIL PALM CLINKER CONCRETE

MUHAMMAD FAISAL JAVED

THESIS SUBMITTED IN FULFILMENT OF THE REQUIREMENTS FOR THE DEGREE OF DOCTOR OF PHILOSOPHY

FACULTY OF ENGINEERING
UNIVERSITY OF MALAYA
KUALA LUMPUR

2018

UNIVERSITY OF MALAYA

ORIGINAL LITERARY WORK DECLARATION

Name of Candidate: Muhammad Faisal Javed

Registration/Matric No: KHA140127

Name of Degree: Doctor of Philosophy

Title of Thesis: Flexural performance of cold formed steel tube filled with oil palm clinker concrete

Field of Study: Structural Engineering & Materials

I do solemnly and sincerely declare that:

(1) I am the sole author/writer of this Work;
(2) This Work is original;
(3) Any use of any work in which copyright exists was done by way of fair dealing and for permitted purposes and any excerpt or extract from, or reference to or reproduction of any copyright work has been disclosed expressly and sufficiently and the title of the Work and its authorship have been acknowledged in this Work;
(4) I do not have any actual knowledge nor do I ought reasonably to know that the making of this work constitutes an infringement of any copyright work;
(5) I hereby assign all and every rights in the copyright to this Work to the University of Malaya ("UM"), who henceforth shall be owner of the copyright in this Work and that any reproduction or use in any form or by any means whatsoever is prohibited without the written consent of UM having been first had and obtained;
(6) I am fully aware that if in the course of making this Work I have infringed any copyright whether intentionally or otherwise, I may be subject to legal action or any other action as may be determined by UM.

Candidate's Signature ____________________ Date: __________________

Subscribed and solemnly declared before,

Witness's Signature _____________________ Date: ___________________

Name:

Designation:

FLEXURAL PERFORMANCE OF COLD FORMED STEEL TUBE FILLED WITH OIL PALM CLINKER CONCRETE

ABSTRACT

The use of concrete filled steel tubes (CFST) in structures is increasing day by day. Cold-formed steel is light weight, highly durable, more fire resistant, and has cheaper and simpler maintenance as compare to hot-rolled steel. The only issue with cold-formed steel is its high initial cost, but it can be offset by lower lifetime cost. The amount of cold-formed steel required is often reduced by filling hollow structural sections with concrete. Agricultural industry produces various types of solid waste. Oil Palm boiler clinker is an agriculture waste from the palm oil industry and considered as a severe threat to the environment. Therefore, channeling oil palm boiler clinker waste material into the concrete industry would help to promote the usage of a sustainable and lightweight member. A combination of oil palm boiler clinker concrete (OPBC) and steel is a compromise between benefits and disadvantages. Therefore, in this study, a new sustainable CFST members consisting of steel tube and OPBC is proposed and investigated. This study focuses on experimental and numerical methods to examine the behavior of oil palm boiler clinker concrete filled steel tubes (OCFST) at ambient and elevated temperature. Full-scale specimens were tested at ambient temperature with monotonic loading while some specimens were tested at an elevated temperature according to ISO-834 heating curve under an-isothermal conditions with a constant static load. Finite element (FE) model was developed using ANSYS and the results from tests in both conditions were used as validation data. An extensive parametric study was performed using the validated ambient temperature model to investigate the influences of the depth-to-thickness ratio (20−200), concrete compressive strengths (2–100 MPa), and steel yield strengths (235–400 MPa) on the fundamental behavior of CFST beams under

flexure load only. The results from parametric studies and experimental data of researchers from the literature were used to check the accuracy of the existing design methods presented in Eurocode (EC4 (2004), CIDECT, AISC (2010) and GB50936 (2014). Furthermore, FE model was developed and verified against experimental test results from this study. The verified FE model was used to analyze the effect of important parameters like strength of steel, strength of concrete, load ratio, cross-sectional dimension and steel ratio on the elevated temperature performance of CFST members. It was concluded that increasing yield strength of steel and load ratio has adverse effect on the fire resistance time of CFST members. The results obtained from this study were compared with the available equations for predicting the member temperature of the steel tube and in-filled concrete. The available equations can be used to predict the temperature of outer steel tube while the equations for predicting the temperature of in-filled concrete needed to be revised.

Keywords: concrete filled steel tubes, flexural behavior, oil palm boiler clinker, elevated temperature, ambient temperature

KEUPAYAAN LENTURAN TIUB KELULI TERBENTUK SEJUK DIISI DENGAN KONKRIT ARANG KELAPA SAWIT

ABSTRAK

Penggunaan tiub keluli terisi konkrit (CFST) dalam struktur semakin meningkat setiap hari. Keluli terbentuk sejuk adalah ringan, sangat tahan lama, lebih tahan api, dan mempunyai penyelenggaraan yang lebih murah dan lebih mudah berbanding dengan keluli tergelek panas. Satu-satunya isu dengan keluli terbentuk sejuk adalah kos awal yang tinggi, tetapi ia boleh diimbangi oleh kos sepanjang hayat yang lebih rendah. Jumlah keluli terbentuk sejuk yang diperlukan boleh dikurangkan dengan mengisi bahagian struktur berongga dengan konkrit. Industri pertanian menghasilkan pelbagai jenis sisa pepejal. Arang kelapa sawit, adalah sisa pertanian dari industri minyak sawit dan dianggap sebagai ancaman teruk kepada alam sekitar. Oleh itu, penyaluran bahan buangan arang kelapa sawit ke dalam industri konkrit akan membantu menggalakkan penggunaan anggota struktur yang mampan dan ringan. Gabungan konkrit arang kelapa sawit (OPBC) dan keluli adalah kompromi antara manfaat dan kekurangan. Oleh itu, dalam kajian ini, anggota CFST yang baru yang terdiri daripada tiub keluli dan OPBC dicadangkan dan disiasat. Kajian ini memberi tumpuan kepada kaedah eksperimen dan berangka untuk mengkaji kelakuan keluli tiub terisi konkrit arang kelapa sawit (OCFST) pada suhu ambien dan tinggi. Spesimen berskala penuh telah diuji pada suhu ambien dengan beban monotonik manakala beberapa spesimen diuji pada suhu tinggi mengikut lengkok pemanasan ISO-834 di bawah keadaan an-isotermal dengan beban statik yang malar. Model unsur terhingga (FE) telah dibangunkan menggunakan ANSYS dan keputusan dari ujian dalam kedua-dua keadaan suhu telah digunakan sebagai data pengesahan. Kajian parametrik yang terperinci telah dilakukan dengan menggunakan model suhu ambien yang disahkan untuk menyiasat pengaruh nisbah kedalaman ke-

ketebalan (20-200), kekuatan mampatan konkrit (2-100 MPa), dan kekuatan keluli (235-400 MPa) pada tingkah laku asas rasuk CFST di bawah beban lenturan sahaja. Hasil dari kajian parametrik dan data eksperimen penyelidik dari literatur digunakan untuk memeriksa ketepatan kaedah rekabentuk bagi kod Euro (EC4 (2004), CIDECT, AISC (2010) dan GB50936 (2014). Tambahan pula, model unsur terhingga yang telah dibangunkan turut disahkan menggunakan keputusan ujian eksperimen daripada kajian ini. Model FE yang telah disahkan turut digunakan untuk menganalisis kesan parameter penting seperti kekuatan keluli, kekuatan konkrit, nisbah beban, dimensi keratan rentas dan nisbah keluli pada prestasi CFST pada suhu tinggi. Kesimpulannya, peningkatan kekuatan yield dan nisbah beban mempunyai kesan buruk terhadap masa rintangan kebakaran anggota CFST. Keputusan yang diperoleh daripada kajian ini dibandingkan dengan persamaan yang sedia ada untuk meramal suhu anggota tiub keluli terisi konkrit. Persamaan yang sedia ada boleh digunakan untuk meramalkan suhu tiub keluli luar, sementara persamaan untuk meramal suhu pada konkrit yang diisi perlu disemak semula.

Kata kunci: tiub keluli terisi konkrit, kelakuan lenturan, arang kelapa sawit, suhu tinggi, suhu ambien

ACKNOWLEDGMENTS

I wish to express my deepest gratitude to my supervisor *Dr Nor Hafizah* and *Dr Shazim Ali Memon* for their time, advice, encouragement, and expertise during the research. This thesis would not have been possible without their elaborate comments, guidance and full encouragement at various stages.

I would also like to thank my best friend *Dr Sardar Kashif-Ur-Rehman* and the laboratory assistant *Mr. Sreedharan* for their cooperation in providing and preparing the required laboratory equipment's.

Special thanks are extended to the financial support of University Malaya Postgraduate Research Fund (PPP – Project no. PG155–2015B) and Fundamental Research Grant Scheme, Ministry of Education, Malaysia (FRGS – Project no. FP047/2013B).

Every challenging work needs self-efforts as well as guidance of elders especially those who were very close to our heart. My humble effort I dedicate to sweet and loving;

FATHER & MOTHER

Whose affection, love, encouragement, and prays of day and nights make me able to get such success and honor.

TABLE OF CONTENT

Abstract iii

Abstrak v

Acknowledgments vii

Table of Content viii

List of Figures xiv

List of Tables xviii

List of Symbols and Abbreviations xx

CHAPTER 1: INTRODUCTION 1

1.1 Background of the Study 1

1.2 Problem Statement 4

1.3 Objectives of the Research 6

1.4 Scope and Limitations 6

1.5 Outline of the Thesis 7

CHAPTER 2: LITERATURE REVIEW 8

2.1 Introduction 8

2.2 Properties of CFST at Ambient Temperature 8

2.2.1 Experimental Tests at Ambient Temperature 8

2.2.2 Numerical Investigations and Analytical Models of CFST at Ambient Temperature CFST 11

2.3 Properties of CFST at Elevated Temperature 13

2.3.1 Experimental Investigations at Elevated Temperature 13

2.3.2 Numerical Models 15

2.3.3 Simple Calculation Models (Design Guidelines) 18

2.4 Properties of Concrete at Elevated Temperature 22
2.4.1 Density 22
2.4.2 Thermal Conductivity 22
2.4.3 Specific Heat 23
2.4.4 Coefficient of Thermal expansion 23
2.4.5 Stress-Strain Curve 26
2.5 Properties of OPBC at Ambient Temperature 29
2.5.1 Density 29
2.5.2 Mechanical Properties 30
2.6 Test Methods 31
2.6.1 Steady State Test 31
2.6.2 Transient State Test 32
2.7 Standard Fire Time-Temperature Curve 32
2.8 Properties of CFS Members at Elevated Temperature 34
2.8.1 Beams 34
2.8.1.1 Un-restrained Members 36
2.8.1.2 Restrained Members 39
2.8.2 Columns 41
2.8.2.1 Un-restrained Members 42
2.8.2.2 Restrained Members 46
2.9 Research Gaps 49

CHAPTER 3: METHODOLOGY 51

3.1 Introduction 51
3.2 Experimental Investigation at Ambient Temperature 51
3.2.1 Test Specimen 51
3.2.2 Material Properties and Mix Proportions 52

3.2.2.1 Steel 52

3.2.2.2 Concrete 53

3.2.3 Test Setup and Procedure 54

3.3 Experimental Investigation at Elevated Temperature 55

3.3.1 Test Plan and Apparatus 55

3.3.2 Specimen Fabrication 57

3.3.2.1 Steel 57

3.3.2.2 Concrete 58

3.3.3 Arrangement of Thermocouples and Displacement Transducers 58

3.3.4 Loading and heating 59

3.4 Finite Element Modeling at Ambient Temperature 60

3.4.1 Model Description 60

3.4.2 Material Constitutive Models 60

3.4.2.1 Steel 60

3.4.2.2 Concrete 61

3.4.3 Surface Interaction 64

3.4.4 Element Description 64

3.4.4.1 3D hexahedral reduced integration solid element 65

3.4.4.2 3D quadrilateral reduced integration solid element 66

3.4.5 Mesh Convergence 66

3.4.6 Parametric Analysis 68

3.5 Finite Element Modeling at Elevated Temperature 68

3.5.1 General 68

3.5.2 Thermal Analysis 70

3.5.3 Material Constitutive Models 71

3.5.4 Initial Geometric Imperfection and Amplitude 74

CHAPTER 4: RESULTS AND DISCUSSIONS...75

4.1 Experimental Results and Discussion for Ambient Temperature Tests....................75

4.1.1 Failure Mode...75

4.1.2 Overall Deflection Curves 78

4.1.3 Strain Distribution Curves 79

4.1.4 Energy Absorption, Specific Energy Absorption and Structural Efficiency ..81

4.1.5 Ultimate Strength...82

4.1.6 Ductility 83

4.2 Evaluation of Test Results by Comparison with Available Literature 84

4.2.1 Moment-Curvature Curve...84

4.2.2 Flexural Stiffness 85

4.2.1 Ultimate Capacity 86

4.3 FE Analysis Results at Ambient Temperature...87

4.3.1 Verification of the FE Model Experimental Results from Literature.............87

4.3.1.1 Ultimate Flexure Strengths of Normal Strength CFST Beams........88

4.3.1.2 Ultimate Flexure Strength of High Strength CFST Beams.............91

4.3.1.3 Moment Curvature Curves..93

4.3.2 Verification of the FE Model Experimental Results from Literature.............95

4.4 Parametric Study for NCFST at Ambient Temperature...97

4.4.1 Effect of Depth to Thickness Ratio..98

4.4.2 Effect of Grade of Concrete 100

4.4.3 Influences of Steel Yield Strengths..103

4.4.4 Effect of D/B Ratio 105

4.4.5 Effect of a/d Ratio..107

4.5 Comparison of Moment Capacities with Design Codes 108

4.5.1 Eurocode (BS EN 1994-1-1:2004)..109

4.5.2 AISC-LRFD-1994 110

4.5.3 CIDECT-1995 111

4.5.4 GB50936 (2014) 111

4.6 Test Results and Discussion for Elevated Temperature Testing 114

4.6.1 Thermal Response 114

4.6.1.1 Furnace Temperature vs ISO-834 Curve 114

4.6.1.2 General Response of Tested Specimen 116

4.6.1.3 Effect of Type of Infilled Concrete 117

4.6.1.4 Effect of Cross-sectional Shape 119

4.6.2 Failure Modes 119

4.6.3 Critical Temperature/ Limiting Temperature 123

4.6.4 Critical Time 124

4.6.5 Fire Concrete Contribution Ratio (FCCR) 126

4.7 Comparison with Previous Data 127

4.7.1 Strength Reduction Factors 127

4.7.2 Temperature of Steel Tube 128

4.7.3 Temperature of Infilled Concrete 130

4.8 Verification of Elevated Temperature FE Model for NCFST 131

4.9 Verification of Elevated Temperature FE Model for OCFST 133

4.10 Parametric Study for NCFST at Elevated Temperature 135

4.10.1 Effect of Strength of Steel 137

4.10.2 Effect of Strength of Concrete 138

4.10.3 Effect of Load Ratio 139

4.10.4 Effect of Cross-Sectional Dimensions (B/D ratio) 140

4.10.5 Effect of Steel Ratio 141

4.11 Parametric Study for OCFST at Elevated Temperature 142

4.11.1 Effect of yield strength of steel 143

4.11.2 Effect of strength of concrete 144

4.11.3 Effect of load ratio 146

4.11.4 Effect of width-to-depth ratio (B/D ratio) 148

4.11.5 Effect of steel ratio 149

CHAPTER 5: CONCLUSIONS AND RECOMMENDATIONS 151

5.1 Conclusions 151

5.2 Recommendations for Future 153

REFERENCES 155

List of Publications and Papers Presented 181

List of Figures

Figure 1.1: Different Types of CFST 2

Figure 2.1: Time-temperature curves given by different codes vs real fire 33

Figure 2.2: CFS profiles working as flexural elements (girders and purlins) (Shedquarters, 2009) 36

Figure 2.3: Scheme of the cross-sections of the tested beams by Luis 41

Figure 2.4: CFS members used as pallet storage racks (Rack, 2016) 42

Figure 2.5: Electric Furnace and loading setup (Heva, 2009).. 43

Figure 2.6: a) Lipped channel 100×56×15×2 without hole b) Lipped channel 100×56×15×2 with hole (Feng et al., 2003)... 45

Figure 2.7: Type A C-Section without additional lips, Type B C-Section with additional lips(Ranawaka & Mahendran, 2009a)... 46

Figure 2.8: Comparison of other distortional failure modes from experiments and FEA. (a) Both flanges moving inward. (b) One flange moving outward while other one moving inward (Ranawaka & Mahendran, 2010).. 46

Figure 3.1: Test setup and location of Strain gauges 52

Figure 3.2: Stress–strain curves for tensile coupon tests 53

Figure 3.3: General view of the experimental test setup.. 56

Figure 3.4: Location of thermocouples and side view of experimental setup 57

Figure 3.5: Schematic sketch of uniaxial stress–strain relation for steel 60

Figure 3.6: Effect of confinement on normal and high strength concrete 64

Figure 3.7: Representation of 3D hexahedral reduced integration solid element 65

Figure 3.8: Representation of 3D Quadrilateral reduced integration solid element 66

Figure 3.9: Study of mesh convergence for sample SOCFST 67

Figure 3.10: Boundary conditions and mesh used for square and rectangular CFST beams........68
Figure 3.11: Test sample showing heated length of specimen........69
Figure 3.12: FE model with load applied and reactions........69
Figure 3.13: Stress-strain curves for 475 MPa steel at different elevated temperatures.72
Figure 3.14: Mid-span deflection of different experimental tests and different FE models with different initial imperfections........74
Figure 4.1: Failure mode of square and rectangular NCFST specimens........76
Figure 4.2: Moment-curvature curve of RNCFST and ROCFST beams........76
Figure 4.3: Moment-curvature curve of SNCFST and SOCFST beams........77
Figure 4.4: Moment-deflection curve of RNCFST and ROCFST beams........77
Figure 4.5: Moment-deflection curve of RNCFST and ROCFST beams........78
Figure 4.6: Deflected Shape for both types of beams........79
Figure 4.7: Strains in beams along its length........80
Figure 4.8: Moment vs Strain Diagram for OCFST and NCFST beam........81
Figure 4.9: Moment -curvature curve predicted by Han et al., (2006) vs experimental results........85
Figure 4.10: Moment curvature curve of FE model and experimental test (B240-2).....93
Figure 4.11: Moment curvature curve comparison of FE model and experimental test sample CB-33........94
Figure 4.12: Load deflection curve comparison of experimental and FE model........95
Figure 4.13 Moment-curvature curve comparison of FE model and experimental test sample ROCFST........96
Figure 4.14: Moment-curvature curve comparison of FE model and experimental test sample SOCFST........96

Figure 4.15:Moment-displacement curve comparison of FE model and experimental test sample ROCFST 97

Figure 4.16: Ultimate Moment capacity of square and rectangular CFST with different D/t ratios 100

Figure 4.17: Load-deflection curve for different compressive strengths of concrete ... 103

Figure 4.18: Comparison of ultimate flexural capacities of CFST members having different steel yield strength 105

Figure 4.19: Capacity of different models having different D/B ratios and strengths .. 106

Figure 4.20: Moment curvature curve of samples having different a/d ratios 108

Figure 4.21: Comparison of the flexural bearing capacity.. 114

Figure 4.22: ISO-834 and furnace temperature throughout the test............................ 115

Figure 4.23: Temperature distribution in SNCFST... 116

Figure 4.24: Temperature of infilled concrete of all specimens 118

Figure 4.25: Temperature of steel tube of all the specimens 118

Figure 4.26: Comparison between the temperature of infilled concrete and steel tube of SOCFST and ROCFST 119

Figure 4.27: Deflection of RNCFST and SNCFST beam at different time intervals ... 120

Figure 4.28: Deflection of SNCFST and SOCFST beam at different time intervals.... 121

Figure 4.29: Failure modes of RNCFST and ROCFST 122

Figure 4.30: Mid-span deflection vs time of all specimens 123

Figure 4.31: Critical time of the tested specimens... 125

Figure 4.32: Comparison of moment reduction factors obtained from this experiment with results presented by (Chung et al., 2009)... 128

Figure 4.33: Comparison of temperature of outer steel of square CFST Beams with equations 4.23-4.26 130

Figure 4.34: Comparison of temperature of infilled concrete of square CFST Beams with available equations 131

Figure 4.35: Comparison of experimental and FE model time-temperature curve for outer steel tube of NCFST specimens 132

Figure 4.36: Comparison of experimental and FE model time-temperature curve for steel tube of OCFST specimens 134

Figure 4.37:Comparison of experimental and FE model time-temperature curve for infilled concrete of OCFST specimens 134

Figure 4.38:Time vs displacement curve for experimental and numerical models of OCFST specimens 135

Figure 4.39: FR time values for different yield strengths of steel 138

Figure 4.40: FR time of beams for different compressive strengths of concrete 139

Figure 4.41: Effect of load ratio on FR time for different yield strengths of steel 140

Figure 4.42: FR time for beam samples of different cross-sections 141

Figure 4.43: Comparison of FR time of different steel ratios with same yield strength 142

Figure 4.44 FR time values for different yield strengths of steel 144

Figure 4.45 FR time of beams for different compressive strengths of concrete 146

Figure 4.46 Effect of load ratio on FR time for different yield strengths of steel 148

Figure 4.47: Comparison of FR time of different steel ratios and cross-sectional dimensions 149

List of Tables

Table 2.1: End support conditions for the simply supported beams analysed 39

Table 3.1: Dimensions of tested specimens 52

Table 3.2: Mix proportions of NMC and OPBC concrete 54

Table 3.3: Properties of different aggregates 54

Table 3.4: Strength and Modulus of Elasticity at 28 days 54

Table 3.5: Dimensions of tested specimens 57

Table 3.6: Properties of steel and concrete used in FE model 71

Table 4.1: Energy absorption and structural efficiency of OCFST and NCFST beams . 83

Table 4.2: Yield and ultimate moment, ductility of OCFST and NCFST beam............. 84

Table 4.3: Comparison between test results and design results of initial flexural stiffness and flexural stiffness at the serviceability limit state for NCFST and OCFST....... 87

Table 4.4: Comparison of experimental and design ultimate capacity of beams............ 87

Table 4.5: Details of the specimens used for the verification of FE model of normal strength CFST 90

Table 4.6: Details of the specimens used for the verification of FE model of high strength CFST 92

Table 4.7: Main properties for CFST models used for studying the effect of D/t ratio .. 99

Table 4.8: Limit ratios of wall dimension to wall thickness for which local buckling is prevented 100

Table 4.9: Main properties for CFST models used for studying the effect of compressive strength 101

Table 4.10: Main properties for CFST models used for studying the effect of yield strength 104

Table 4.11: Main properties for CFST models used for studying the effect of D/B ratio 106

Table 4.12: Details of models used to study the effect of a/d ratio.............................. 107

Table 4.13: Comparison of limitations of different codes 109

Table 4.14: Average, maximum and minimum values from different code comparison 113

Table 4.15: Critical temperature of the tested specimens 124

Table 4.16: Fire concrete contribution ratio of all tested specimens 127

Table 4.17: FR time comparison for experimental and Numerical models for NCFST133

Table 4.18: Details of specimens used for parametric studies 136

Table 4.19 Main properties for CFST models used for studying the effect of yield strength of steel 143

Table 4.20 Details of models used to study the effect of compressive strength of concrete 145

Table 4.21 Main properties for CFST models used for studying the effect of load ratio 147

Table 4.22: Details of models used to study the effect of B/D ratio and steel ratio 149

LIST OF SYMBOLS AND ABBREVIATIONS

3D		Three dimensional
3R	:	Recycle, Reduce, Reuse
ASTM	:	American Society for Testing and Materials
B/t	:	Width to thickness ratio
CFS	:	Cold-formed Steel
CFST	:	Concrete Filled Steel Tube
CFT	:	Concrete Filled Tube
COV	:	Coefficient of Variance
CTE	:	Co-efficient of thermal expansion
D/t	:	Depth-to-Thickness
EA	:	Energy Absorption
FDS	:	Fire Dynamics Simulator
FE	:	Finite Element
FEA	:	Finite Element Analysis
FRDM	:	Fire and Rescue Department of Malaysia
FRR	:	Fire Resistance Rating
HSC	:	High Strength Concrete
LCB	:	Lipped channel beam
LVDT	:	Linear Variable Displacement Transducers
MPa	:	Mega Pascal
NCFST	:	Steel tube filled with natural aggregate concrete
NMC	:	Natural mix concrete
NRC	:	National Research Council of Canada
OCFST	:	Steel tube filled with oil palm boiler clinker concrete

OPB	:	Oil-palm-boiler clinker
OPBC	:	Oil-palm-boiler clinker concrete
SD	:	Standard Deviation
SE	:	Structural Efficiency
SEA	:	Specific Energy Absorption
A_s	:	Area of steel tube
A_C	:	Area of concrete
a/d	:	Shear span-to-depth ratio
E_c	:	Modulus of Elasticity of concrete
E_s	:	Modulus of Elasticity of steel tube
ξ	:	Confinement factor
ε_{cc}	:	Strain of confined concrete
ε_e	:	Strain of steel at proportional limit
ε_y	:	Strain of steel at yield strength
ε_y	:	Strain of steel at ultimate strength
F_S	:	Flexural stiffness of steel
F_C	:	Flexural stiffness of concrete
f_c'	:	Compressive strength of concrete at 28 days
f_{cc}	:	Maximum compressive strength of concrete
f_p	:	Proportional Limit of steel
f_y	:	Yield strength of steel
f_u	:	Ultimate strength of steel
ρ_c	:	Density of concrete
K_i	:	Initial flexural stiffness obtained from experiments (kN/m^2)
K_c	:	Flexural stiffness calculated using equations suggested by codes

K_s	:	Flexural Stiffness at serviceability level
M_{exp}	:	Moment capacity obtained from experiments
Mu_{Num}	:	Moment capacity obtained from FE model
M_{EC4}	:	Moment capacity calculated using EC4 code
M_{AISC}	:	Moment capacity calculated using AISC code
M_{CIDECT}	:	Moment capacity calculated using CIDECT guidelines
M_{GB}	:	Moment capacity calculated using GB code
M_u	:	Ultimate moment
M_y	:	Yield strength
l_T	:	Buckling length of CFST column in mm
δ_u	:	Deflection at ultimate moment in mm
δ_y	:	Deflection at yield moment in mm
$t_{fi,Rd}$	:	fire endurance of CFST column
μ	:	Ductility index

CHAPTER 1: INTRODUCTION

1.1 Background of the Study

It is notable that steel and concrete are the most utilized construction materials as a part of structural designing works. The steel members have higher load carrying capacity to weight proportion as compared to concrete yet buckling will decrease the structural effectiveness as the full section capacity can't be used. Moreover, steel members are prone to elevated temperatures and corrosion. As compared to steel members, the concrete members are bulky and are prone to tensile forces. As a result, the chances of concrete cracking and spalling at higher temperatures are increased.

The main objective of steel-concrete structure is to make use of the advantages of concrete and steel materials. In this research, steel-concrete composite beam is studied. Concrete filled steel tube (CFST) members have many benefits over conventional reinforced concrete and steel members, like high load carrying capacity, ductility, and ease of fabrication and construction (Liew, 2004a, 2004b). Different types of CFST members used are shown in Figure 1.1. The benefits of filling hollow steel sections with concrete core were recognized earlier, indeed the first known patent related to circular concrete filled steel tubes dates from 1898 (Hicks et al., 2005). CFST beams and columns is an economical load bearing structure. Webb & Peyton (1990) compared the costs of CFST, steel, and concrete structures (Webb & Peyton, 1990). The costs were calculated and presented in the form of cost/meter^2. It was concluded that for a 10-storey building, the cost of the concrete structure was 10% lower than CFST structure. However, the cost of CFST structure was 50% lower than the steel structure. Whereas for 30-storey building the cost of CFST structure was equal to the cost of the concrete structure and 40% lower than the steel structure. Thus, CFST structures will be more efficient and economical for high-rise buildings.

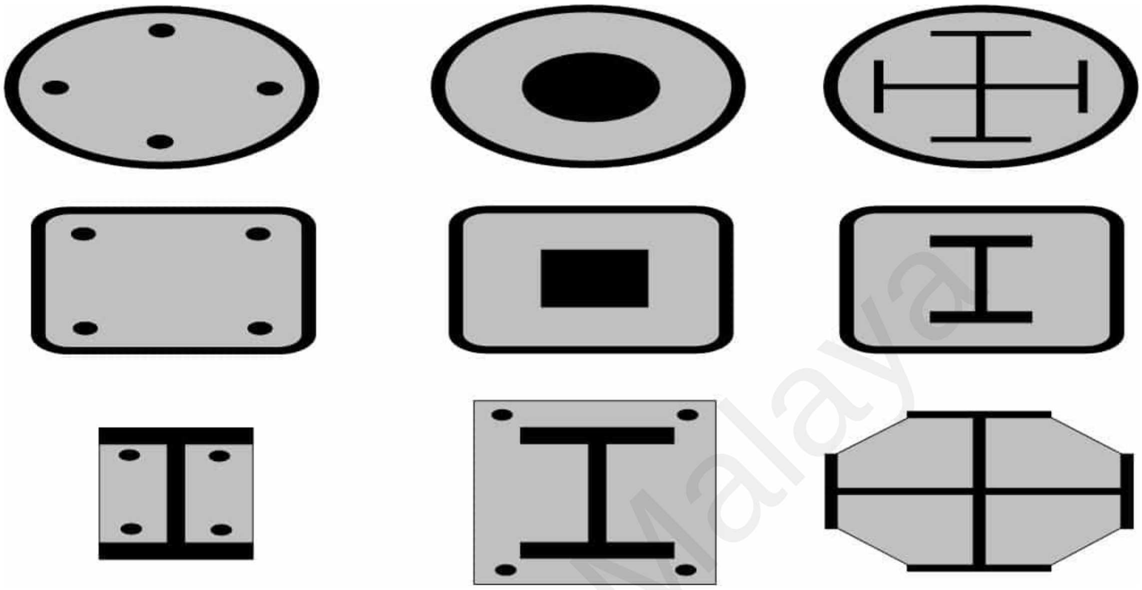

Figure 1.1: **Different Types of CFST**

Fire resisting capacity of CFST member is better than pure steel members because of the heat absorption of concrete from the steel tube. Furthermore, steel tube prevents the spalling of concrete in fire thus increasing the fire resistance of CFST member. Due to this better performance of CFST in fire, the required amount of external fire protection in case of CFST is lower as compared to bare steel members thus reducing the cost of fire protection. CFST members also have better residual fire resistance as compared to steel member, as the residual capacity after fire can still be 50%-90% of that of ambient temperature (Jingsi, 2002).

Solid waste products originating from various industries need proper management and disposal to ensure healthy and cleaner environment. The agricultural industry in Malaysia is developing very rapidly and progressively to support the country's economy. It has been reported that 80 million dry solid biomass waste yielded in 2010 only and is expected to reach up to 110 million by 2020 (Malaysia, 2011; Ng et al., 2012). The Malaysian palm oil industry is the 2nd largest palm oil industry having more than half a million employees (Johari et al., 2015; Michael, 2012). As this industry becomes bigger and wider, a substantial amount of oil palm wastes is generated and create the problem of waste overload. This problem tends to burden the operators with disposal difficulties and escalates the operating cost (Mahasneh & Gharaibeh, 2005). Various types of solid wastes like palm fiber, oil palm shell, oil palm boiler clinker and empty fruit branches are produced at the end of palm oil processing stages. Oil-palm-boiler clinker (OPB) is a waste material obtained by burning off solid wastes during the process of palm oil extraction (Aslam et al., 2016b). Most of the OPB is used for covering the potholes on the roads within the vicinity of the plantation areas, which affects the environment directly (Kanadasan & Abdul Razak, 2015) and this is why in most countries oil palm industries are known for their wide range of negative environmental impacts (Craveiro et al., 2015). Hence, by utilizing the agricultural waste for example in the construction industry will be a smart choice, as it will reduce the harm of agricultural industry to the environment. OPB is a lightweight waste material that has been successfully utilized in the past for sustainable and lightweight composite members. OPB concrete (OPBC) behaves differently from other types of lightweight concrete and can be designed for high grades and ductility (Aslam et al., 2016a; Chai et al., 2017). In the last decade, many researchers have shown that OPBC can be used as coarse aggregate in concrete (Ahmmad et al., 2016; Aslam et al., 2016a). Besides, for sustaining green environment due to the use waste materials, OPBC is a smart choice as it has lower density and can be used in the construction industry to produce lightweight concrete. Hence, by using the OPBC as coarse aggregate in concrete instead of using natural aggregate would be a better way to improve the cost and sustainability of a structure. Hence the performance of concrete made with natural coarse aggregate and concrete made with OPBC aggregate filled inside the steel tubes needs to be compared and analyzed. Steel tubes filled with concrete made with natural aggregates are denoted by NCFST and steel tubes filled with OPBC are denoted by OCFST in this thesis.

1.2 Problem Statement

Fire safety has become a very important concern in building design, especially after the collapse of the World Trade Center twin towers. Fire and Rescue Department of Malaysia (FRDM) attended to 33,640 fires in 2013 over the country or an average of 92 cases per day. This figure was the highest annual figure recorded, continuing the generally upward trend since 2007 (FRDM, 2014). A sharp increase of fire incidents in 2012 had killed 72 civilians but this was the lowest number of fatalities for the last seven years. The behavior of CFST members at elevated temperature is very different from steel hollow sections as in steel hollow sections the temperature in the member is throughout uniform. As the steel and concrete have significantly different thermal conductivities, their combination produces a transient heating behavior. This behavior is characterized by temperature differentials across the section. Due to the complex evolution of temperature distribution in CFST sections, section factor based simple calculation models cannot be used to predict the strength of CFST members at elevated temperature. Hence, advanced calculation tools are needed which consider the time-dependent thermal properties of different materials and resulting thermal transients. The different parts of the CFST members have different strength reduction factors when exposed to fire, depending on the position of the part within the cross section of the member (Twilt et al., 1994). The steel tube is exposed directly to the fire, so its capacity reduces significantly after a short period of exposure time. On the other hand, concrete core with low thermal conductivity and high mass, resist the elevated temperature for longer duration of time mainly in the areas closer to the center of the section. Similarly, in case of reinforced concrete CFST members, the reinforcement is located closer to the steel tube but covered with concrete cover, so their rate of strength reduction is lower than steel tube. The number of experiments carried out to date to study the structural behavior of CFST members in fire made it possible to create a list of different parameters which contribute in the failure of these members after exposure to fire. For example, diameter to thickness ratio, concrete strength, steel strength, aggregate type, load level and member slenderness (Ana et al., 2010, 2011, 2012).

The load transfer and bearing mechanisms in the CFST subjected to pure flexural load are like that of axially loaded CFST. However, the response is different in some way because there will be no tri-axial stress state in the concrete. A lot of studies have been conducted on CFST columns at ambient and elevated temperature (Kodur, 1998; Kodur & MacKinnon, 2000; Lie & Kodur, 1996a; Lie & Stringer, 1994). However, there are very limited studies on the flexural behavior of CFST at ambient temperature while to date no study has been conducted on the behavior of CFST beams at elevated temperature. One would doubt the meaning to study the flexural behavior of the CFST members as the CFST members are seldom subject to pure bending. This may be true for building structures, where CFSTs are mainly used as column members. However, CFSTs are also widely used for bridge construction and in pole structures where they are subject to predominately flexural action (Chen et al., 2017). Besides, when designing CFST columns under combined axial force and bending moments in high-rise structures, one may have to determine the bending resistance according to the moment-axial force (M-N) interaction curves. Therefore, a comprehensive research study is required to study the flexural behavior of CFST members at ambient and elevated temperature.

1.3 Objectives of the Research

Main objectives of this research are given as follows.

1. To investigate experimentally the behavior of rectangular and square NCFST and OCFST beams at ambient temperature and elevated temperature.
2. To develop and validate a 3D FE model for predicting and analyzing the structural behavior of NCFST and OCFST beams at ambient and elevated temperature.
3. To conduct parametric studies on NCFST and OCFST beams, identifying various variables and determining their influence and to evaluate the accuracy of existing four design codes for the flexural capacity of CFST members.

1.4 Scope and Limitations

The scope of this thesis is restricted to un-protected CFST beams of square and rectangular shape, filled with OPBC and normal strength concrete subjected to only flexural loads. With the limitations surrounding the environmental issues of negative effects of oil palm industry and construction industry, a new type of member is proposed. The study covers the full-scale experimental tests, FE modeling, parametric studies and evaluation of four different current design codes. The experimental test consists of four in room temperature and four in elevated temperature.

The evaluation of performance of CFST members is normally performed using monotonic loading. ISO-834 curve is applied using a heating furnace. An-isothermal method is used for the elevated temperature tests in which the load is kept constant and the temperature varies. FE studies are performed using multi-purpose FE analysis program, ANSYS. The FE model is validated with existing data in literature as well as with the present experiments. The parametric studies examine the variations of different properties and its effect on the performance of CFST member. The FE results are used for the evaluation of the four different existing methods for the design of CFST member. The effect of infilled concrete and different cross-sectional shapes was examined for elevated temperature conditions. The field of application of this thesis is limited to simply supported CFST members subjected to flexural loads only.

1.5 Outline of the Thesis

This thesis is divided into five chapters. Chapter one provides the basic introduction about the research area and specifies the research needs, objectives and the scope of work. A comprehensive critical review on the use of cold formed steel, concrete and CFST at ambient and elevated temperature is presented in chapter two. Part of the literature provided in this chapter is already published as a review paper entitled “Recent research on cold-formed steel beams and columns subjected to elevated temperature: A review”. The methodology of experimental tests at ambient temperature and elevated temperature is presented in the first part of chapter 3. Furthermore, the details of FE model are also discussed in chapter 3. Test results from experiential tests and Finite element model are discussed in chapter 4. Results from the parametric studies of CFST members at ambient and elevated temperature are also presented in chapter 4. Finally, chapter five presented the cumulative conclusions of the major findings of the present research investigation, as well as some future recommendations were also suggested.

CHAPTER 2: LITERATURE REVIEW

2.1 Introduction

Experimental, numerical and analytical research has been performed to study the behavior of square, rectangular and circular CFST members at elevated temperatures. Most of the research is carried by using ASTM E-119 standard. Different parameters like type and strength of material, cross-sectional shape and loading are included in the research. In this section, prior research on rectangular and square CFST and factors affecting their performance at ambient and elevated temperature is summarized. The behavior of steel and concrete material in fire is also discussed in this chapter. In section 2.1, prior experimental tests on rectangular and square CFST using standard ambient temperature and fire conditions are discussed. The results of these experimental data are used in Chapter 4 for the validation of FE model. In section 2.3, main parameters and their effect on the performance of CFST members at elevated temperature are discussed. In section 2.4, different properties of concrete material at elevated temperature are discussed. In section 2.5, properties of OPBC concrete at ambient temperature are discussed. In section 2.6, different test methods used for steel testing at elevated temperature is presented. In section 2.7, standard fire time temperature curve is discussed. In section 2.8, different properties of steel member at elevated temperature are discussed.

2.2 Properties of CFST at Ambient Temperature

2.2.1 Experimental Tests at Ambient Temperature

One of the earliest tests on the flexural performance of CFST members at ambient temperature were reported in 1976 (Matzumoto et al., 1976). The author performed 2 experimental tests on the circular CFST members. All the members were 4000 mm long, and 30 mm in diameter. The author compared the performance of expansive and normal concrete used as infill in CFST member. The author concluded that CFST members filled with expansive concrete performs better due to the initial pre-stress action produced. Lu & Kennedy (1994) examined the effects of different D/t ratio and different shear span to depth ratio on twelve square and rectangular steel beams. The steel tubes with yield strength of 350 MPa were filled with normal strength concrete of 30 MPa while the shear span to depth ratio was kept in the range of 1-5. The length of the CFST beam varies from 1975 to 4260 mm. They reported that the flexural strength of the CFST is increased by 10-30% over that of hollow steel sections, depending on relative proportions of concrete and steel. The flexural stiffness is also increased due to concrete infill. The shear-span to depth ratio has no significant effect on ultimate strength of CFST. Formulae for the strength of square and rectangular CFST under flexure load were suggested.

Hunaiti (1997) performed 8 tests on lightweight CFST having square cross-section. 3 unfilled similar samples were also tested for comparison. It was observed that beams filled with lightweight aggregate showed good ductility as compared to hollow beams. The author concluded that lightweight aggregate can be utilized in composite construction to increase the flexural capacity of hollow steel sections. Uy (2000) performed 5 experiments on square CFST beams filled with normal strength concrete. The strength of the concrete infill was in the range of 38 to 50 MPa while the yield strength of the steel tubes was 300 MPa. The main parameters were D/t ratio and strength of infill concrete. The author concluded that D/t ratio have significant influence on the flexural performance of CFST member. Elchalakani et al (2001) performed experiments on circular CFSTs subjected to pure bending. They reported that the concrete filling in the steel tubes increased the ductility, energy absorption and strength of thinner sections.

Yang & Ma (2013) performed 14 experiments on square CFST beams. The infill concrete used was made of recycled aggregate having infilled concrete strength of more than 50 MPa. It was observed that recycled aggregate CFST have similar failure pattern as that of normal CFST. It was concluded that current design codes gave conservative values for the ultimate flexural capacity of CFST beams. Assi et al (2003) reported the results of an experimental investigation on lightweight aggregate and foamed concrete-filled hollow steel beams. Thirty-four simply supported beam specimens of rectangular and square specimens of different d/t ratios were used at a span length of 1000 mm. Normal mix concrete specimen and hollow steel sections also were tested for comparison purposes. It was concluded that beams filled with foamed and lightweight aggregate concrete can develop the full flexural strength of their sections.

Han (2004) performed experiments on sixteen rectangular and square CFST members. The D/t ratio was in the range of 20-50, while the yield strength of steel and concrete were kept as 300 MPa and 30 MPa, respectively. All samples were 1100mm long. The author concluded that infilling square and rectangular hollow steel tubes increased the ductility of samples. (Wang et al., 2014) compared the performance of sand dune filled CFST with normal CFST. Six experimental tests were reported. The length of the specimens was kept as 4000 mm. The author reported that the failure mode of dune sand filled CFST and normal CFST are similar and hence dune sand concrete can be used as infill material in CFST members subjected to flexural loads.

Soundararajan & Shanmugasundaram (2008) performed experiments on square CFST members. The specimens were made of normal mix concrete, fly ash concrete, quarry waste concrete and low-strength concrete (LSC) with compressive strength ranging from 21 MPa to 32.6 MPa. The D/t ratio of the steel tube was kept as 20.5. All specimens were tested under the two-point flexure loads. The yield strength of steel tubes was 345 MPa while the ultimate stress was 510 MPa. The author concluded that quarry waste concrete can be used as infill while low strength concrete has negative effect on the flexural performance of CFST member.

Recently, Xiong et al (2017) studied the flexural performance of CFT with high strength steel and infilled ultra-high strength concrete. Yield strength of steel used in this study was more than 780 MPa while the compressive strength of infilled concrete was more 180 MPa. A total number of 8 specimens were tested. The length of all the specimens were kept as 3000 mm. 3 of the test samples were circular while the rest were square. All specimens were subjected to two-point loading. The author concluded that the yield strength of the steel tube and compressive strength of infilled concrete has significant influence on the flexural behaviour of CFST members.

2.2.2 Numerical Investigations and Analytical Models of CFST at Ambient Temperature CFST

Hu et al., (2010) proposed material constitutive model for circular CFST columns subjected to pure bending. They performed finite element analysis (FEA) and validated the theoretical results with the experimental data and concluded that the concrete acts as ideal material to resist compressive loading in the typical applications, only when the depth-to-thickness (D/t) ratio is greater than 74. In addition, the infilled concrete has no significant effect on the strength of CFST columns when the D/t ratio is less than 20. Lakshmi & Shanmugam (2002) proposed a semi-analytical method by using an iterative process, the relationship between moment-curvature-thrust is generated to investigate the behaviour of CFST columns. They considered different cross-sections including square, rectangle and circle of compact section in the FE analysis. The pin-ended columns subjected to bi-axial or uniaxial loads were studied. They verified the theoretical and experimental results and concluded that the moment capacity of columns decreases with an increase in axial load.

Liang et al. (2005) studied the FE behaviour of simply supported composite beams subjected to combined shear and flexure loading. A 3D FE model was developed to consider the material and geometric non-linear behaviour of composite beams and is verified by experimental results. The verified FE model was then used to study the effects of different factors effecting the combined moment and shear capacities of concrete slab and composite beams. It was concluded that the presence of moment significantly affects the shear capacity of composite beams.

Jiang et al (2013) developed an FE model for thin-walled CFST and verified using the results of the experiments. The increase in corner strength due to cold forming, welding residual stresses and confined concrete material properties were considered in the FE model. It was concluded that the FE model accurately predicts the load-strain curves of tested specimens provided that the effect of cold-forming is considered. Yang & Ma (2013) performed 14 experiments on square CFST beams by using recycled aggregate as infill material. The authors presented an analytical model to calculate the flexural capacity of recycled aggregate CFST. It was concluded that the recycled aggregate CFST performs like normal CFST, if the compressive strength of concrete is kept constant. After conducting a series of experiments on square and rectangular CFST beams, Han (2004) proposed a model that can predict the structural behaviour of CFST and used that model to assess the accuracy of existing design codes. The author concluded that the moment capacities of CFST beam predicted by BS5400 (1979), LRFD-ASIC (1999), EC4 (1994) and AIJ (1997) were lower than the experimental values. However, the model is only valid for D=100-2000 mm; f_y=200-500 MPa and f_c=20-80 MPa and cannot be used for high strength and ultra-high strength concrete.

2.3 Properties of CFST at Elevated Temperature

2.3.1 Experimental Investigations at Elevated Temperature

Kodur & Mackinnon (2000) performed experimental study on CFST columns to study the effect of different types of cross-sections and infilled concrete on the performance of CFST columns at elevated temperature. Overall 58 CFST members were tested including rectangular, square and circular members with different infills. Behavior of three different types of infill including plain concrete, reinforced concrete and steel-fiber reinforced concrete were studied in the experimental program. Different diameters/widths in the range of 140-410 mm are used in the experimental work. The slenderness ratio (length to width ratio) selected for the study was in the range of 10 to 20, whereas strength of the infill used in the experiments ranges from 20-55 MPa. Both axial and fire loading were applied to CFST members used in the experiments. Fire loading was applied with the help of large furnace built at NRC. The axial load was generally applied as a factor of total axial capacity and is sometime referred as axial load ratio. Various load ratios were used in the experimental work at NRC ranging from 10-60%. Fire loading is applied to the CFST members by increasing the temperature of the air inside the furnace. The temperature was increased according to the curve given by ASTM E119. Buckling was the main cause of failure in all columns. By analyzing the results, it can be concluded that columns having plain concrete as infill have approximately 2 hours of fire resistance time. Whereas, columns filled with fiber reinforced concrete and reinforced concrete have resistance time of approximately 3 hours (Kodur, 1998; Kodur & MacKinnon, 2000; Lie & Kodur, 1996a; Lie & Stringer, 1994).

Few standard ambient and fire tests have been carried out in Japan on square CFST members. Focus of the research was to find the design fire resistance rating (FRR) values for CFST. However, different kinds of fire protections including fire-resistant steel, ceramic protection and intumescent coating, were used on the tested samples. Different axial load ratios (20-30%) and eccentric loadings were applied to the samples. The effect of load levels and eccentricity of the thermal and structural behavior of square CFST columns were investigated. Furthermore, the fire resistance of different types of steel tubes used in CFST were also investigated. In addition to, the performance of protected square CFST members are compared with the performance of unprotected square CFST members (Kimura et al., 1990; Saito & Saito, 1990; Sakumoto et al., 1994). From the experimental work, it was concluded that the total fire resistance time of unprotected fire-resistant CFST members is about 30 minutes (Sakumoto et al., 1994). Furthermore, the fire-resistant steel and conventional steel CFST members have the equal FRR values. However, fire-resistant steel is more sensitive to flexure loading as compare to conventional steel.

Han (2004) performed reported numerous experimental tests on the elevated temperature performance of CFST columns. Both square and rectangular CFST members were tested for their performance in fire. Both fire protected, and unprotected members were tested. Load ratio was kept constant. However, the value of load ratio selected was 77%, which is much higher as compare to other studies. Chinese code was used to evaluate the design values of the members at room temperature. Constant axial load was applied with different eccentricities on different members to study their structural and thermal behavior. Fire resistance time was also investigated. Furthermore, in these experiments, ISO 834 fire curve was used instead of ASTM E119 time temperature curve. Rectangular and square CFST columns mostly failed in buckling in most of the experiments. The author concluded that fire resistance of CFST members can be increased significantly by applying fire-protection material to the steel of CFST. More experiments have been recently done in China on CFST members. Some of the conclusions of these studies are given below.

1. Both the cross-sectional shape and dimensions of CFST members significantly affects its structural and thermal behavior and fire resistance of the member.
2. Effect of load eccentricity has little influence on the fire resistance and thermal behavior of CFST members when all the other factors are kept constant.
3. Effect of fire protection has substantial influence on the fire resistance and thermal behavior of CFST members.

All the above studies were performed on the axial behavior of CFST members at subjected to axial load at elevated temperature. According to author's knowledge, to date there is no study reported on the flexural behavior of CFST members at elevated temperature and very few studies are reported on the flexural behavior of CFST members at ambient temperature. The experimental tests performed on the CFST members subjected to flexural members at ambient temperature are presented in next section below, while they are also presented in tabulated form in Chapter 4.

2.3.2 Numerical Models

Main numerical studies present in the literature are summarized and reviewed below.

From all the global structural models, the models presented by Wang (1999) and Bailey (2000) got more attention. Wang (1999) used a global model to study the effects of the continuity of circular CFST members on fire resistance. FE was used to study the structural behavior of CFST members and the distribution of temperatures around the cross-section of the member. To conduct the thermal analysis, the author used one-dimensional finite elements with two nodes, thus representing the circular slice of the cross-section. The author developed his own FE computer program to obtain the structural response of steel and composite frames at elevated temperature. Thermal resistance of the steel-concrete interface was neglected, and the composite cross-section was assumed to be continuous material with changing thermal properties. It was concluded that the effective length of column which is continuous at one end, is 0.7 times the total length of column.

A global structure model is presented by Bailey (2000) to investigate the effective lengths of CFST members at critical temperature. A finite element embedded computer model was developed to include the structural behavior of square CFST members at ambient and elevated temperatures. One dimensional two-nodded element with 7 degrees of freedoms was selected to represent the square CFST. Complete cross-section was divided into numerous rectangular and square segments. For material, constitutive models in fire, the recommendations given in EN 1994-1-2 were used. Tensile strength of concrete is taken as 10% of its compressive strength at each temperature. A two-dimensional thermal computer package TFIRE was used to obtain the temperature distribution through the cross section. It was concluded that the effective length of column which is continuous at both ends, is 0.75 times the total length of column.

In literature, one-dimensional, sectional and three-dimensional models can be found to be used for member analysis. Both Wang (1999) and Bailey (2000) used one-dimensional member models. One-dimensional member models are good from the computational point of view, but some simplified assumptions are needed to be made.

Hence, two and three-dimensional models can be found abundantly as compare to one-dimensional model. Some of the most highlighted work is briefly described here in chronological order.

Lu et al. (2009) performed experimental studies and FE analysis for understanding the structural behavior of high strength self-consolidating short square CFST columns at elevated temperature. Commercial FEA software ABAQUS was used for FE analysis. A sequentially coupled thermal-stress analysis was used. The model presented by Kodur (2007) was used for representing the thermal properties of high strength self-consolidating concrete whereas, the models presented by Lie & Stringer, (1994) were used for the thermal expansion of concrete and steel. Uni-axial stress-strain relationships proposed by Lie & Stringer, (1994) for steel in fire and uni-axial stress strain relation from Han et al. (2003)for concrete were also used in the model. To take into account, the thermal resistance at the contact between concrete core and steel tube, a heat contact conductance parameter of 100 W/mK^2 was used. Four-nodded shell elements and three-dimensional eight-nodded solid elements were used for steel tube and concrete core respectively. The model was capable for predicting and explaining the failure mechanism of CFST columns at elevated temperature.

Song et al. (2010) presented a FE 3D model to simulate the experiments of CFST short columns under different mechanical and thermal loading conditions. The studies were previously done by Yang et al. (2008) by simplifying many factors. The sequentially coupled thermal-stress analysis module was used. The studies were performed by using a commercial FE software ABAQUS. Various stress-strain relationships at ambient temperature, heating, cooling and post-fire conditions were used as explained by Yang et al. (2008). Three-dimensional eight nodded brick elements and four nodded shell elements were used for concrete core and steel tube respectively. For modeling of thermal resistance at steel-concrete interface, a surface-based interaction model with Coulomb friction and contact pressure model was used. The coulomb friction model was in tangential direction and contact pressure model was in normal direction.

2.3.3 Simple Calculation Models (Design Guidelines)

Researchers taking keen interest in the development of simple calculation methods for calculating the Fire resistance time of CFST axial members, due to the increase in demand of usage of this structural typology. However, very limited research has been carried out to develop the design guidelines for CFST flexural members. The calculation methods developed by the researchers are then use by designers to obtain the minimum protection cover and dimensions for the required elevated temperature behavior.

Several design guides have been developed in the past by researchers for estimating the fire resistance of CFST members, amongst which the CIDECT and Corus tubes guide are needed to be highlighted. At the end of these guides, designers can find a variety of design charts viable for commonly used cross-sectional dimensions. In these design charts the ultimate load bearing capacity of the CFST member exposed to elevated temperature for certain period of time is given as a function of cross-sectional dimensions, effective length and percentage of steel reinforcement. Rush et al. (2011) and Zhao et al. (2010) reviewed the existing methods for evaluating the fire resistance of CFST members. Some of the commonly used methods are mentioned here.

Kodur (1998) along with other researchers developed design equations for fire resistance of CFST members. These design equations are based on the vast experimental study conducted at National Research Council of Canada. Kodur (1998)has suggested that the fire resistance of CFST circular or square column can be expressed as

$$t_{fi,Rd} = f_1 \left(\frac{f_c'+20}{l_T-1000}\right) D^2 \sqrt{\frac{D}{N_{fi,ED}}} \quad \text{……………………………………..(2.1)}$$

Where,

$t_{fi,Rd}$= fire endurance of CFST column

f_1= factor, to be selected from table (depends on type of aggregate used in concrete, siliceous or carbonate)

f_c' = compressive strength of concrete in MPa

l_T = Buckling length of CFST column in mm

D = Side length of the square column or diameter of circular column

$N_{fi,ED}$ = Load applied during the test (kN)

The above design equation is only valid for square and circular CFST columns. However, they can be used for both high and normal strength infill concrete with various types of reinforcement i.e., steel fibers and longitudinal reinforcement. Kodur's Model is basically a best-fit semi empirical model based on both experimental and numerical results (numerical results were obtained from the numerical model based on the experimental results).

Wang (2000) made minor modifications in Lawson and Newman (1986) method to be used for the prediction of the temperature in the CFST member. The CFST is assumed to be without any external fire protection. In case of reinforced CFST members, the temperature of the reinforcement should be taken as that of the concrete around it. Han et al (2003) presented a model for the prediction of fire resistance of rectangular and square CFST members without fire protection.

Nowadays, different design codes, developed by different research groups are used in different parts of the world. The equations proposed by Han et al. (2003) have been embedded in Chinese Code DBJ13-51 (2003), for calculating the thickness of the fire protection material, applied externally, to attain certain fire resistance. Furthermore, Han et al (2003) expressions are used for developing the equations for calculating the strength index of CFST column without fire protection exposed to elevated temperature.

The research work done by Kodur (1998) and his research group have been incorporated into the National Building Code of Canada (NRCC, 2005), ASCE/SFPE 29-99 (ASCE 1999), ACI 216 (ACI 2007) and AISC Steel Design Guide 19 (Ruddy et al. 2003) and is being used in North America. The method consists of simple equation incorporating different factors affecting the fire resistance of CFST columns. In Europe, the detailed methods for the calculations of fire resistance of CFST columns are incorporated in EN 1994-1-2. Three methods for designing CFST columns are allowed i.e., tabulated data, simple calculation model and advanced calculation model. The tabulated data is presented in clause 4.2.3.4 in the tabulated form which gives reinforcement and minimum cross-sectional dimensions of CFST column for a standard fire exposure and given load level. This method is the most simplistic method available, however, is very conservative according to Rush et al. (2011). Simple calculation models are based on elastic buckling theory and are presented in clause 4.3.5.1. These methods are widely used and consist of a full method for calculating the fire resistance of composite columns. More specific method for CFST columns without external fire protection is also given in Annex H of the Euro Code. Advanced calculation model allows the use of FE models for simulating the original fire behavior of elements using real thermo-mechanical problem. The advanced calculation model provides highest accuracy as compare to other models. However, this method can't be used by practitioners in normal routine and due to limited resources and time, it is used very rarely is designing.

Different authors Wang (1997, 2000, 2008), Aribert et al. (2008), Ribeiro et al. (2008) and Leskela (2009) have put emphasis on the study of simple calculation model in EN 1994-1-2. However, the specific method presented in annex H is complicated and does not produced accurate results for slender columns (Wang & Orton 2008, Aribert et al. 2008), most researchers use the general guidelines presented in clause 4.3.5.1, which is accurate for all types of CFST columns. However, the accuracy and applicability of general guidelines present in clause 4.3.5.1 is checked by only few studies in France (Renaud et al. 2004, Aribert et al. 2008). The results of these studies are presented in French National Annex to EN 1994-1-2 (AFNOR 2007).

Recently, Espinos (2012) 's model proposed a model for circular CFST columns based on the results of the FE study (Ana et al., 2011; Ana et al., 2010, 2012). The author performed simulation of 176 CFST columns. The procedure given in this model is similar to the model given in Eurocode 4. First the temperature field across the section of CFST is calculated by using two different equivalent temperature equations for steel and concrete. The equations for the equivalent temperature of concrete is based on two approaches i.e., flexural stiffness approach and plastic resistance approach. In both the approaches, the cross-section of concrete core is divided into many layers.

2.4 Properties of Concrete at Elevated Temperature

2.4.1 Density

Mostly, the density of concrete increases with decrease in temperature and vice versa (Shin et al., 2002). The density of concrete at high temperature depends of several factors including moisture content, density of aggregates, temperature and curing conditions. The density of siliceous concrete aggregate decreases rapidly during the temperature change from 20 to 700 due to rapid expansion of siliceous aggregate as compare to carbonate aggregate (Anand & Arulraj, 2011; Naus, 2006; Schneider et al., 1982). However, in case of limestone concrete, the density remains constant from 20 to 700C and decreases significantly after further heating due to loss of water and de-carbonation process. However, around 1200˚C, the density starts to increase due to sintering. As Basalt have lower thermal expansion, therefore it shows the smallest decline in density (Shin et al., 2002). Curing or storage conditions at ambient temperature are important as wet specimens will lose water more rapidly resulting in rapid decrease in density as compare to dry specimens.

2.4.2 Thermal Conductivity

Thermal conductivity is the property of any material to conduct heat and is influenced by temperature. Moisture in concrete is present in different forms. The amount and type of moisture effects the thermal conductivity of concrete (Kodur & Khaliq, 2010). However, compressive strength of concrete has no effect on thermal conductivity (John et al., 1997). Water content, pore distribution, hardened cement paste, and pore volume are some of the important factors affecting the thermal conductivity of concrete. When concrete is in moist condition, it gives very high values of thermal conductivity at lower temperature. Thermal conductivity keeps on increasing up to 100°C, then due to development of more cracks, it decreases (Naus, 2006).

In most of the studies for thermal conductivity, it has been concluded that by increasing temperature thermal conductivity decreases (Adl-Zarrabi et al., 2006; Harada et al., 1972; Harmathy, 1970; Kodur & Khaliq, 2010; Lie & Kodur, 1996b; Marechal, 1972; Shin et al., 2002; Xing et al., 2011). The thermal conductivity of concrete changes linearly with moisture content. Concrete thermal conductivity increases with the increase in conductivity of aggregates. In addition, concrete with lower amount of cement shows lower conductivity as compare to lean mixes.

2.4.3 Specific Heat

The specific heat is the amount of heat per unit mass required to raise the temperature by one degree Celsius. Aggregate type, moisture content and density of concrete are the main factors that influenced the specific heat (Kodur & Khaliq, 2010). At lower temperatures, the specific heat increases with an increase in moisture content of concrete. Heat capacity of concrete rises up to 500℃ and then becomes constant or decline when temperature approaches to 1000℃ (Harmathy & Allen, 1973).

2.4.4 Coefficient of Thermal expansion

Coefficient of thermal expansion (CTE) is an important factor that affects the performance of concrete at elevated temperature. It represents the change in volume of a material due to change in temperature. Structural movement and thermal stresses caused by temperature change can be calculated by measuring CTE. As concrete is a homogeneous material, its thermal expansion is complicated because each of its component has its own CFT. Huge difference in CFT can cause micro-cracking and micro-stresses and results in the disruption of concrete microstructure. Experimental observations of thermal expansions are also very complicated due to a number of external changes that occurs at elevated temperatures (like change in volume due to change in moisture content, micro-cracking and creep due to non-uniform thermal stresses and chemical reactions that causes dehydration and conversion) (Naus, 2006) .

It can be concluded from results present in the literature that main factors that influence the CTE of concrete can be divided into following three main groups.

a) Aggregate type and content
b) Temperature
c) Moisture content

(a) ***Aggregate Type and Content***

70-80% volume of concrete consists of coarse and fine aggregates whereas 2/3 volume of aggregates consists of coarse aggregate (Pereira et al., 2009). Therefore, coarse aggregate is the major factor that affects the CTE of concrete (Naik et al., 2010). Thermal expansion of concrete is a combination of the shrinkage of cement paste at elevated temperature due to dehydration and expansion of aggregates. The expansion of aggregates is predominant and is the main reason of the positive slope of thermal expansion-temperature curve (Cruz & Gillen, 1980; Harmathy & Allen, 1973).

The type of aggregate is the main factor affecting thermal strain. Coarse aggregate fraction plays an important role in thermal strain, as it is the major portion of concrete (Naus, 2010; Nielsen, 2003; Schneider & Kassel, 1985). Therefore, cracks in mass concrete can be prevented by using the coarse aggregate with lower CTE (Khoury, 2006; Kodur & Sultan, 2003; Naus, 2006; Weigler et al., 1972). Thermal expansion of concrete is also affected by quartz content (Harmathy & Allen, 1973). Aggregates with smaller amount of silica (limestone) have the lowest CTE (Naus, 2010; Nielsen, 2003). By changing the type of aggregate and keeping the aggregate content constant, free thermal strains can be varied (Khoury et al., 1985). Free thermal strains are found to be different for siliceous and basaltic gravel aggregates. As compare to coarse aggregate type, the type of cement has no significant effect on free thermal strain. At temperatures above 550°C, higher quartz content of sand causes a larger expansion of concrete. Concrete made with quartz containing aggregates expands significantly at 573°C owing to the α to β inversion of quartz (Cruz & Gillen, 1980; Khoury et al., 1985; Kodur & Sultan, 2003; Takeuchi et al., 1993; Uygunoğlu & Topçu, 2009; Weigler et al., 1972). In case of carbonate aggregates, the thermal expansion increases rapidly at 500°C due to the presence of dolomite. However, due to complete deformation of crystal structure of cement paste, thermal strain decreases suddenly at 850°C and above. In case of plain concrete, due to shrinkage and dehydration, the thermal expansion decreases at 800°C and above. As thermal expansion of limestone aggregate is more than basalt aggregate, thermal strain causes greater expansion in limestone aggregate concretes (Khoury, 2006). However, due to its fine crystalline structure, basaltic aggregate concrete has lower thermal expansion than siliceous aggregate.

(b) ***Temperature***

Many researchers have demonstrated that thermal expansion of concrete is a non-linear function of temperature and increases with increase in temperature (Abrams, 1979; Khoury et al., 1985; Neville & Brooks, 1987; Bekoe, 2008; Schneider & Kassel, 1985; Takeuchi et al., 1993; Weigler et al., 1972). In ASCE (1992), the CTE of concrete at 20°C is given as $6.16x10^{-6}$/°C, and increasing to 10.88×10^{-6}/°C.

(c) ***Moisture Content***

At temperature, lower than 200°C, the moisture content starts affecting the thermal expansion of concrete as both free and bonded water has vanished (Naus, 2010; Naus, 2006; Schneider & Kassel, 1985; Takeuchi et al., 1993; Weigler et al., 1972). The peak rate of moisture loss and minimum thermal strain occurs at temperature range between 150-200 °C (Khoury, 2006; Kodur & Sultan, 2003). Partially dry concrete samples have highest thermal expansion followed by oven dried concrete and is minimum for saturated concrete (Khoury et al., 1985; Nielsen, 2003; Bekoe, 2008; Takeuchi et al., 1993), due to drying shrinkage which results in reduction of overall expansion. The difference between the maximum value and minimum value is almost 15%. According to Nielsen (2003), the difference is caused by two components, true thermal coefficient and hydrothermal expansion co-efficient. True thermal co-efficient is caused by the movement of molecules with in the paste. Hygro-thermal co-efficient is caused by the increase internal water vapor pressure at elevated temperature. No hygro-thermal expansion occurs in saturated and totally dry samples as there is no change in water vapor pressure. However, in concrete the of hygro-thermal expansion is smaller as compared to cement paste.

2.4.5 Stress-Strain Curve

Stress-strain of concrete is different for elevated and ambient temperature. By increasing temperature, the modulus of elasticity decreases. Before reaching to peak load, due to decrease in modulus of elasticity, concrete becomes weaker at elevated temperature. The descending branch after the peak load is bigger at elevated temperature than ambient temperature. Hence, concrete at elevated temperature has higher ultimate strain than at ambient temperature (Castillo, 1987; Shi et al., 2002; Weigler et al., 1972).

As mentioned earlier, the type of aggregate is the most influential factor that affects the behavior of concrete at elevated temperatures. From various experiments, it is concluded that the performance of siliceous aggregate concrete is poor than carbonate aggregate concrete (Abrams, 1971; Cheng et al., 2004). Another important factor which affects the performance of concrete at elevated temperature is the moisture content (Bertero & Polivka, 1972; Castillo, 1987; Cheng et al., 2004; Yong et al., 2009; Lankard et al., 1971; Phan, 1996).

Some researchers concluded that high strength concrete is more prone to strength loss at high temperatures than normal-strength concrete. This is because of the shrinkage of cement paste and expansion of aggregates at higher temperatures. The shrinkage of cement pastes and expansion of aggregates causes loss of bond. That's why, in lean mixes the internal stresses developed are smaller and results in lower strength loss. As the destruction of cement paste is temperature dependent but is more considerable in high strength concrete as compare to normal strength concrete. There are two main reasons for this. First, in case of high strength concrete (HSC), the cement paste carries higher loads i.e., homogeneous stress distribution between cement paste and aggregate. As cement paste in high strength concrete is thicker than that of normal strength concrete, it dries slowly at elevated temperatures and hence drying hardening does not occur in high strength concrete.

The second reason is the contribution of absorbed water at lower temperatures of 100-300°C. When high density concrete is saturated with water, most of the water is adsorbed between the cement paste particles and little water is filled in capillary pores resulting in higher loss of strength. Both actions explained above are causing higher strength loss in high strength concrete than normal strength concrete. Due to the loss of water, high strength concrete is more vulnerable to spalling (Castillo, 1987; Cheng et al., 2004; Diederichs et al., 1988; Phan, 1996). It is worth mentioning here that concrete with a compressive strength higher than 55 MPa is defined as HSC. HSC is further divided into three broad classes depending on its strength. Concrete with a compressive strength between 55 and 60MPa is Class 1, with 70 and 80 MPa is class 2 while with 90 MPa compressive strength is class 3.

HSC losses significant amount of strength in the temperature range between 100 and 200°C. During this stage, the process of water removal begins. Adsorbed water and moisture spread to the surface of concrete section during this stage, influencing the internal forces and thus reducing the overall strength. Hence, higher the initial strength of concrete, the greater its loss of strength in fire. However, concrete recovers it strength with further increase in temperature due to the hardening of cement gel. With the removal of adsorbed moisture, the forces between the gel particles also increases. The porosity of concrete is the main factor in determining the temperature of the removal of adsorbed water. At 400°C and above, due to the dehydration of cement gel and its disintegration, HSC loses its compressive strength rapidly. As aggregates expands and paste contracts at elevated temperatures, the bond between paste and aggregate becomes weaker resulting in the reduction of compressive strength of concrete (Castillo, 1987; Yong et al., 2009).

The condition of concrete at the time of testing also affects the residual strength of concrete. Concrete tested in hot state gives higher compressive strength than tis residual compressive strength due to absorption of moisture from the surrounding atmosphere. This kind of observations are also made when concrete is tested at different cooling rates and states. The hot specimens contain more evaporable water at the time of testing than colder specimens (Abrams, 1971; Bamonte & Gambarova, 2012; Sarshar & Khoury, 1993). Furthermore, the hot-specimens gives higher compressive strength when tested with an applied load as compare to tested with no load. This is because when compressive stress is applied at elevated temperature during testing, the propagation of the cracks development gets slower. In case of unstressed specimens, this propagation is free (Abrams, 1971; Castillo, 1987; Fu et al., 2005; Phan, 1996; U Schneider, 1976).

Both normal and oil-palm boiler clinker concrete (OPBC) is used as infill in hollow steel tubes in this study. As there are no studies reported to date on the performance of OPBC at elevated temperature, only the ambient temperature studies are presented in the following section. Furthermore, a lot of studies are reported for OPB as partial/full replacement of fine aggregate, however, little research is performed on the concrete having OPB replaced completely with coarse aggregate.

2.5 Properties of OPBC at Ambient Temperature

2.5.1 Density

To check the density of OPBC and compare it with normal and light-weight aggregate in plastic state, Abdullahi et al. (2008) performed experimental tests. The author reported that the density of OPBC is in the range of 1900 – 1970 kg/m^3. However, the density is affected by several factors including the w/c ratio and mix proportions of concrete. The author also reported that fresh density of OPBC is 200-400 kg/m^3 more than saturated density of concrete due to the water absorption of aggregate. Various researchers reported the density of hardened OPBC to be in the range of 1440-1850 kg/m^3, when OPB was replaced as fine and coarse aggregate (Abdullahi et al., 2008; Kanadasan & Razak, 2014; Mohammed et al., 2014; Mohammed et al., 2011, 2013). However, when only coarse aggregate is replaced by OPB, the density was in the range of 1850-2100 kg/m^3 (Mannan & Neglo, 2010). Furthermore, the density of OPBC tends to increase by 1-4%, when 10% of cement is replaced by fly ash (Ahmad et al., 2007).

2.5.2 Mechanical Properties

Zakaria (1986) compared the compressive strength of concrete of normal concrete and OPBC concrete. Only coarse aggregate was replaced by OPBC aggregate. Natural sand was used as fine aggregate in all samples. The author kept the range of w/c ratio in the range of 0.7 and 1. The author achieved the compressive strength of 15-28 MPa for OPBC. The lower strength achievement was due to the use of higher w/c ratio. The research was continued by keeping the aggregate ratio same with lesser w/c ratio (Mannan & Neglo, 2010). The authors achieved higher strength of concrete ranging from 27 to 36 MPa.

Zakaria (1986) reported that modulus of rupture of OPBC is approximately in the range of 3-5 MPa, or 15-20% of its compressive strength. (Ahmad et al., 2007) reported performed experimental study to study the effect of 10% cement replacement with fly ash on the modulus of rupture of OPBC. Only coarse aggregate was replaced with OPC aggregate. The author concluded that addition of fly ash results in 15% reduction of modulus of rupture. Furthermore, researchers reported that modulus of rupture of OPBC depends on the cement content and aggregate to binder ratio increased (Mohammed et al., 2011, 2013).

Zakaria (1986) conducted experimental tests to study the effect of replacement of coarse aggregate with OPC on tensile strength of concrete. The authors reported that tensile strength of concrete reduces up to 10% when OPC is replaced with natural aggregate. However, these results were only valid for w/c ratio 0.20-0.60. Furthermore, the tensile strength varies with the cement content and w/c ratio. (Mohammed et al., 2011, 2013) reported the tensile strength of OPBC when 10% cement is replaced with fly ash.

The author observed increased in tensile strength when compared with zero fly ash concrete.

The modulus of elasticity of the concrete depends upon the moduli of elasticity of its constituents and their quantities by volume in the concrete; its value is reduced when natural aggregates were replaced by waste aggregates (Neville, 2008). Only two studies are found in the literature on finding experimentally the modulus of elasticity of OPBC and is reported by the same author (Mohammed et al., 2011, 2013). The author used OPC as replacement of fine and coarse aggregate and reported the modulus of elasticity in the range of 9-27 GPa. The author concluded that modulus of elasticity of OPBC varies with different w/c ratio and natural aggregate replacement ratio.

2.6 Test Methods

The response of steel structural elements to elevated temperatures is usually studied by conducting either steady-state test or transient-state test.

2.6.1 Steady State Test

In steady state tests, the sample is heated up to a specific temperature and when the temperature becomes stable, the sample is loaded gradually till failure. The heating rate in steady state test is normally in 10-50°C/min range; however, the temperature is kept constant during the application of load till failure. The stress-strain relationship at a particular temperature are obtained directly while other mechanical properties are obtained from stress-strain curves.

2.6.2 Transient State Test

In this type of test, the sample is loaded to some stress level by applying load statically. Thereafter, the temperature is increased gradually by using different standard fire time-temperature curves recommended by different testing methods, until failure. The heating rate usually varies from 5°C/min to 50°C/min. As a result, a temperature-strain curve is obtained directly from the test. The stress-strain curves are then obtained at different elevated temperatures by the methods described in (Maljaars et al., 2009; Outinen, 2007). The other mechanical properties (yield strength and modulus of elasticity) are obtained from the stress-strain curves. Although, steady state test is more common as it is easier to perform but, temperature would always rise in actual fire scenario. Hence, the transient state test is more accurate in predicting the response of a specimen under fire (Chen & Young, 2006). Kay et al.(1996) compared results from transient state test and steady state tests and concluded that strength of steel obtained by steady state test was higher than the transient state test.

2.7 Standard Fire Time-Temperature Curve

All building codes uses standard fire time-temperature curves for rating the performance of building materials, designing fire protection as well as selecting the size of structural members through fire resistance ratings (in mins/hours). The standard fire time-temperature curves given in different codes are shown in Figure 2.1. Of all the standard time-temperature curves, ISO 834 is mostly used across the globe.

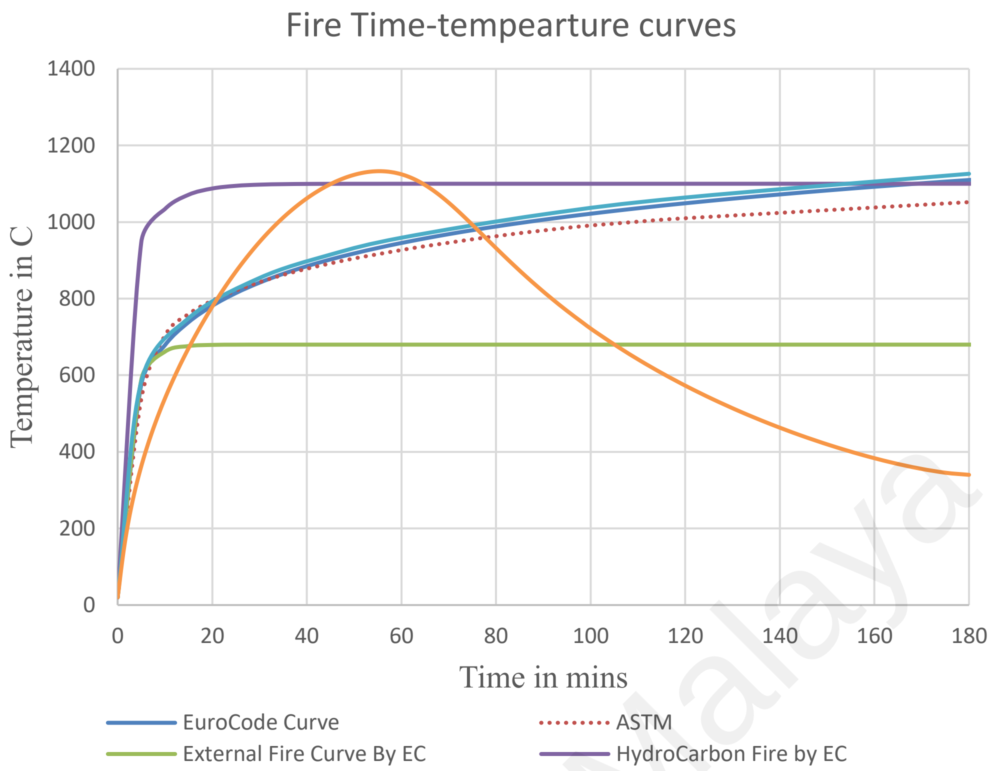

Figure 2.1: Time-temperature curves given by different codes vs real fire

All standard fire tests have the primary purpose of comparing the performance of building materials and small-scale members, even if they are not a good representative of real fires. The standard fire tests are considered different from real fire in terms of rise/fall in temperature with time, structural behavior and of fire loading (uniform vs. non-uniform). In terms of rise/fall in temperature with time, in real fire, the temperature increases up to certain level and then becomes constant followed by the decrease in temperature also known as growth, full development and decay phases while in most of the patterns given by different standard testing procedures, the temperature keeps on increasing until the failure of the member. With respect to structural behavior, the standard fire tests cannot estimate the full scale complex structural behavior of the building including the thermal expansion, large deflections, connection behavior and development of another path load and loss of stability. Finally, in terms of fire loading, in case of real fires the members may be subjected to fire from all the four sides like the case of most of the columns (uniform fire loading), or less than four sides like columns embedded in walls (non-uniform fire loading). However, furnace tests usually involve short-span samples, which may be difficult for extrapolation to full scale. It must be noted that non-uniform distribution of temperature can lead to non-uniform distribution of mechanical properties and affects the pre-buckling stresses in axially loaded members (Bronzova & Garifullin, 2016; Cheng, 2015; Cheng, Wu et al., 2014). It is worth mentioning here that from the testing methods used for establishing fire rating, only ASTM E119 puts specific emphasis on restrained and unrestrained end condition for beams, floors and roof assemblies. As most of the research on cold formed steel (CFS) members in fire is conducted on uniformly distributed temperature, hence, in this paper only uniform fire studies are considered. Moreover, emphasis is put on the latest research mainly from 2010 and onwards. Experimental and numerical studies regarding the performance of CFS beams and columns at elevated temperature are discussed extensively in the subsequent sections.

2.8 Properties of CFS Members at Elevated Temperature

2.8.1 Beams

CFS beams are progressively being utilized as load bearing components because of obvious advantages such as high strength-to-weight ratios and adaptability of profiles Figure 2.2. However, because of their low torsional stiffness and slenderness, CFS beams are substantially more vulnerable to instability failures (Local, distortional and lateral-torsional buckling) even at ambient temperatures even when protected by fire proof coatings (Chen et al., 2015; Kodur & Arablouei, 2015; Mirmomeni et al., 2016; Sinaie et al., 2014). The thin walled structural steel members subjected to bending may possibly fail by both local and global buckling modes. The local buckling mode occur due to compression of thin plates in the cross section while the lateral–torsional buckling, which is global buckling mode for members subjected to bending is characterized by rigid body movements of the whole member i.e. individual cross-sections rotate and translate but do not distort in shape (Ghafoori & Motavalli, 2015; Hancock, 1997). Distortional buckling, also known as "stiffener buckling" or "local-torsional buckling", is a mode characterized by rotation of the flange at the flange/web junction in members with edge stiffened elements. Compared to local buckling, lateral-torsional buckling and the distortional buckling is a relatively new concept, have a very short history and occur only in cold-formed steel sections. In this paper, only lateral-torsional and distortional buckling of beams is studied as they are more common in cold formed steel beams subjected to elevated temperatures. Moreover, based on restrained conditions, we have divided the literature on CFS beams at elevated temperature into two categories. The beams that are tested individually without considering the effect of surrounding structure is discussed under the unrestrained category while the studies on beams in which the effect of surrounding structures is discussed under restrained category. It must be noted that most of the research has been done by performing testing on un-restrained member whereas very few studies have been performed on restrained members.

Figure 2.2: CFS profiles working as flexural elements (girders and purlins) (Shedquarters, 2009)

2.8.1.1 Un-restrained Members

Lateral–torsional buckling behavior of both hot-rolled and cold-formed steel beams is complicated at ambient and elevated temperatures. Both experimental (Bilotta et al., 2016; Nadjai et al., 2016; Real et al., 2003) and numerical (Bailey et al., 1996; Dharma & Tan, 2007; Real & Franssen, 2000; Real & Franssen, 2001; Real et al., 2004; Real & Franssen, 1999; Yin & Wang, 2003) investigations have been done on lateral-torsional buckling behavior of stainless steel beams (Lopes et al., 2006; Real et al., 2008; Berg & Bredenkamp, 1994) and hot-rolled steel members in fire. In case of cold-formed steel, few experimental and numerical investigations are reported on this topic at ambient temperature (Li, 2004; Yang et al., 2015; Yu & Schafer, 2006). For example, the lateral-torsional buckling behavior of CFS beams at ambient temperature has been studied both numerically and experimentally by Kankanamge & Mahendran (2012a). As far as the performance of cold-formed steel at elevated temperature is concerned, the researchers have numerically investigated the lateral-torsional buckling performance at elevated temperatures (Dolamune Kankanamge & Mahendran, 2008; Kankanamge, 2010; Kankanamge & Mahendran, 2011, 2012; Kesawan et al., 2015).

Finite element analysis was performed for studying the structural behavior of CFS beams at elevated temperatures under steady-state method (Dolamune Kankanamge & Mahendran, 2008; Kankanamge, 2010; Kankanamge & Mahendran, 2011, 2012). For this purpose, a CFS lipped channel beam (LCB) under uniform bending moment was considered with idealized simply supported boundary conditions at supports, allowing warping displacements as well as both major and minor rotations whereas preventing in-plane and out-of-plane twisting and translations. For ambient temperature, eight tests were also conducted. The main parameters considered were thickness of steel (1.90 and 1.95 mm), grade of steel (G250 and G450) and span of the beam (1500, 2000, 2500 and 2900 mm). For parametric studies, 9 LCB cross-sections were selected with different thicknesses, different spans and different grades of steel at seven different temperatures varying from 20 to 700°C. Moreover, all the beams were loaded at two quarter points of the beam. By comparing the results of the above mentioned finite element studies with the design codes like EN1993-1-2(Eurocode, 1993) and with AS/NZS4600 (AS/NZS, 2005), it was observed that the design method recommended in EN1993 was accurate for very slender members, however, it was over conservative for most of the non-slender members. Because of residual stresses and initial imperfections, the ultimate moment capacities of beams with intermediate slenderness decreased considerably relative to the elastic buckling moment capacities. However, as the beam slenderness increased, the beam capacity approached elastic buckling moment capacity. It was also found that the moment capacity data for intermediate slenderness were very scattered and hence separate buckling curves should be used for different high temperatures so as to get accurate design predictions. Furthermore, in EN1993-1-2, the recommended temperature limit (350 °C) for CFS beams in fire was found to be over conservative. For similar beams and boundary conditions, the authors in (Lu et al., 2007; Outinen, 2007; Outinen et al., 2001; Outinen & Mäkeläinen, 2004) suggested temperature limit of 700°C.

As most of the CFS members are exposed to distortional failure, the present design specifications included special provisions like strength curves for the design of CFS beams and columns against distortional buckling failures. However, all such strength curves for CFS members were developed and used by researchers at ambient temperature (Borges & Camotim, 2010; Haidarali & Nethercot, 2012; Hancock et al., 1994; Kwon & Hancock, 1992; Yu & Schafer, 2006) and very limited research has been carried out to investigate that either such curves (with or without slight modifications) can be used at elevated temperatures or not. Distortional failure of cold-formed steel lipped channel beams under ambient and elevated temperatures was studied numerically by Landesmann and Camotim (2016). Three different end conditions for simply supported beam, i.e. free warping and rotation, prevented warping and rotation as well as free rotation and prevented warping, were considered. The details of end conditions are given in Table 2.1. Using steady-state method and with four different cross-sections of lipped channel beam, nine different temperatures in the range of 100-800°C were considered. It was concluded that both cross-sectional dimensions and end conditions significantly affected the failure moment and distortional post buckling response of CFS lipped channel beams. Also, due to significant stress-strain non-linearity curve at temperatures higher than 300°C, the current DSM did not predict adequately the failure moments of CFS beams. However, the above research focused on simply-supported lipped channel beams with three types of end conditions. Hence it is recommended that research should be carried out with different boundary conditions and cross-sectional dimensions. Moreover, experimental investigations should be carried out using different models available in literature (Chen & Young, 2007; Kankanamge & Mahendran, 2011; Ranawaka & Mahendran, 2009b).

Table 2.1: End support conditions for the simply supported beams analysed

Support conditions	**F**	**PF**	**P**
Wrapping	Free	Prevented	Prevented
Minor-axis flexural rotations	Free	Free	Prevented

2.8.1.2 Restrained Members

One of the important shortcomings of standard fire tests is that they are carried on individual structural members instead of complete structural assemblies. Also, for a member analysis, Part 1.2 of Eurocode 3 (Eurocode, 1993) states that "the internal forces and moments at supports and ends of members applicable at time *t*=0 may be assumed to remain unchanged throughout the fire exposure". As a result, the structural interactions are difficult to evaluate. Moreover, the Cardington fire tests (Newman, 1999), Broadgate fire (Weller, 1992) and some theoretical analysis of these tests (Bailey, 1998; Bailey, 2000; Wang & Moore, 1994) have shown that there exists a strong interactions between beams, columns and slabs. Hence, it can be deduced that in comparison to un-strained member, individual restrained steel members tested in fire is an effective and appropriate way.

Various studies were conducted on compression members (restrained) made up of hot-rolled steel members (Correia et al., 2013; Franssen, 2000; Valente & Neves, 1999). However, members' restraintment is more relevant to horizontal members like slabs and beams, i.e., the members which are not designed for compressive forces at room temperature. Some researchers reported that axial restraint is not so severe phenomena

(Correia et al., 2013; Franssen, 2000) however, others found axial restraint is more important (Ali & Connor, 2001; Valente & Neves, 1999).

Experimental and numerical investigations were carried out to evaluate the structural behavior of thermally, axially and rotationally restrained CFS beams both at ambient temperature (Rodrigues, et al., 2013a; 2013b) and at elevated temperature (Rodrigues, & Silva, 2013; Laím & Rodrigues, 2016; Laím et al., 2014, 2015; 2016). In total, 54 fire tests were performed on six different sections of CFS beams including C-, Lipped I-, R- and 2R- (Figure 2.3) (Laím et al., 2014; 2015; 2016; Rodrigues, et al., 2013a; 2013b). Out of 54 samples, 18 were just simply supported beams, other 18 were the same beams but with restrained thermal elongation while the remaining 18 were beams with axial and rotational restraint. One of the reasons for this great number of tests was that three repetitions were considered for each type of beam and for each series of fire tests. The overall length of the beam was kept as 3.6m with span length of 3.0m while transient-state method was used during heating of beam. From these researches and depending on the cross-sectional shape of beams, it was concluded that the structural response of beams in fire is completely different with web stiffeners. At elevated temperatures, the beams without axial restraints and web stiffeners showed the best behavior while the behavior of close or built-up sections were found to be better than the open sections. The geometric imperfections reduced up to 20% of the critical temperature of CFS beams whereas hollow beams showed up to 50% increase in fire resistance time as compared to open CFS beams. The critical temperature of all CFS beams was up to 700°C, which was much higher than recommended by EN1993-1-2 (2005). It was shown that the critical temperature is greatly affected by the stiffness of the surrounding structures i.e. beams and the relation between there stiffness. Amongst all sections used in this experimental work, R and 2R sections showed the best structural response at elevated temperature.

Hence, to increase the use and efficiency of CFS beams, accurate design guidelines are the need of time.

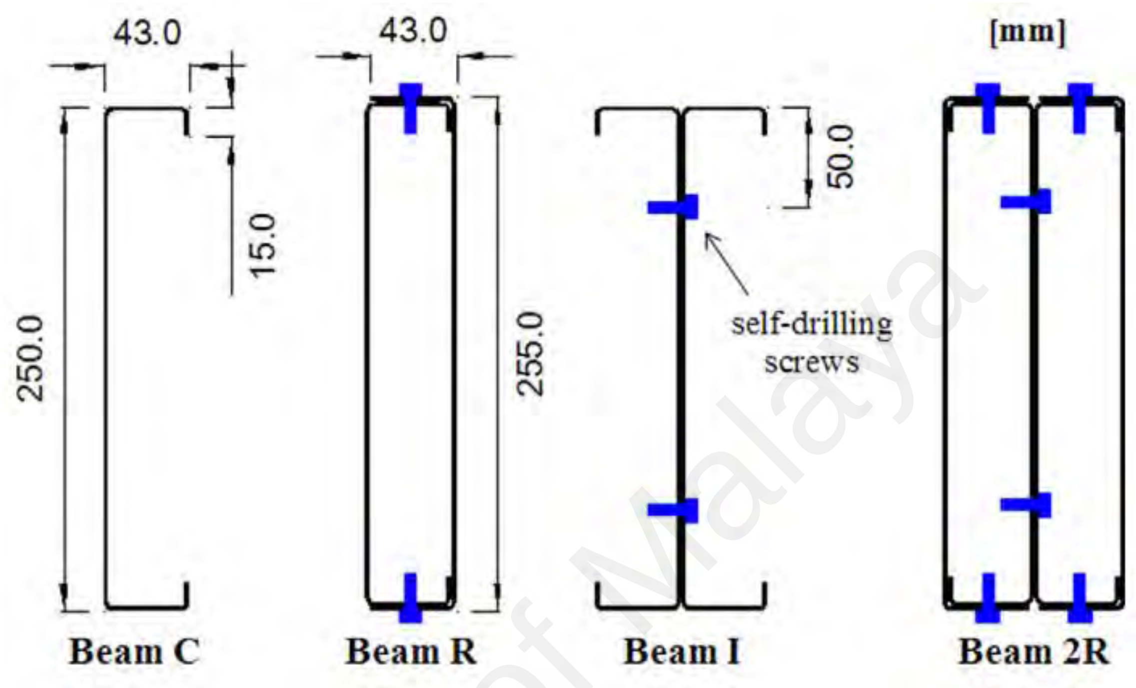

Figure 2.3: Scheme of the cross-sections of the tested beams by Luis

2.8.2 Columns

Compared to beams, CFS columns (Figure 2.4) under elevated temperature have been studied relatively more. Structural behaviors of columns like modal interactions, altered buckling modes, yielding and time-temperature dependence are like that of beams. Existing research shows that fire resistance for columns and beams is less than 30 minutes (Han et al., 2014; Wastney, 2002). CFS columns are susceptible to three main buckling modes, a) local, b) Euler (flexural or flexural-torsional) and c) distortional buckling (Cava et al., 2016; Schafer, 2002). Short columns mostly fail in local and distortional buckling while long columns commonly fail in flexure and flexural-torsional buckling.

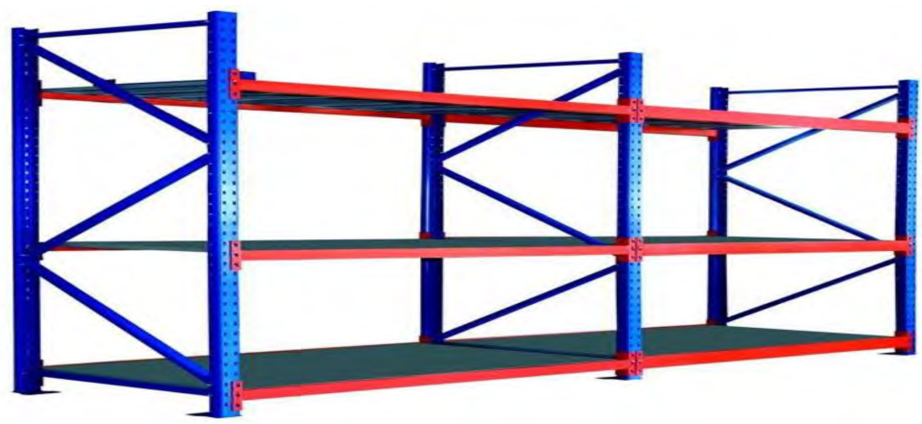

Figure 2.4: CFS members used as pallet storage racks (Rack, 2016)

2.8.2.1 Un-restrained Members

The flexural-torsional buckling of CFS compression members both at ambient and elevated temperature was experimentally investigated by Heva (2009). The author performed 39 tests consisting of different lengths (2800mm and 1800mm), thicknesses (0.95mm, 1.90mm, 1.95mm) and grades of steel (G550, G250, G450) for both lipped and un-lipped channel respectively. The furnace and loading setup used in these experiments is shown in Figure 2.5. By using steady-state method, the ultimate load bearing capacity of the short columns were found at different temperatures (20, 100, 200, 300, 400, 500, 600 and 700℃) and the results were than compared with different codes. The author found that the present design rules for both ambient and elevated temperatures were conservative, especially over conservative for elevated temperatures. Hence, Heva and Mahendran (2013) suggested important guidelines for CFS column designs at elevated temperature so as to overcome existing overdesign. Based on these guidelines, Gunalan et al. (2014a; 2014b) performed detailed parametric studies for columns having lengths varying from 1500 to 4000 mm with different boundary conditions (pin supports, fix supports) for variety of lengths (1500-4000 mm), thickness (0.95-1.95mm), grade of steel (G450, G250, G450) and temperature (100-700 °C). By comparing the results of FEA with Euro Code 1.3, it was found that the current design rules are more precise for pin ended columns while less accurate for fixed ended columns. Thus, it was recommended to use suitable buckling curves for fixed ended columns. It is worth mentioning here that further research is required to include the effects of non-linear characteristics of stress-strain curves within the guidelines of AISI S100 and AS/NZ 4600.

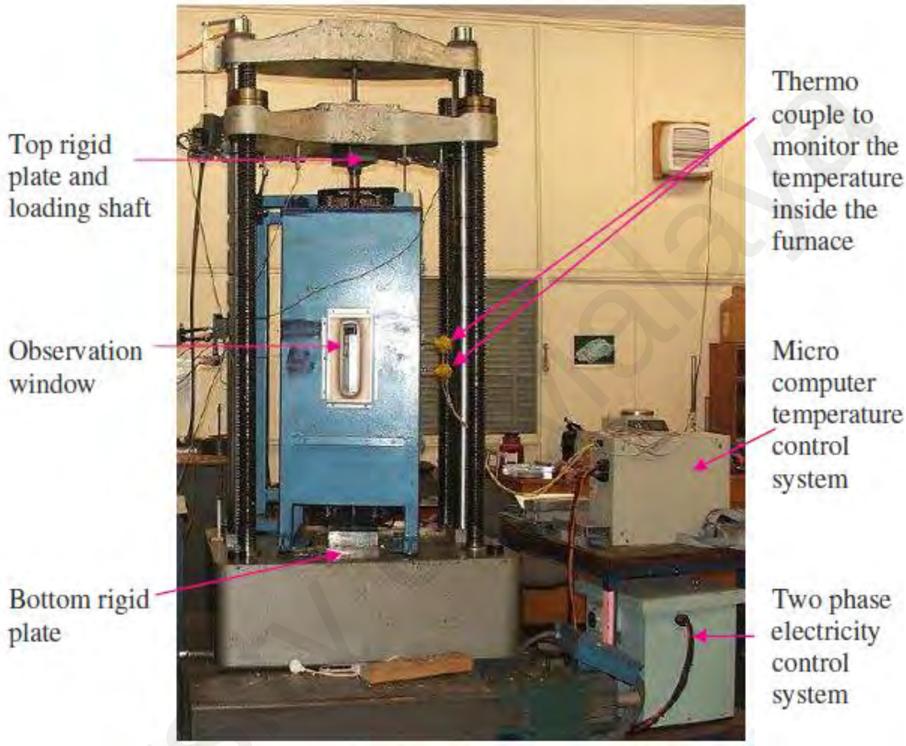

Figure 2.5: Electric Furnace and loading setup (Heva, 2009)

In order to study local buckling of CFS compression members both at room temperature and in fire, Gunalan et al. (2015) performed 27 tests in the structural laboratory of Queensland University of Technology. Lipped and un-lipped channels were tested at seven different elevated temperatures (up to 700°C) using steady-state method. The length of the specimens was selected as the multiple of half wave lengths for local buckling, which was calculated by using CUFSM. The test results were then compared with the available design standards including American, Australian, British and European steel standards and DSM (Gunalan et al., 2015; Gunalan & Mahendran, 2013a, 2013b, 2013c). The comparison showed that current ambient temperature rules can be used confidently at elevated temperature with suggested reduced mechanical properties. The DSM predictions were closest to test results but un-conservative for some sections. Furthermore, the author suggested that the current design rules can further be improved by including the non-linear stress-strain characteristics at high temperatures.

To study the distortional and local buckling behavior of CFS columns with and without initial imperfections, Feng et al. (2003) performed 52 tests (both at ambient and elevated temperature) followed by numerical studies on cold-formed lipped and un-lipped channel compression members. The elevated temperature tests were carried out under steady-state condition and without thermal restraints. Initial imperfections were considered in both experimental and numerical studies. The buckling of lipped channel with and without hole at ambient temperature is shown in Figure 2.6. Test results showed that depending on the initial imperfections, the failure modes of nominally identical columns can be different both at ambient and elevated temperatures. Moreover, regardless of the difference in the failure modes, the ultimate buckling loads of nominally identical columns were almost same.

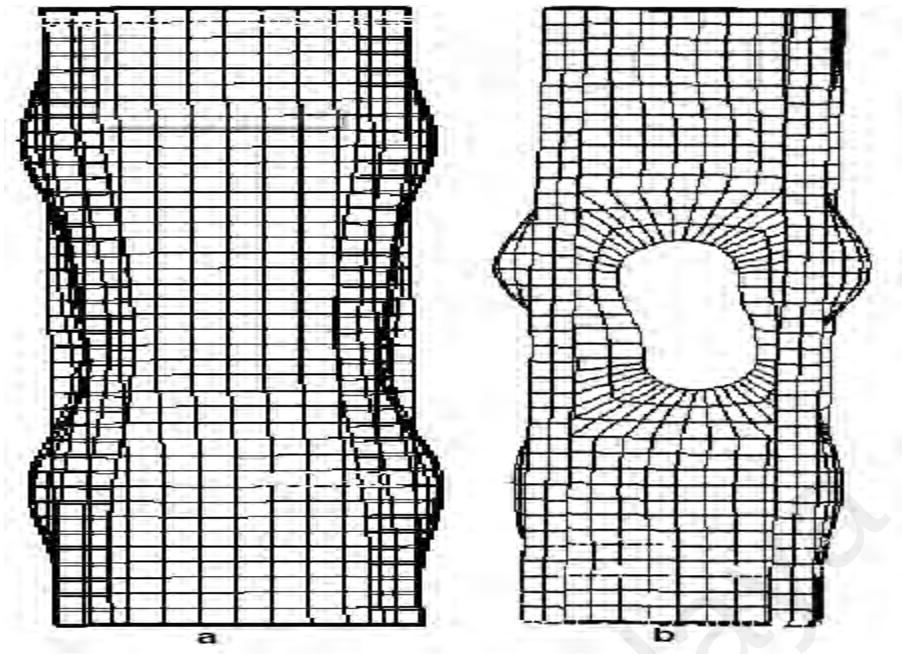

Figure 2.6: a) Lipped channel 100×56×15×2 without hole b) Lipped channel 100×56×15×2 with hole (Feng et al., 2003)

Ranawaka & Mahendran (2009a, 2010) performed series of experiments and carried out numerical modeling by considering two grades of steel (G250 and G550), three thicknesses (0.60,0.80 and 0.95mm) and two lipped C-sections (with and without additional lips). The difference between lipped C-sections with and without additional lips is shown in Figure 2.7. The compression members were analyzed at six different temperatures varying from 20 to 800°C with support condition selected as fixed. Overall, 72 cases were studied by using steady-state method. The FEM model included initial geometric imperfections, residual stresses and mechanical properties as a function of temperature. The comparison of FEA and experimental failure modes is shown in Figure 2.8. The authors concluded that the design methods in current design codes including DSM were accurate at room temperature however, further research was recommended for the elevated temperatures.

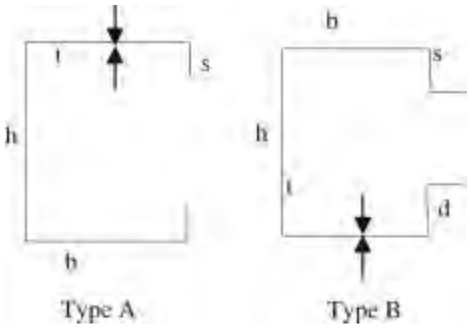

Figure 2.7: Type A C-Section without additional lips, Type B C-Section with additional lips(Ranawaka & Mahendran, 2009a)

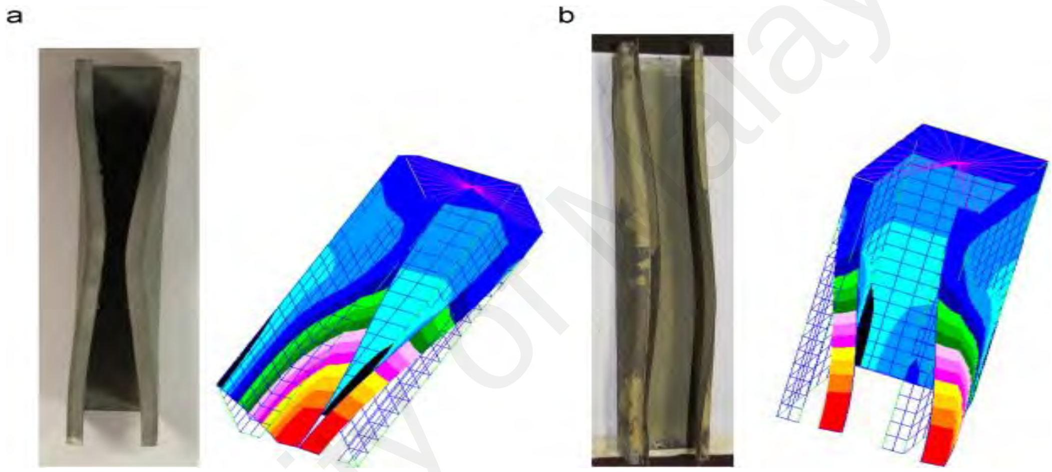

Figure 2.8: Comparison of other distortional failure modes from experiments and FEA. (a) Both flanges moving inward. (b) One flange moving outward while other one moving inward (Ranawaka & Mahendran, 2010)

2.8.2.2 Restrained Members

Most of the experimental studies on CFS short columns at elevated temperatures have been performed for evaluating their buckling behavior (Outinen & Myllymäki, 1995; Han et al., 2003; Heva, 2009; Lee, 2004; Ranawaka & Mahendran, 2009a). Also, for this purpose, different numerical methods (Feng et al., 2003, 2004; Ranawaka & Mahendran, 2006) have been used. However, in case of built-up cross sections, which are most commonly used in building construction, limited research was done at ambient and elevated temperatures (Georgieva et al., 2012; Stone & LaBoube, 2005). Moreover, in most studies, the effect of surrounding structures on the buckling behavior of columns was not considered (Outinen & Myllymäki, 1995; Han et al., 2003; Heva, 2009; Lee, 2004; Ranawaka & Mahendran, 2009a).

An experimental investigation was recently carried out at Coimbra University, Portugal by Craveiro et al. (2014) so as to study the influence of the thermal restraints or effect of surrounding structure on the structural behavior of single lipped channel and built-up cross-section (double lipped channel) compression members both at ambient and elevated temperatures by implementing transient-state method. 48 experiments were performed by using standard fire curve ISO-834 (Standard, 1999) by keeping the load levels, stiffness of the surrounding structure, type of cross-section and thermal restraints as variables. The experimental setup consisted of 3D restraining steel frame adaptable for various level of stiffness and a 2D reaction steel frame. According to the test results (Almeida et al., 2012; Craveiro et al., 1993; 2015), for higher initial load levels and stiffness, the effect of the level of axial and rotational restraints on critical temperatures were found to be higher. The distortional buckling was more clearly visible in the semi-rigid end support condition. The limiting temperature predicted by Eurocode 1.3 gave accurate values for open and built-up cross-sections but were found to be conservative for lipped channel columns. The authors suggested that further research is needed to find out the optimal cross-section shape for thermal restraint. Moreover, the results showed that C cross-sections are mostly affected by thermal elongation restraints as compared to 2R and I section, and it was recommended that critical temperature should be measured at mid height.

In real life, most of the CFS compression members are protected by insulations and plasterboards, mostly made of gypsum. After an event of fire, the plasterboards can be removed with ease for inspection and identification of damage in compression members. In this scenario, the final decision regarding the use of member must be taken by the structural engineer. In past, the behavior of hot-rolled structural steel studs after the fire event was studied by number of authors including Tide (1998), Dill (1960), Chan (2009) and Kirby et al. (1986). However, very limited research has been done regarding the structural behavior of CFS members after an event of fire. According to the best of author's knowledge, so far there are no standard rules/guidelines available for evaluating CFS members exposed to fire. Due to this, the structural engineers must make some over-conservative decisions while assessing the residual capacities of CFS members affected by fire. Furthermore, the current design standards contain very little information regarding the mechanical properties of CFS members after being exposed to fire.

Gunalan and Mahendran (2014) performed series of experiments followed by numerical modeling by considering different grades of steel (G300, G500 and G550) and three thicknesses (0.95, 1.00 and 1.15mm) for lipped C-section. All specimens were heated to eight different temperatures ((400, 500, 550, 600, 650, 700, 750 and 800 °C) before testing for ultimate capacity. The results of the study are presented in (Gunalan & Mahendran, 2014a, 2014b, 2014c, 2014d). Based on these studies, it was found that the values of mechanical properties (at 300°C) were less than values of mechanical properties determined at ambient temperature. The CFS compression members regained 90% of their initial distortional buckling strength after being exposed to elevated temperatures less than 500°C. After being exposed to 1000°C, the yield strength of CFS members reduced to 40%. The trend in reduction of ultimate capacity was same to that of yield strength reduction. Moreover, the residual compression can be predicted accurately by using the design rules of ambient temperature if the maximum temperature experienced by short or laterally restrained CFS compression member is known (Gunalan &

Mahendran, 2014c). The accuracy of design methods mentioned in current codes was assessed and a detailed review of FEA of thin walled compression members was presented by Ellobody (2013). In addition, some assumptions were also suggested by Ellobody (2013) for performing a consistent FE analysis both at ambient and elevated temperatures.

2.9 Research Gaps

The critical review of the literature on the structural behavior of CFST subjected to flexural load revealed many gaps in the available literature. It was shown that studies conducted so far are few, very limited in scope, with conclusion that are preliminary. These limited studies lack experimental insight into the response of CFST members when used as structural member subjected to a combination of flexural load and elevated temperature. It was also noted that no study of validated FE model has been reported on simulation of the flexural load performance at elevated temperature of CFST member. Some studies have been performed on the CFST columns with small to large eccentricity, but they do not represent the pure flexural performance of CFST. Moreover, most of these limited studies are performed on circular CFST members. The influence of various parameters was not investigated. Furthermore, the mechanical properties of OPBC at elevated temperature under different types of loading and confinement should be studied in detail.

Based on these shortcomings, it is important to investigate the flexural behavior of CFST members both at ambient and elevated temperature. For this purpose, both experimental and numerical studies are needed to be conducted to gain an insight into the effects of various structural and non-structural parameters on the response of CFST member and figure out the key factors accountable for the failure of these members. These insight and understanding are necessary for the development of practical design codes and methods. Unavailability of any study on difference in the performance of CFST at ambient and elevated temperature under flexural loading also necessitates a research to assist designers in choosing a member size and type that has better performance under a flexural load scenario. Two steps should be taken to achieve these objectives. Firstly, an experimental study should be planned and implemented. Secondly, a numerical model should be developed to be validated against the experimental data to provide for a tool to expand the investigation without having to conduct expensive and time-consuming tests. Furthermore, the mechanical properties of OPBC at elevated temperature under different types of loading and confinement should be studied in detail.

CHAPTER 3: METHODOLOGY

3.1 Introduction

This chapter describes an experimental work and numerical work which has been carried out in this study. Details of the experimental investigation, development of FE model and the description of the specimens' preparation are presented. In the first stage, experimental work was conducted at room temperature followed by the FE modeling. In the 2nd stage, by keeping the dimensions same as that of ambient temperature testing, the specimens were tested at elevated temperature. In last, FE modeling for specimens subjected to elevated temperature was performed.

3.2 Experimental Investigation at Ambient Temperature

3.2.1 Test Specimen

A total of 4 CFST beams, which were divided into two groups, were prepared for ambient temperature testing. The specimens filled with normal mix concrete (natural coarse aggregate) were abbreviated as NCFST while the specimens filled with Oil-palm-boiler clinker concrete were abbreviated as OCFST. Furthermore, naming the beams, the first letter indicates the cross-sectional shape of the beam. Hence, RNCFST means the rectangular beam filled with natural aggregate concrete. To get a good comparison, the compressive strength of both types of concrete was kept same. The length of all specimens was kept as 3200 mm while the nominal depth, width and thickness of the steel tube for all the specimens were 200mm, 100mm, and 6mm, respectively. To avoid the local buckling of CFST beams, Depth/thickness ratios of the specimens were kept lower than 52s. The details and dimensions of steel tubes measured by using Vernier caliper are shown in Figure 3.1 (not drawn according to scale) and Table 3.1 respectively.

Table 3.1: Dimensions of tested specimens

Type of infilled concrete	Cross-sectional Shape	Specimen Name	Height, h (mm)	Width, b (mm)	Thickness, t (mm)
OPBC	Rectangular	ROCFST	200.2	100.1	5.99
	Square	SOCFST	150.4	150.1	6.01
NMC	Rectangular	RNCFST	199.7	99.9	5.99
	Square	SNCFST	150.3	150.2	6.02

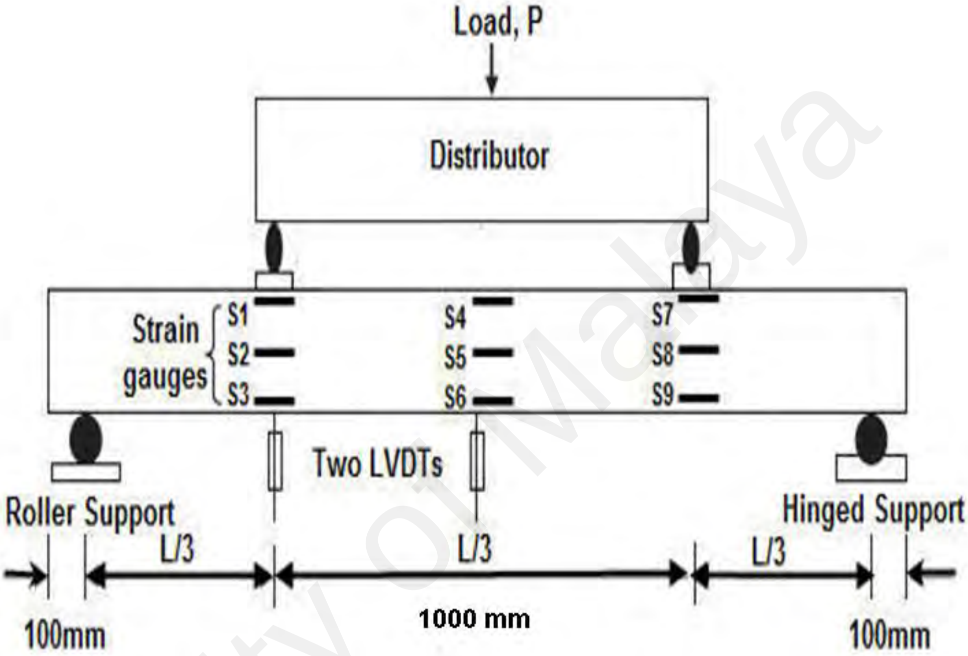

Figure 3.1: Test setup and location of Strain gauges

3.2.2 Material Properties and Mix Proportions

3.2.2.1 Steel

The steel tubes in all specimens were cold formed from steel plates by press bending and seam welding. The tubes were provided from a 12m length of hollow rectangular steel tube. Tensile tests were performed on steel coupons obtained from the original tubes. A 0.2% proof stress was adopted for cold-formed steel tubes, as recommended in a previous study (Yang & Han, 2006b). The stress–strain curves for three coupon tests are plotted in Figure 3.2. The measured yield strength, ultimate strength, elastic modulus and maximum elongation were found to be 394 MPa, 458 MPa, 201.3 GPa and 29%, respectively.

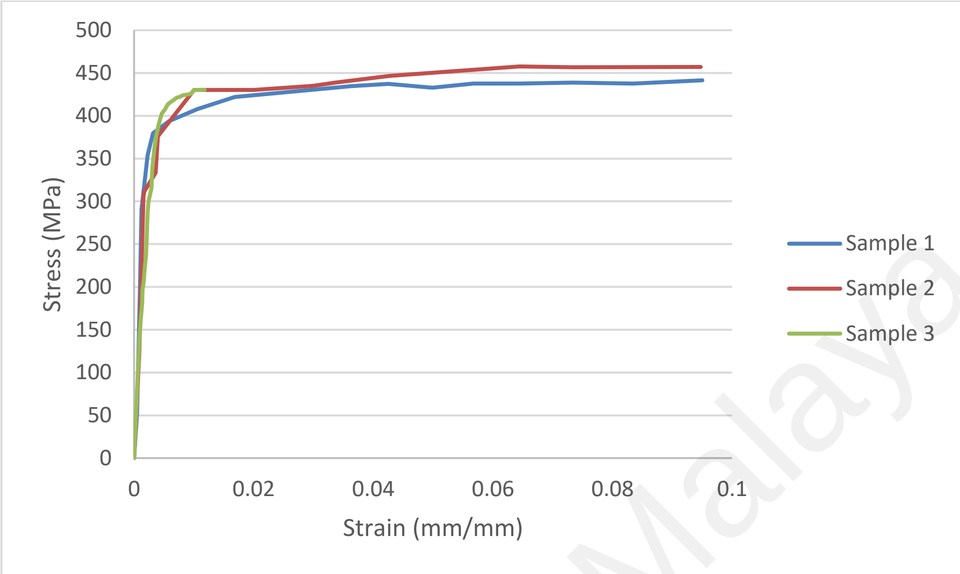

Figure 3.2: Stress–strain curves for tensile coupon tests

3.2.2.2 Concrete

As one of the main aims of this research was to compare the flexural behavior of OCFST with NCFST. For this purpose, two different types of concrete having same compressive strength were prepared by using the pan mixer. The ACI mix design method was used for designing the NMC while the mix design method suggested by Kanadasan & Razak (2014) was used to design the OPBC of required strength. Ordinary Portland Cement (OPC) with a specific gravity of 3.14 g/cm^3 was used for all the mixes. A high range water reducing admixture, Sika viscocrete-2199 was used as it was chloride free in accordance with BS 5075. POC was washed and dried after collecting from the palm oil factory to remove the dust from the raw materials. After crushing the POC using the stone crushing machine, it was then sieved to particle sizes between 12.5 mm and 4.75 mm to be used as coarse aggregate.

The mix proportions and slump of both types of concrete are summarized in Table 3.2 while the details of the physical properties of aggregates are shown in Table 3.3. The compressive strength of concrete was determined by testing 100 mm x 100mm x 100mm cubes while the elastic modulus and stress-strain behavior of concrete was determined by testing concrete cylinders having size of 100mm x 200mm at the age of 28 days. The results are presented in Table 3.4.

Table 3.2: Mix proportions of NMC and OPBC concrete

Mix Type	Cement (kg/m^3)	w/c	SP (%)	Granite CA (kg)	OPBC* (kg)	Sand (kg)	Slump (in)
NMC	440	0.40	1.5	980	--	855	4
OPBC concrete	550	0.35	2	--	980	648	6

*OPBC aggregate was used in saturated surface dry condition in concrete

Table 3.3: Properties of different aggregates

Aggregate	Specific Gravity	Apparent specific gravity	Bulk density (kg/m^3)	Absorption (%)
Granite CA	2.64	2.65	1600	0.32
OPBC	1.80	1.81	782	3.56

Table 3.4: Strength and Modulus of Elasticity at 28 days

Type of Concrete Mix	f'_c at 28 days (MPa)	E_c at 28 Days (MPa)	Density (kg/m^3)
NMC	52	31.2	2398
OPBC	51.2	32	2019

3.2.3 Test Setup and Procedure

All the members were loaded in pure flexural (without any shear and axial load) by applying two-point loads (L/3 distance apart) through spreader beam along constant moment zone. A 600 kN capacity hydraulic jack was used to apply the load to the test specimens while the results were monitored through INSTRON program. All members were subjected to a loading rate of 2 kN/min until failure.

Two linear variable displacement transducers (LVDT) were used to measure the vertical displacement of the beam while a total of 9 strain gauges (S1 to S9) with a 10mm gage length were installed on each specimen to measure the strain in steel tube at different depths. The readings of strain gauges and two LVDTs were recorded at an interval of one second by using Data logger TBS-530. The test setup and detailed location of strain gauges are shown in Figure 3.1.

3.3 Experimental Investigation at Elevated Temperature

3.3.1 Test Plan and Apparatus

The elevated temperature experimental tests on square and rectangular CFST members were conducted at the Heavy Structures Laboratory of the University Malaya, in Malaysia. Figure 3.3 shows different parts of the experimental test setup used in the elevated temperature tests of CFST beams along with labeling of components. The setup consists of one vertical frame (1) and two horizontal "A frame" (2). The vertical 2D frame consists of 4.5m long beam connected with two 6.6m tall columns through 8 M24 grade bolts. An ENERPAC hydraulic jack of 150 kN capacity in compression (3) was installed on the vertical 2d frame (1) and controlled by a hydraulic central unit (4) and beneath this one, a load cell of 100 kN (6) capacity was placed to monitor the applied load during the tests. Beneath the load cell, a stub column (5) was placed to prevent the exposure of hydraulic actuator to elevated temperature and to transfer the load from hydraulic actuator to the beam specimen. The specimen was placed inside the furnace and is supported by two small beams attached to horizontal A-frames, thus simulating simply-supported boundary conditions. For heating of the specimen, a horizontal electric furnace capable of replicating the ISO-834 fire curve (Standard, 1999) was used. The dimensions of the internal chamber of the furnace were 2000mm (L) x 1000mm (W) x1000mm (H) while the length of specimen beam exposed to elevated temperature was 2 meters as shown in Figure 3.4. The experimental program consisted of 4 fire resistance tests, 2 of which were performed on NMC filled CFST (NCFST) while the other 2 were performed on OPBC filled CFST (OCFST). Both NCFST and OCFST samples were further divided into square and rectangular cross-section. The details of experimental program are summarized in Table 3.5, where the investigated parameters included type of infilled concrete and cross-sectional shape of the specimen. The steel ratio is kept constant for all the specimens. The nominal load ratio, n of all the specimens was 0.30. All specimens were labeled so that the types of beams can be easily identified. As an example, the sample ROCFST indicates a fire resistance test on a rectangular OCFST beam.

Figure 3.3: General view of the experimental test setup

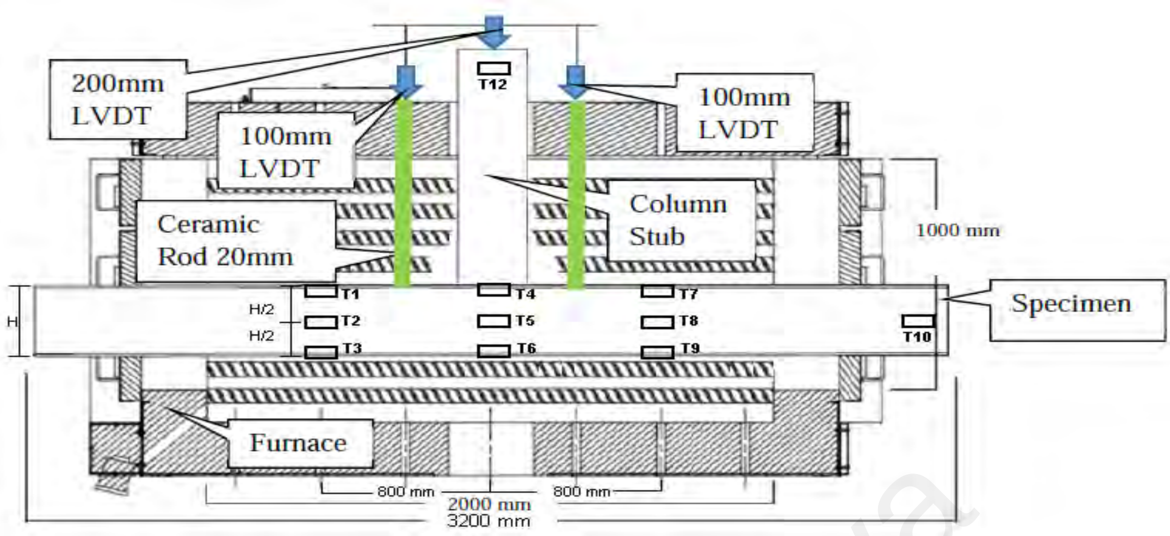

Figure 3.4: Location of thermocouples and side view of experimental setup

Table 3.5: Dimensions of tested specimens

Specimen Name	**Height, H (mm)**	**Width, B (mm)**	**Thickness, t (mm)**	**Load Ratio, n**	**Cross-Sectional shape**	**Type of concrete**
ROCFST	200.2	100.1	5.99	0.3	Rectangular	OPBC
RNCFST	200.4	100.1	6.01	0.3	Rectangular	Normal
SOCFST	150.8	150.8	5.99	0.3	Square	OPBC
SNCFST	150.7	149.9	5.99	0.3	Square	Normal

For each tested specimen, one end of the tube was first welded on a steel end plate concentrically, followed by concrete casting. Due to elevating temperature, which is more than 250˚C, moisture in concrete core evaporates. Therefore, the welded steel plate from one end of the tube is removed after concrete filling.

3.3.2 Specimen Fabrication

3.3.2.1 Steel

Two different types of cross-sectional shapes (square and rectangular) were selected for the composite members. The cross-sectional dimensions of square and rectangular beams were selected in such a manner that the amount of steel remains constant. All the tubes were provided from 12m length of hollow rectangular steel tube while the tensile tests were performed on steel coupons cut from the original tubes. The measured yield strength, ultimate strength, elastic modulus and maximum elongation were 394 MPa, 458 MPa, 201.3 GPa and 29%, respectively.

3.3.2.2 Concrete

Both NMC and OPBC of grade 50 were prepared with pan mixer. The steel tubes were then filled with their respective type of concrete. A poker vibrator was used to vibrate the concrete and remove air voids trapped in it. The compressive strength of concrete was determined by testing concrete cubes of size 100 mm while the elastic modulus and stress-strain behavior of concrete was determined at 28 days by testing concrete cylinders of 100mm x 200mm. The moisture content was obtained according to the procedure described in ISO 12570:2000 (12570:2000, 2000). The results of measured compressive strengths and elastic modulus of both concretes at 28 days and the measured compressive strength of concrete at the time of testing of the CFST are presented in Table 3.4.

3.3.3 Arrangement of Thermocouples and Displacement Transducers

To obtain the temperature distribution along the length of each specimen, 10 K-type thermocouples were installed on steel tube as shown in Figure 3.4. One thermocouple was embedded at the mid-height of concrete to measure the temperature of infilled concrete (T11). Three displacement transducers were placed on two sides in the top-side of each specimen to measure the deformation of the specimen under elevated temperature. The detailed arrangement of thermocouples and displacement transducers is shown in Figure 3.4.

3.3.4 Loading and heating

The elevated temperature tests were conducted under transient state heating conditions as it is closer to real-life scenarios. In transient state test, the sample is loaded to some stress level by applying load statically. Thereafter, the temperature is increased gradually by using different standard fire time-temperature curves recommended by different testing methods, until failure.

The experimental test was divided into two basic stages; loading stage and heating stage. For the loading stage, the applied load ratio was selected as 30% of the design value at room temperature because it replicates the common serviceability load of a CFST flexural member of real building structures (Rodrigues & Laim, 2017). The design value was calculated by using Chinese code (GB50936, 2014). During the loading stage, the flexural load was applied to the specimens 30 min before igniting the furnace. The load was applied slowly to the specimen at a rate of 2 kN/min. When the load reached the desired level, it was maintained there for 2 minutes. During the second stage, the furnace was ignited, and the beam was exposed to elevated temperature in such a manner that the average temperature of the furnace followed the ISO 834 fire curve closely. It is pertinent to mention that at the time of igniting the furnace, the room temperature was 27°C.

To measure the temperature of the furnace, 4 type-K thermocouples (T13-T16) were embedded at different location in the furnace. The thermocouples readings were recorded with the help of the assembly attached to the furnace. A TDS-530 data logger was used to record the readings from load cell and LVDTs at every second.

3.4 Finite Element Modeling at Ambient Temperature

3.4.1 Model Description

The structural behaviour of a square and rectangular CFST beams filled with normal strength concrete and high strength concrete was investigated using nonlinear FE models in ANSYS software. The loading rate was kept constant at 2kN/min.

3.4.2 Material Constitutive Models

3.4.2.1 Steel

A model for structural steel as suggested by Han et al. (2001) was used for uni-axial stress-strain relation of steel. In this model, the effect of strain hardening of steel was considered. The deformation of steel included elastic, elastic-plastic, plastic, hardening and fracture as shown in Figure 3.5. Where, f_p, f_y, and f_u represents the proportional limit, yield, and ultimate strength of steel, at their respective strains while ε_e= $0.8\varepsilon_y$, f_y/E_s, ε_y= $1.5\varepsilon_e$, ε_{uy}=$10\varepsilon_y$, ε_u= $100\varepsilon_y$.

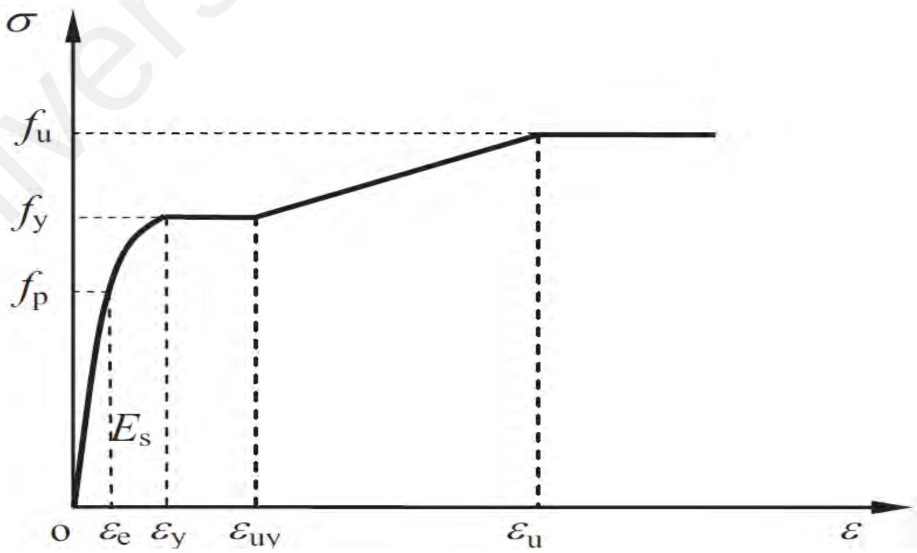

Figure 3.5: Schematic sketch of uniaxial stress–strain relation for steel

The Von-Mises yield function with associated plastic flow was used in multi axial stress states. The structural steel was assumed to have isotropic hardening behaviour, so that yield stresses increase or decrease in all stress directions when plastic straining occurs. Moreover, when Mises stress reaches the yield stress of the steel, the stress can still increase when subjected to further plastic straining. The modulus of elasticity and the Poisson's ratio for the steel were taken as $2x10^5$ MPa and 0.3, respectively.

3.4.2.2 Concrete

For this research, concrete having compressive strength less than 50 MPa was termed as normal strength concrete while concrete having compressive strength more than 50 MPa was termed as High-strength concrete. As the structural behaviour, effect of confinement and mode of failure of normal and high strength concrete are completely different from each other, therefore both were modelled separately (Cusson & Paultre, 1995; Kim, 2007; Mander et al., 1988; Saatcioglu & Razvi, 1992; Scott et al., 1982). The effect of confinement on normal and high strength concrete is shown in Figure 3.6.

Although the confinement effect of different CFST cross-sections is different (Qiu et al., 2016), yet a same average model for different cross-sections can be used (Chen et al., 2016; Sundarraja & Prabhu, 2011). For normal strength concrete, the equations given by Elchalanki (2016) for circular CFST members were used. The model is known as concrete damaged plasticity model and uses the combination of different equations. The combination includes equations for an unconfined compressive behaviour of concrete as given by (Carreira & Chu, 1985) in equation 3.1 and the effect of confinement of concrete presented by (Richart et al., 1928) in equation 3.2 and 3.3.

$$\frac{f}{f_c} = \frac{r\left(\frac{\varepsilon}{\varepsilon_c}\right)}{1+(r-1)\left(\frac{\varepsilon}{\varepsilon_c}\right)^{\beta}} \qquad \ldots\ldots\ldots\ldots\ldots\ldots\ldots\ldots\ldots\ldots(3.1)$$

$$f_{cc} = f_c + 4.1\sigma_{lat} \qquad \ldots\ldots\ldots\ldots\ldots\ldots\ldots\ldots\ldots\ldots(3.2)$$

$$\varepsilon_{cc} = 5\varepsilon_c\left[\frac{f_{cc}}{f_c} - 0.8\right] \qquad \ldots\ldots\ldots\ldots\ldots\ldots\ldots\ldots\ldots\ldots(3.3)$$

The modulus of elasticity was calculated by using the following equation.

$$E_c = 0.043{\rho_c}^{1.5}{f_c}^{0.5} \qquad \ldots\ldots\ldots\ldots\ldots\ldots\ldots\ldots\ldots\ldots(3.4)$$

In the above equations, f and ε is the strength and deformation of concrete, f_{cc} and ε_{cc} is the maximum compressive strength and strain of confined concrete, r is material parameter, β is $r/(r$-1), ρ_c and f_c is the average density and compressive cylinder strength of concrete at 28 days.

For high strength concrete, the model used by Han (2007) for CFST square columns was used. It considers the effect of confinement on the plasticity of concrete in compression as well as in tension. The plasticity of high strength infill concrete increases due to the confinement effect from outer steel tube and hence strain corresponding to the maximum stress increases (Han, et al., 2001). The increase in the plastic behaviour was considered by using a confinement factor, which can be calculated by using the equation 4.5. As shown in equation 3.5, the confinement factor highly depends on strength and area of concrete and steel.

$$\xi = \frac{A_s f_y}{A_c f_{ck}} = \alpha \frac{f_y}{f_{ck}} \qquad \text{(3.5)}$$

The stress-strain model presented by Han (2007) for high strength concrete was used to model the CFST with high strength concrete infill. The model is based on Han (Han et al., 2005) but slightly modified by Han (2007). The equation is given below.

$$y = f(x) = \begin{cases} 2x - x^2, & x \leq 1 \\ \frac{x}{\beta_0 (x-1)^{\eta} + x}, & x > 0 \end{cases} \qquad \text{(3.6)}$$

where,

$\eta = 1.6 + 1.5x$

$\beta = \frac{(f'_c)^{0.1}}{1.2\sqrt{1+\xi}}$

In the above equations, ξ is the confinement factor, f_y is the yield strength of steel, f_{ck} is the characteristics strength of concrete and is equal to$0.67f'_c$; f'_c is the compressive strength of concrete in MPa, A_s and A_c is the area of steel tube and infilled concrete respectively. For tensile softening behaviour of concrete, the fracture model presented by Hillerborg (1976) was used. Finally, the modulus of elasticity was calculated by using equation 3.7 (Omar et al., 2000).

$$E_c = 3320\sqrt{f'_c + 6690} \qquad \text{(3.7)}$$

For both normal and high strength concrete, the Poisson's ratio was assumed to be 0.2.

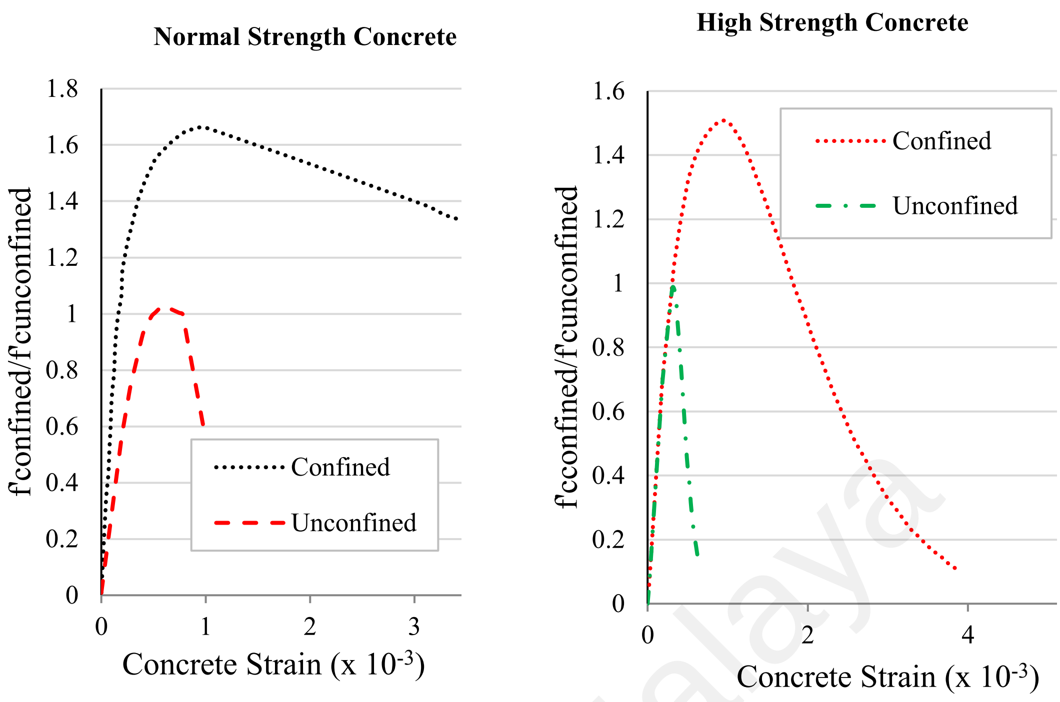

Figure 3.6: Effect of confinement on normal and high strength concrete

3.4.3 Surface Interaction

The interface between the infilled concrete and the steel tube of the CFST was modelled in the tangential and normal directions. The "hard point contact" formulation was used for the normal direction, which permits any pressure value when the surfaces are in contact and zero pressure when the surfaces are separated. For the interaction in the tangential direction, the penalty friction formulation with a Coulomb friction coefficient of 0.6 and maximum shear interfacial stress of 0.41 MPa was taken, as suggested by AISC 360-10 (Zhai et al. 2012). The slippage at the interface could occur when the applied shear stress exceeds 0.3 times the contact pressure.

3.4.4 Element Description

Different element used in analysis may provide different results, which is possible due to the different degrees of freedom provided. Solid elements for example are stiffer than line elements but solid elements are a closer simulation of actual experimental tests if model deformation and interaction are necessary to the study. In addition, the elements may not have the attached function relevant to the study, including temperature effects as with certain elements. Hexahedral shaped elements are commonly used in previous studies (Zhai et al. 2012). The size of element is determined by performing mesh convergence study.

3.4.4.1 3D hexahedral reduced integration solid element

This type of element is termed as "C3D8" element in Abaqus. 3D hexahedral reduced integration solid element is as represented in Figure 3.7, showing an 8-node solid brick element. The element can be used as a general-purpose element for all analysis types. However, under bending loads shear locking may occur. Shear locking occurs due to the linear nature of the element, where the element is unable to form a curvature, similar to actual materials under bending and thus causes shear to develop. This was avoided by using a smaller mesh size as suggested by (Hallquist, 2006).

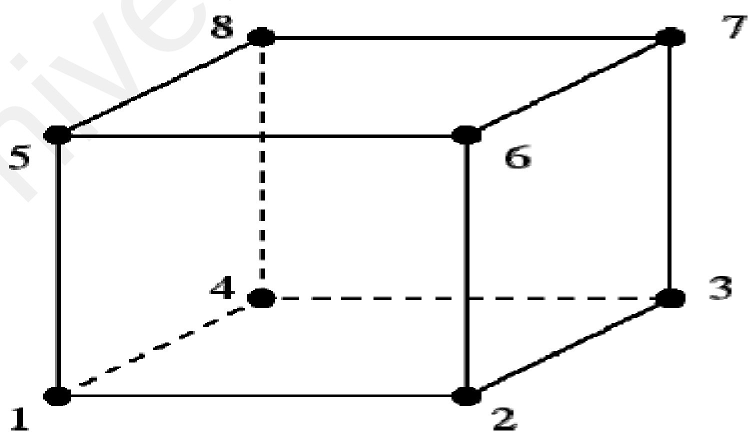

Figure 3.7: Representation of 3D hexahedral reduced integration solid element

3.4.4.2 3D quadrilateral reduced integration solid element

3D quadrilateral reduced integration solid element with "constant stress" solid element formulation was selected in this study for concrete modelling as they are known to provide accurate and efficient results under a wide range of conditions even under severe deformation (LSDYNA Aerospace Working Group, 2013). Figure 3.8 shows 3D quadrilateral reduced integration solid element. Fully integrated solid formulation has relatively low cost as it saves on computer time and does not encounter the problem of being very stiff in many situations and unstable in large deformation applications when compared with single point integration (Hallquist, 2006).

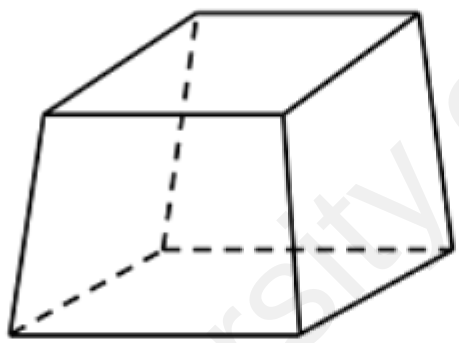

Figure 3.8: Representation of 3D Quadrilateral reduced integration solid element

3.4.5 Mesh Convergence

The ANSYS FE software provides various types of solid elements that could be used to model the steel, concrete and interface between steel and concrete. However, the results are highly dependent on the mesh size. Undoubtedly, a few methods exist to partition the solid; however, the main concept is the definition of a cutting line that would serve to partition the whole component in the selected direction. Whole model is selected for partitioning to increase mesh uniformity. One of the main procedures in producing hexahedral meshing would be the utilization of the Partition method to split the solid into smaller sections which can be sweep meshed. Meanwhile, the mesh seed size is commonly defined as 5mm size in general, in which the mesh is verified to check for unusual meshes, which may increase computational loads or result in analysis error.

A convergence study was performed to select the appropriate mesh size of the FE model of the square CFST beam. Optimization of mesh was done based on ultimate flexural capacity. Ultimate flexural capacity calculated from different meshes were compared with experimental results of this study for SOCFST sample. The change in ultimate capacity was less than 0.1% for the last two models with 13080 and 60960 elements as shown in Figure 3.9. The FE model with 13080 elements was selected based on the time taken by the workstation and without compromising the accuracy of the FE model. The steel tube and concrete were divided into 7200 and 5880 elements respectively, for the selected model.

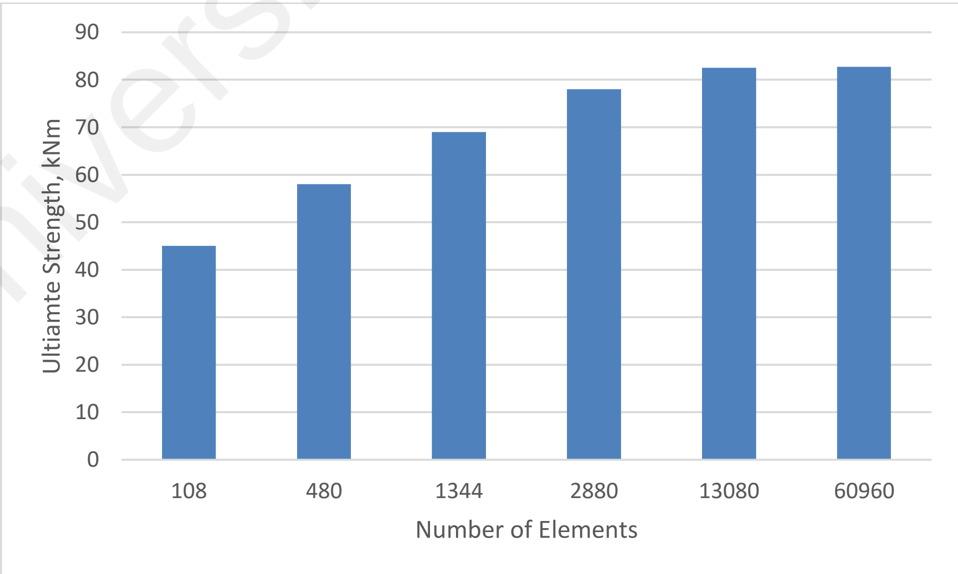

Figure 3.9: Study of mesh convergence for sample SOCFST

The mesh used for square and rectangular CFST beams are shown in Figures 3.10. Adequate size and number of elements were selected by performing mesh convergence study on some models.

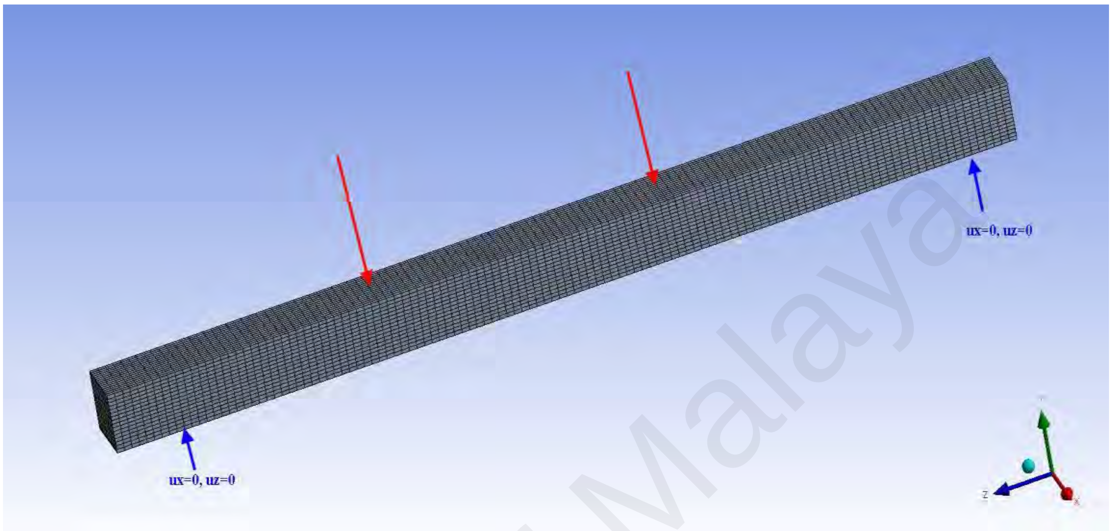

Figure 3.10: Boundary conditions and mesh used for square and rectangular CFST beams

3.4.6 Parametric Analysis

The FE model that was developed to validate the experimental testing was further extended for parametric analysis. The analyzed parameters were as follows: depth-to-thickness ratio, strength of concrete, yield strength of steel, depth-to-width ratio and shear span-to-depth ratio. The discussion on parametric analysis is presented in the next chapter of this study.

3.5 Finite Element Modeling at Elevated Temperature

3.5.1 General

For the simulation of test results accurately, detailed information of the test has been included in the FE model. Recently, many researchers employed 2D model for thermal analysis and prediction of temperature distribution across the member. The total length of the beam in the tests was 3200 mm, where only the central part of length 2800mm was exposed to fire. The temperature of beam specimen was uniform in the fire exposed area. The temperature of area of beam outside the furnace has relatively low temperature as compared to central part of beam due to no-direct exposure to fire. Hence, the beam shows slightly long critical time as compare to "uniform temperature assumption' along the beam. Furthermore, the thermal expansion of the beam was influenced by the heated length of the beam. Therefore, the FE model with only central part heated was used to model the temperature distribution. The details of beam and application of load and reactions are shown in Figure 3.11 and Figure 3.12, respectively.

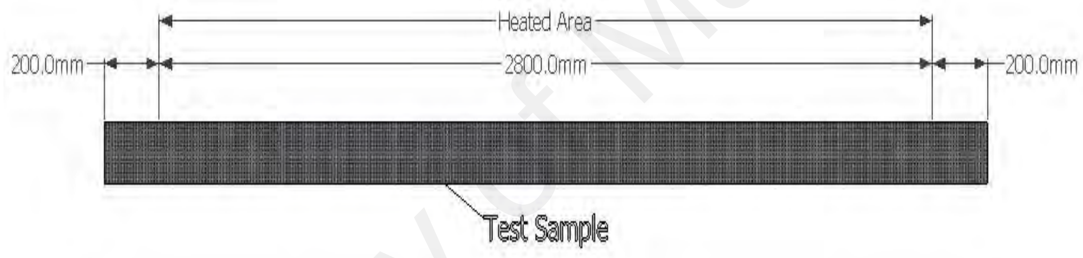

Figure 3.11: Test sample showing heated length of specimen

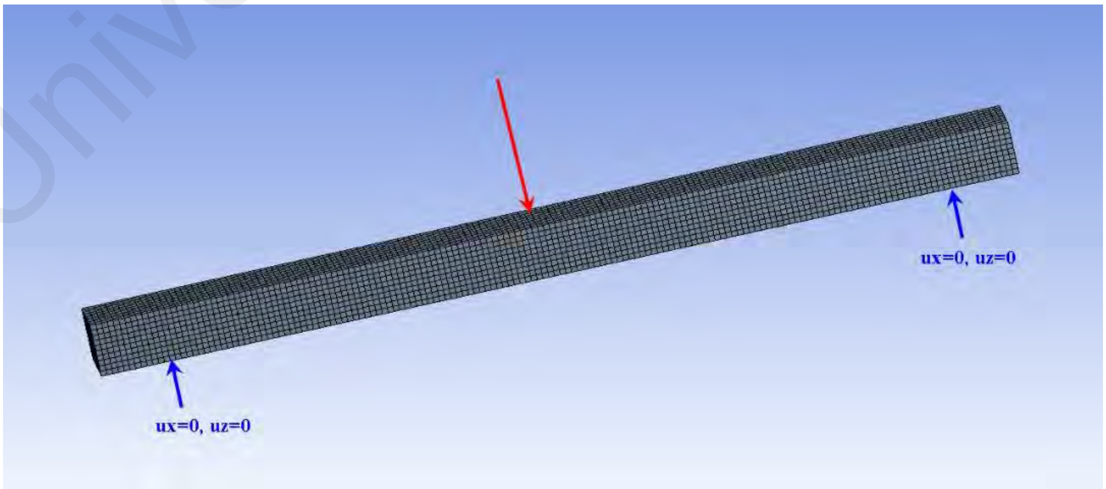

Figure 3.12: FE model with load applied and reactions

The modeling and analysis of structural fire behavior of CFST members is a complex process because it involves several variables including initial geometrical imperfections of CFST members, interaction between steel and concrete, changes in the material properties and strength reduction during exposure to fire. Further variables include fire growth, duration of fire and temperature distribution in concrete and steel. The type of element and the size of mesh also require careful selection as they affect the accuracy and computational time of the model.

3.5.2 Thermal Analysis

Thermal analysis was performed in the thermal field to determine nodal temperature and temperature distribution and profile in the member. In the thermal field the heat transfer was modelled using radiation, convection and conduction; Radiation was modelled in ANSYS by creating a space node which represents the fire environment or furnace and a radiating (receiving and emitting) surface on the exposed surface of the member. The fire was simulated by applying the appropriate temperature – time curve on the space node which represents the fire or furnace temperature. An example of a temperature −time function used in ANSYS is given in Equation 3.8. The ambient and reference temperature for thermal calculations was taken as 20°C.

$$T_g = 20 + 345 log_{10}(8t + 1) \tag{3.8}$$

Where T_g is furnace temperature and t are exposure time.

Table 3.6 shows the values of different parameters used in thermal analysis. The values of different governing parameters like constant convective coefficient for exposed and unexposed surface, steel emissivity value and radiative heat flux were used according to

EC1. Thermal conductivity and specific heat of normal concrete and steel were calculated according to EC2 and EC3, respectively. The values recommended by Hong and Varma for thermal expansion coefficient were used (Hong & Varma, 2009).

Table 3.6: Properties of steel and concrete used in FE model

Parameters	**Values**	**References**
Constant convective coefficient for exposed	25 W/m^2 K	(Wang & Young, 2013)
Constant convective coefficient for unexposed	9 W/m^2 K	(Wang & Young, 2013)
Steel emissivity value	0.8	(Wang & Young, 2013)
Stefan–Boltzmann constant	5.67 x 10^{-8} W/m^2K^4	(Wang & Young, 2013)
Thermal expansion coefficient for steel	12 x 10^{-6}/°C	(Hong & Varma,2009)
Thermal expansion coefficient for concrete	6 x 10^{-6}/°C	(Hong & Varma,2009)
Thermal conductivity of NMC	1.6 Wm^{-1} K^{-1}	(Eurocode, 2005)
Thermal conductivity of OPBC (Lightweight concrete)	0.43 Wm^{-1} $°C^{-1}$	(Eurocode, 2005)

3.5.3 Material Constitutive Models

The effect of degradation of strength of material with the rise in temperature is considered in FE model. Both mechanical and thermal properties related to temperature were adopted. For steel, the model proposed by Espinos (2012) is employed. As Poisson's ratio is not affected by temperature, so it's assumed to be 0.3. The strength reduction factors suggested by (Kesawan & Mahendran, 2018; Li & Young, 2017) were used to calculate the yield stress and elastic modulus at elevated temperature. The stress-strain curve for f_y= 450 MPa obtained from the model used for different temperatures is shown in Figure 3.13. Thermal expansion coefficient for steel and concrete are presented in Table 3.6 and were suggested by (Hong & Varma, 2009; Wang & Young, 2013). Previous studies shows that the inclusion of slip between concrete and steel interface has very minor effect of the fire resistance (FR) time of CFST member (Ding & Wang, 2008), hence, it is not included in the current FE model.

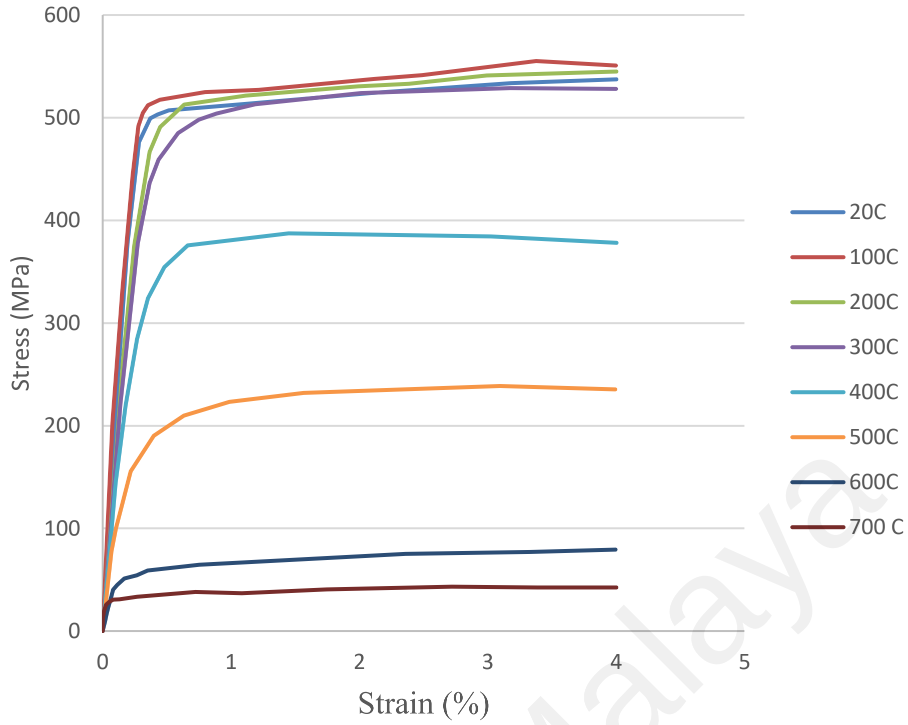

Figure 3.13: Stress-strain curves for 475 MPa steel at different elevated temperatures

For the concrete properties, the elastic stress − strain model for ambient temperature was used and concrete's tensile strength was taken as 10% of its compressive strength at elevated temperatures. Transient strain model is shown in equation 3.9 is taken from Anderberg and Thelandersson (1976). For the thermal properties and thermal strain of NMC and OPBC, the model proposed in the Eurocodes was adopted, as it considers the moisture content of the concrete and the variation of response of concrete at elevated temperatures due to aggregate type. Concrete density was taken as a constant value of 2400 kg/m^3 without considering any variation due to elevated temperatures for NMC while it was taken as 2100 kg/m^3 for OPBC. Creep strain was not considered in the model due to computational and convergence difficulties as it has been reported by Anderberg and Thelandersson (1976), Jensen et al. (2010) and Li and Purkiss (2005) that creep strain is very small and can be neglected.

$$\varepsilon_{tr} = -2.35\left(\frac{f}{f_{c0}}\right)\varepsilon_{thc} \quad (3.9)$$

Where ε_{tr} and ε_{thc} are transient strain and thermal strain of concrete at high temperatures respectively.

For modelling brittle behavior of concrete in ANSYS, Extended Drucker-Prager model was selected (ANSYS, 2010). This model is suitable for modelling soils, rocks, concrete and other brittle material. This model is adequate for modelling concrete because it accounts for tensile and compressive behavior of concrete and it has temperature dependency. The yield function is given by Equation 3.10 (ANSYS, 2010).

$$F = \sigma_e + \alpha\sigma_m - \sigma_k = 0 \quad (3.10)$$

Whereas F and σ_k are yield function and yield stress respectively, α is pressure sensitivity parameter.

$$\sigma_e = \sqrt{\frac{3}{2}\{S\}^T[M]\{S\}} \quad (3.11)$$

Where [M] and {S} are mass matrix and deviatoric stress vector, respectively.

The specific heat and thermal conductivity of concrete was calculated according to Eurocode (2005)

3.5.4 Initial Geometric Imperfection and Amplitude

Different researchers recommend different initial geometric imperfection values (Han et al., 2013; Tao et al., 2009; Wang & Young, 2013). Imperfections in form of the lowest global elastic buckling model were included in the current study. Since the geometric imperfections were not calculated at the time of experiment, three assumed values of imperfections were considered for the initial geometric imperfection sensitivity analysis. Figure 3.14 shows the comparison of time deflection curve FE model with different values of imperfections and experimental result for SNCFST. Assuming smaller imperfections results in higher FR time but significantly decreases the computation time. The imperfection value of L/2000 gives the most favorable comparison, where L is the total length of the beam specimen. This value of L/2000 was used by Han et al., (2013) for stainless steel tubes. Hence, based on results of Figure 3.14, the initial geometric imperfection value of L/2000 was used in verification and parametric studies.

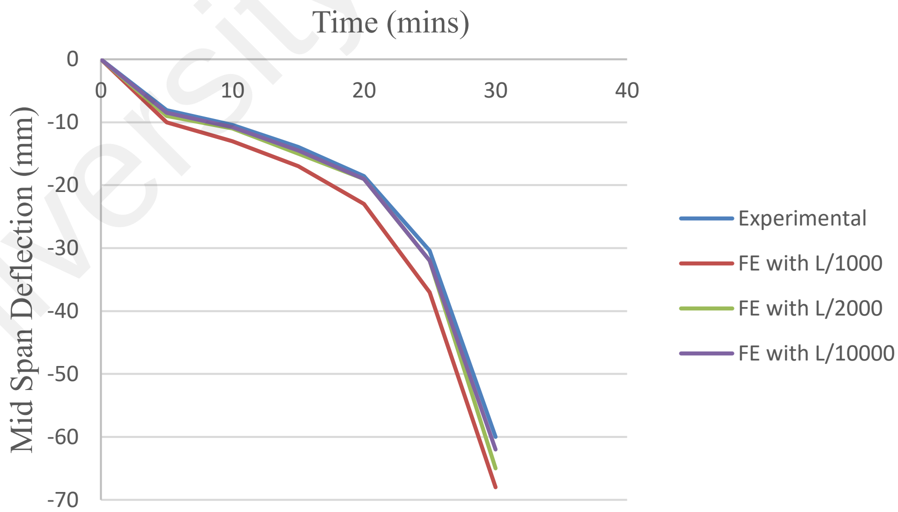

Figure 3.14: Mid-span deflection of different experimental tests and different FE models with different initial imperfections

CHAPTER 4: RESULTS AND DISCUSSIONS

4.1 Experimental Results and Discussion for Ambient Temperature Tests

The mode of failure, overall deflection curves and load vs strain curves obtained from the experimental tests are presented in this section to discuss the energy absorption, structural efficiency, ductility and ultimate strength of the CFST members. The comparison of the performance of OCFST and NCFST reveals the suitability of OPBC as infill material in hollow steel tubes.

4.1.1 Failure Mode

The photograph of failure state for RNCFST and SNCFST are shown in Figure 4.1. It was observed that all specimens failed due to flexural buckling. The absence of local buckling shows that the hollow steel tubes were properly filled with concrete. Moreover, no tensile fracture was observed on the tension flange. The moment-curvature curves of RNCFST, ROCFST, SNCFST and SOCFST are shown in Figure 4.2 and Figure 4.3. Similarly, the moment-deflection curves of RNCFST, ROCFST, SNCFST and SOCFST are shown in Figure 4.4 and Figure 4.5. Both square and rectangular CFST shows similar behavior except for ultimate capacity. Hence, from here onwards, only rectangular samples were used for the discussions. It can also be seen in Figures 4.2-Figure 4.5, that both NCFST and OCFST samples failed in a ductile manner with a maximum curvature exceeding $150x10^{-6}$. The specimens showed elastic behavior in the start of the loading followed by elastic-plastic behavior. This elastic-plastic behavior of OCFST samples is due to the ductility of steel tube. Furthermore, the initial flexural stiffness for both NCFST and OCFST are same. Hence, it can be concluded that OCFST can be a better alternative to NCFST in near future.

Figure 4.1: Failure mode of square and rectangular NCFST specimens

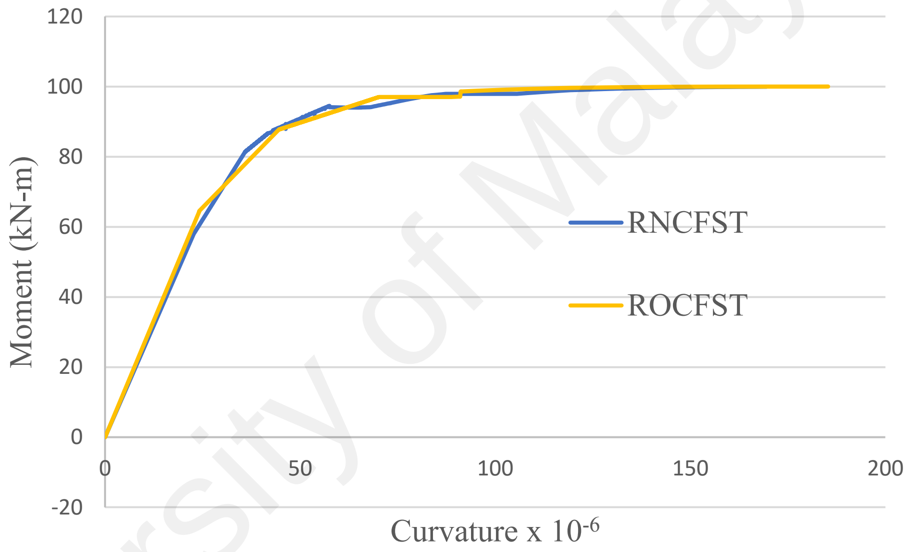

Figure 4.2: Moment-curvature curve of RNCFST and ROCFST beams

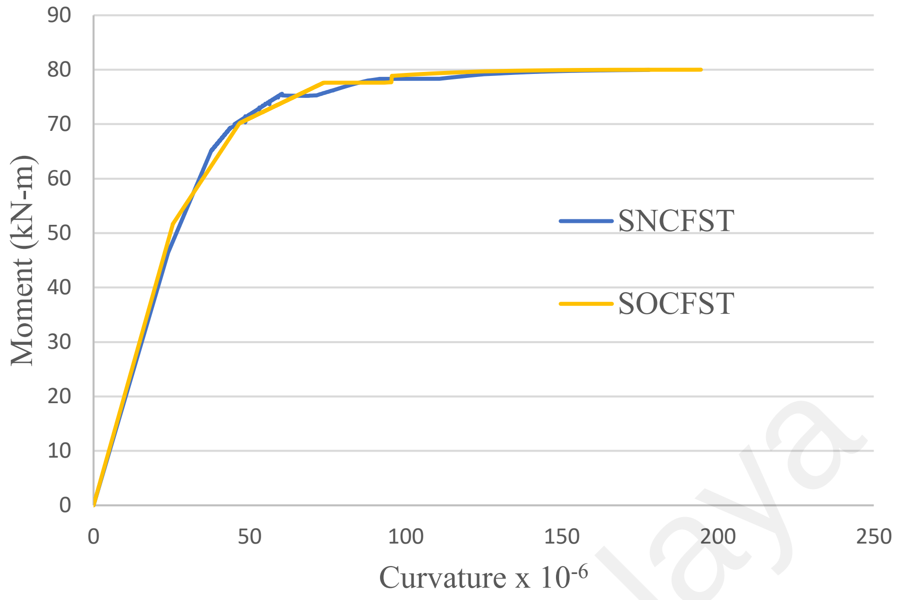

Figure 4.3: Moment-curvature curve of SNCFST and SOCFST beams

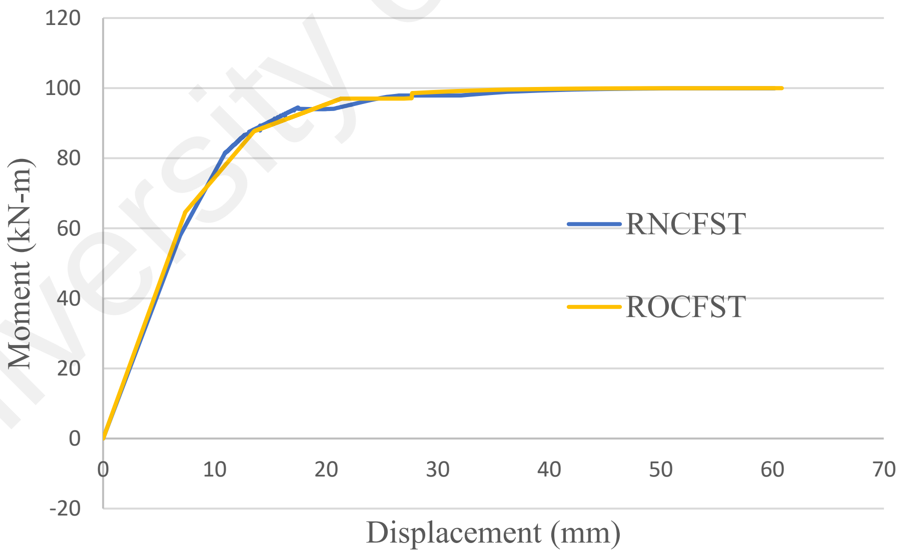

Figure 4.4: Moment-deflection curve of RNCFST and ROCFST beams

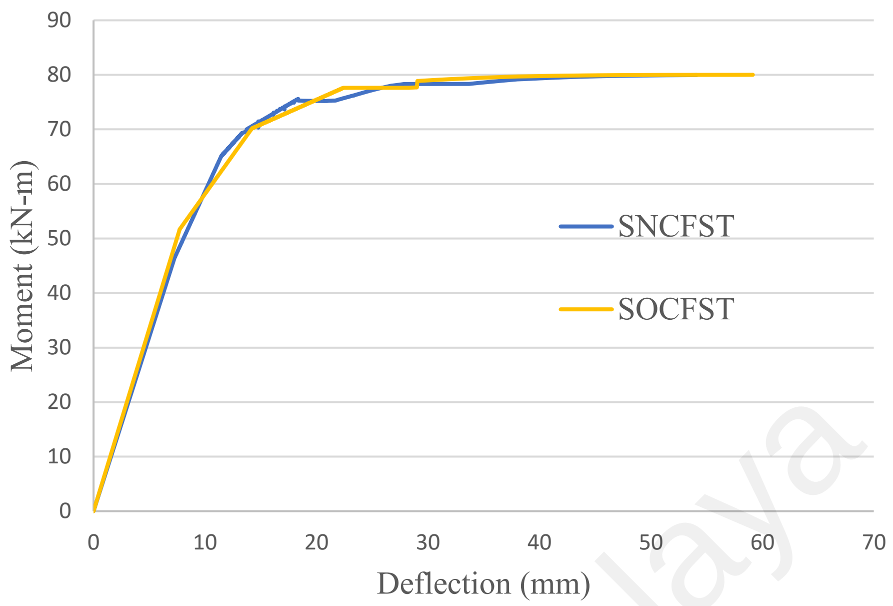

Figure 4.5: Moment-deflection curve of RNCFST and ROCFST beams

4.1.2 Overall Deflection Curves

The deflections in the longitudinal direction of test specimens were obtained from the two LVDT readings. For the two test specimens (one from each group), the deflections for different load levels (0 to Mu) are shown in Figure 4.6. The overall deflection curves for both types of specimens under different load levels resemble a half-sine curve. Similar kind of behavior was observed by Han (2004) for rectangular NCFST with concrete strength up to 40 MPa. The deflections in both types of beams developed gradually at low load levels (up to 0.8 Mu) and then increased at a faster rate after 0.8Mu load level. This is due to the yielding of steel as well as the development of cracks in infilled concrete at ultimate load level. Similar observations were made by Tang et al., (2017) where they tested circular hollow beams filled with recycled aggregate concrete for seismic loads.

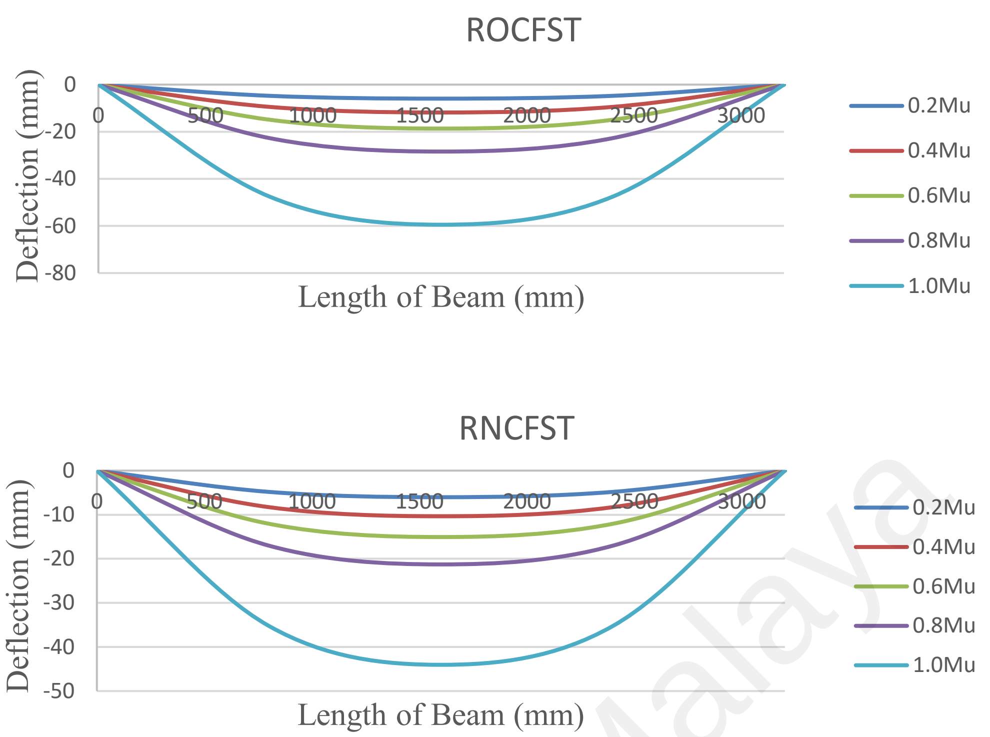

Figure 4.6: Deflected Shape for both types of beams

4.1.3 Strain Distribution Curves

For the tested specimens, the strain readings taken from S4, S5 and S6 strain gauges at different load levels are shown in Figure 4.7. The compressive strains obtained from the strain gauges attached to the top of the specimen are taken as negative, whereas, the tensile strains obtained from the strain gauges attached to the bottom of the specimen are taken as positive. The strains are zero around h/3 distance, showing that the position of a neutral axis of CFST is slightly higher than that of hollow steel tubes (which is at h/2). It is known from available literature (Chen et al., 2017) that the position of neutral axis varies for different grades of concrete. It can be also seen that the position of neutral axis does not change with the changing load levels. Besides this, the strains at the bottom of tensile zone and the top of compression zone are proportional until 0.8 Mu. This means that the assumption of "plane section remains plane" can be adopted to analyze and design the NCFST and OCFST up to 0.8Mu. However, the development of strains increases significantly after the 0.8 Mu load level showing the transition of an elastic stage to plastic stage.

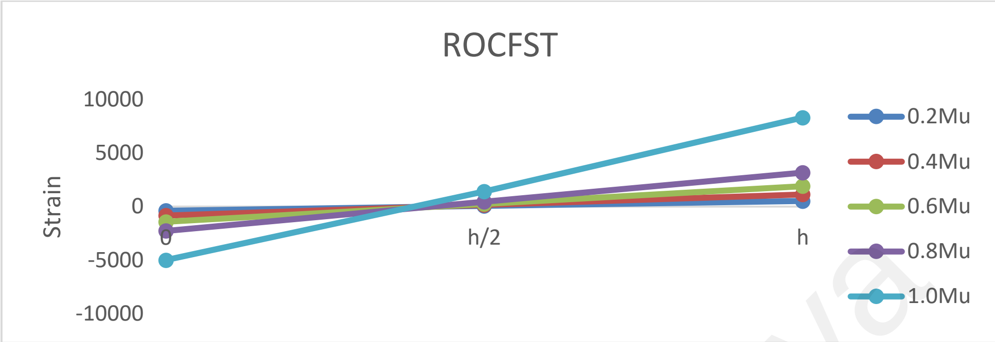

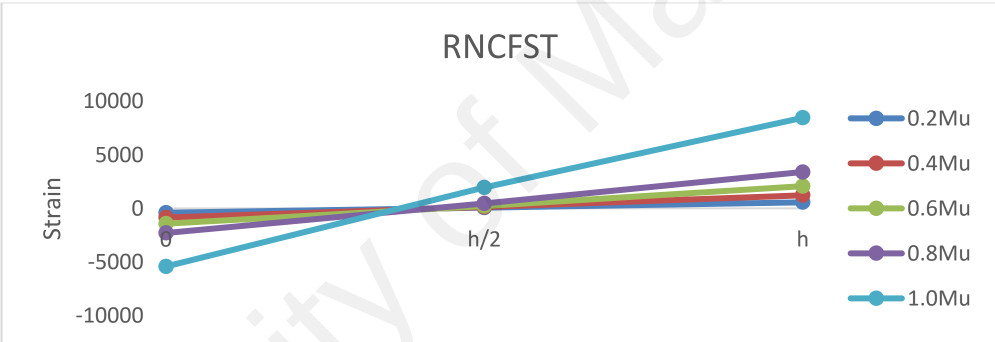

Figure 4.7: Strains in beams along its length

The conventional bending moment versus strain curves of NCFST and OCFST are shown in Figure 4.8. The compressive strains are plotted as negative while tensile strains are plotted as positive. The readings obtained from the strain gauges attached to the upper section of the beam are in compression while the strain gauges at the lower section are in tension. Due to the ductile nature of OPBC, the absolute tensile stresses are greater than absolute compressive stresses in OCFST, whereas in NCFST, the absolute compressive stresses are almost equal to absolute tensile stresses. Furthermore, the maximum tensile stresses produced in OCFST members are higher than the maximum tensile stresses produced in NCFST indicating the better performance and ductility of OCFST under flexural load.

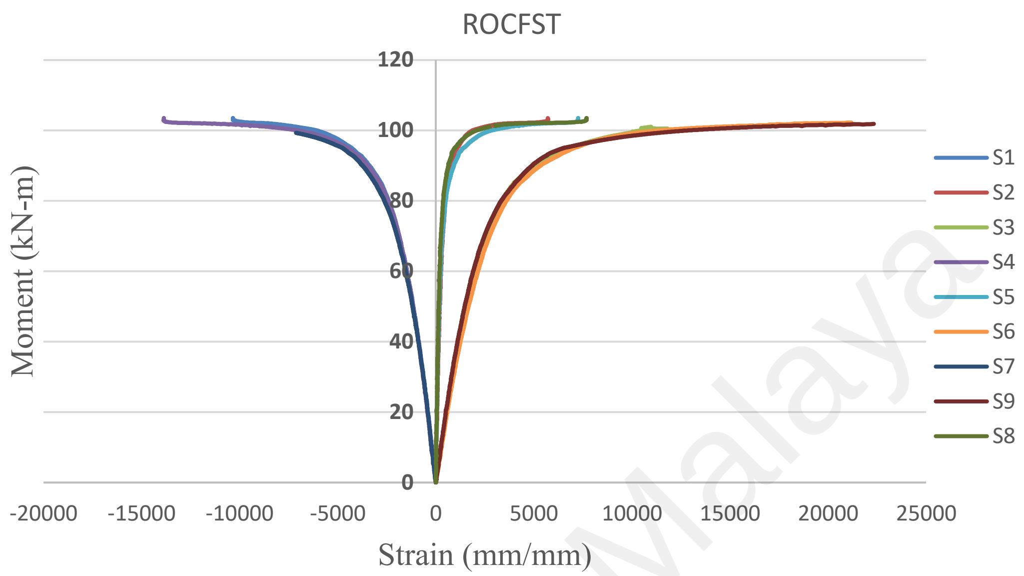

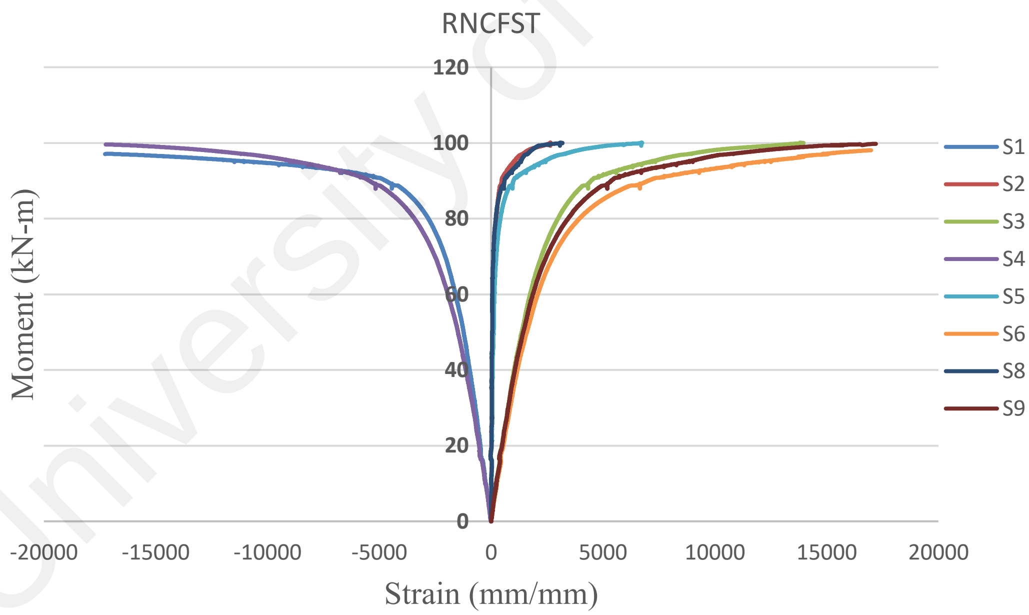

Figure 4.8: Moment vs Strain Diagram for OCFST and NCFST beam

4.1.4 Energy Absorption, Specific Energy Absorption and Structural Efficiency

The area under the load-deflection curve for a given direction of load gives an estimation about the energy absorption (EA) of the element. The energy absorption is the major index used for evaluating the seismic performance of structures: the greater the energy absorption, the better is the performance of structure during earthquake. Specific energy absorption (SEA) is a relatively new term and includes the effect of mass of the element on the EA capability. The values of EA and SEA for all the specimens are given in Table 4.1. The difference between EA values for NCFST and OCFST is not significant, however, a significant increase (up to 12%) is observed in the SEA values.

As mentioned earlier that there is no considerable difference between the peak loads of NCFST and OCFST, but the unit weight of infilled concrete is different. To correctly portray the effect of unit weight on the performance of member, the percentage structural efficiency of NCFST and OCFST is compared. The structural efficiency (SE) of a CFST member is the ratio between its peak load and unit weight. The values of SE for all the specimens are given in Table 4.1. OCFST shows 20% higher values of SE than NCFST and is significant. Moreover, the weight of NCFST is 10% more than OCFST. Therefore, it can be concluded that OCFST can be used as a new composite section with a high-energy absorption capacity and lower unit weight as compared to NCFST.

4.1.5 Ultimate Strength

The ultimate strength of NCFST and OCFST under flexural load is summarized in Table 4.2. For each specimens, the measured yield and ultimate moment are presented in Table 4.2, where Mu is taken as the moment corresponds to the deflection of Le/50 (Han, Tao, et al., 2001), and My is the moment corresponds to the yielding of steel tube. By comparison, the average ultimate strength of OCFST is higher than NCFST. As oppose to other lightweight and waste aggregate CFST (Rawi & Ghannam, 2011; Ismail et al., 2013; Zhong et al., 2011), the ultimate moment of OCFST is found to be 3% greater than NCFST (Table 3.6). However, the enhancement in ultimate capacity is not significant and both types (NCFST and OCFST) can be treated as having the same ultimate capacity. It is pertinent to mention here that the increase in strength of OCFST can be attributed to the rough texture of OPBC, which results in a better bond between steel tube and concrete (Aslam et al., 2016b).

Table 4.1: Energy absorption and structural efficiency of OCFST and NCFST beams

	Ultimate Load, P_{max} (kN)	Density (kg/m^3)	Energy Absorption, EA (kJ)	Specific Energy Absorption, SEA (kJ/kg)	Structural Efficiency, SE (kN-m^3/kg)%
RNCFST	188	3339.8	4072.5	2.81	2.81
SNCFST	160	3340.2	4122.3	2.84	2.84
ROCFST	198	3020.39	4256.65	3.28	3.28
SOCFST	162	3010.14	4069.81	3.15	3.15

4.1.6 Ductility

"Ductility" of a member is often defined as the ability of a member to sustain deformation after elastic point while carrying a significant load until failure. Hence, the demand of ductile members has increased in the seismically active areas to reduce the design seismic forces and hence reducing the overall cost of the project. Moreover, ductile structures perform well in extreme manmade and natural events like a cyclone, blast and fire. Currently, the design of structures mainly depends on perspective detailing provisions. For instance, EC4 restricts the load ratio, cross sectional dimensions and concrete strength of CFST to resist seismic loads in case of earthquake. To quantify the effect of type of concrete on the ductility of the member, ductility index defined in the following equation is used (Hamidian et al., 2016).

$$\mu = \delta u/\delta y \qquad \text{………}(4.1)$$

In the above equation, μ represents the ductility index (DI) of the member, δy and δu represent the deflection at mid-span when the moment in the CFST reaches yield moment and ultimate moment, respectively. The ductility calculations are presented in Table 4.2.

OCFST shows 15% better ductility than NCFST. This response is different from other lightweight filled CFST and is believed to be due to the ductile nature of OPBC. Moreover, the rough texture of OPBC aggregate as well as the stronger bond between steel tube and concrete is responsible for the increase in ductility of OCFST. Hence, OCFST can potentially be used in seismically active areas where high-ductility demand is required.

Table 4.2: Yield and ultimate moment, ductility of OCFST and NCFST beam

Ductility	Strain at yield point, (10^{-6})	Yield Moment, M_y (kN-m)	Ultimate Moment, M_u (kN-m)	Deflection at yield moment, δ_y (mm)	Deflection at Ultimate moment, δ_u (mm)	Ductility, $\mu=\delta_u/\delta_y$	Average μ
RNCFST	2000	58.5	94.00	20.75	59.2	2.85	2.87
SNCFST	2085	50.2	80.00	20.78	60.1	2.89	
ROCFST	2002	57	97.50	18.14	59.8	3.29	3.31
SOCFST	2078	51.6	81.00	18.02	59.9	3.33	

4.2 Evaluation of Test Results by Comparison with Available Literature

In this section, the moment curvature curve, ultimate capacity, initial flexural stiffness and flexural stiffness at serviceability level obtained from the experimental results are compared with their respective values obtained from analytical method available in the literature and four different design codes.

4.2.1 Moment-Curvature Curve

The moment-curvature of NCFST and OCFST obtained from the experimental results are compared with the simplified bi-linear moment-curvature curve (Han et al., 2006) for NCFST (Figure 4.9). Han's model for predicting moment-curvature of RNCFST can be used safely for ROCFST. The maximum difference between the predicted and experimental moment-curvature was found to be less than 20%.

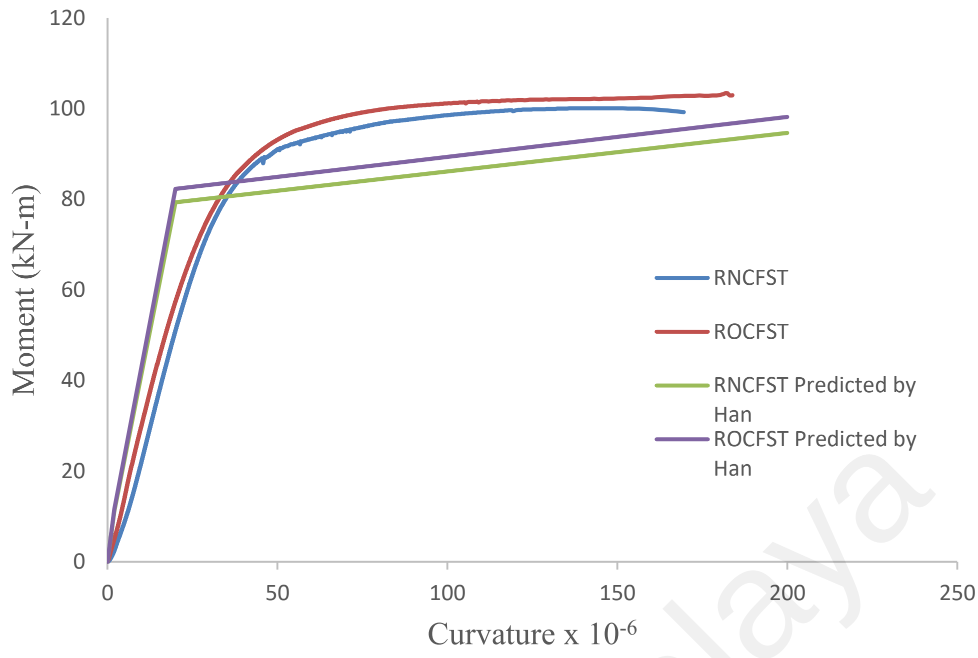

Figure 4.9: Moment -curvature curve predicted by Han et al., (2006) vs experimental results

4.2.2 Flexural Stiffness

The flexural stiffness of NCFST and OCFST obtained from the experiments were compared with the design flexural stiffness calculated from Eurocode 4 (2005), AIJ standard (1997), AISC specification (2005) and BS 5400 (2005) respectively (Equations 4.2 to 4.5). The initial flexural stiffness and flexural stiffness at serviceability level correspond to the secant stiffness under the uniaxial bending of 0.2Mu and 0.6 Mu, respectively (Chen et al., 2017). The comparison is presented in Table 4.3.

$K = F_S + 0.6F_C$ EC4 (2005) ……………………….(4.2)

$K = F_S + 0.2F_C$ AIJ (1997) ……………………….(4.3)

$K = F_S + (0.6 + 2\frac{A_s}{A_c})F_C$ AISC (2005) ……………………….(4.4)

$K = 0.95F_S + 0.45F_C$ BS-5400 (2005) ……..………….(4.5)

Where F_S is the flexural stiffness of steel and is equal to$E_S I_S$, F_C is the flexural strength of concrete and is equal to$E_C I_C$, As and Ac is the area of steel and concrete, respectively.

It can be seen from Table 4.3 that the initial flexural stiffness ratio (K_i/K_c) are unsafe (The ratio K_i/K_c is less than one) for NCFST. However, the K_i/K_c ratio obtained from AIJ gave closer results with an average of value 0.99 while the values calculated from AISC are mostly overestimated with the maximum deviation of 0.62. The predicted flexural stiffness at serviceability level for NCFST is found to be conservative for AIJ (up to 20% higher than experimental value) while precise for BS code. Moreover, for NCFST, the values obtained from EC4 and AISC are found to be unsafe for the flexural stiffness at serviceability level (all values less than 1). However, the initial flexural stiffness and flexural stiffness at serviceability level are all quite precise for OCFST for all codes except AISC. Hence, it can be concluded that the current design codes except AISC can be used confidently for predicting the flexural stiffness of OCFST.

4.2.1 Ultimate Capacity

The ultimate capacity of the test beams was calculated by using different available design codes. Four different international design codes namely EC4, AISC, CIDECT and GB were used for calculating the ultimate capacity of rectangular beams. The calculated values were compared with the experimental results. All the material partial safety factors were set to unity in the calculation of ultimate moment capacity. The ratio between calculated values from codes and experimental values are shown in Table 4.4. The design codes EC4, AISC and CIDECT underestimate the ultimate moment capacity of NCFST and OCFST. The calculated values given by EC4, AISC and CIDECT were about 40%, 53% and 41% higher than experimental results. However, GB predicts the ultimate flexural capacity safely and accurately with the maximum difference of only 15% and mean difference of 10%. Therefore, GB code can be used confidently used to predict the ultimate moment capacity of OCFST. The mean value and standard deviation values shown in Table 4.4 with GB code showing the best results.

Table 4.3: Comparison between test results and design results of initial flexural stiffness and flexural stiffness at the serviceability limit state for NCFST and OCFST

	Initial flexural stiffness K_i (kN/m^2)	Flexural Stiffness at serviceability level K_s (kN/m^2)	EC4		AIJ		AISC		BS	
			K_i / K_c	K_s / K_c	K_i / K_c	K_s / K_c	K_i / K_c	K_s / K_c	K_i / K_c	K_s / K_c
RNCFST	2232.84	2683.47	0.76	0.92	0.99	1.20	0.63	0.76	0.87	1.04
SNCFST	2185.69	2648.96	0.75	0.91	0.98	1.18	0.62	0.75	0.85	1.03
ROCFST	3110.54	2950.41	1.06	1.01	1.39	1.32	0.88	0.83	1.21	1.15
SOCFST	3254.87	3002.85	1.11	1.03	1.45	1.34	0.92	0.85	1.27	1.17
Where K_c=Flexural stiffness calculated from the equations given in code										

Table 4.4: Comparison of experimental and design ultimate capacity of beams

Sample	M_{exp}	M_{exp}/M_{EC4}	M_{exp}/M_{AISC}	M_{exp}/M_{GB}	M_{exp}/M_{CIDECT}
RNCFST	94.00	1.41	1.54	1.09	1.41
SNCFST	95.00	1.43	1.55	1.11	1.43
ROCFST	99.00	1.49	1.62	1.15	1.49
SOCFST	95.00	1.43	1.55	1.11	1.43
Mean		1.45	1.56	1.11	1.43
SD		0.04	0.04	0.03	0.03
COV		0.03	0.03	0.03	0.03

4.3 FE Analysis Results at Ambient Temperature

4.3.1 Verification of the FE Model Experimental Results from Literature

The accuracy and efficiency of the developed FE model was demonstrated by making comparison with the experimental results reported in literature for many CFST beams with different parameters. For the verification of FE model, the ultimate flexure load, moment-curvature curves and load-deflection curves of CFST beams were considered. To check the accuracy and validity of FE model for different parameters, the structural performance of more than 50 samples were compared.

4.3.1.1 Ultimate Flexure Strengths of Normal Strength CFST Beams

The following experimental investigations reported herein were used to verify the FE model for normal strength CFST beams subjected to flexure load only. The comparison between experimental and FE ultimate flexural capacity of beams is shown in Table 4.5. Specimens RB1-1 to RB-8-1 given in Table 4.5 were tested by Han (2004). All the beams were constructed with mild steel tubes filled with normal strength concrete. The compressive strength of the infill concrete was in the range of 27.3 to 40 MPa while modulus of elasticity was 26 GPa. Both square and rectangular beams having different cross-sectional dimensions with D/B ratio in the range of 1-2 and D/t ratio in the range of 20-50 were tested. The yield strength of steel tubes was about 300 MPa. All the beams having length of 1100 mm were tested using two-point loading. In these experiments, the ultimate flexural strength of the CFST beams was defined as the load corresponding to a maximum steel tube tensile strain of 0.01.

For the verification of FEA model, the CFST beams tested by Lu and Kennedy (1994) were also used. The test parameters considered for 12 specimens having square and rectangular cross-sections and designated by CB1-12 are shown in Table 4.5. The steel tubes with yield strength of 350 MPa were filled with normal strength concrete of 30 MPa while the shear span-to-depth ratio was kept in the range of 1 to 5. The length of the CFST beam varied from 1975 to 4260 mm. For the test performed by Lu and Kennedy (1994), the yield strengths of steel (f_y) were taken as the stresses at the strain value of 0.018, which approximately corresponded to the maximum shear forces. We would like to mention here that the authors also calculated the maximum slip between concrete and steel at ultimate loads, but these results were not utilized for the verification of FE model.

The experimental details of CFST beams tested by Soundararajan and Shanmugasundaram (2008) are given in Table 4.5. The specimens were made of normal mix concrete (NMC), Fly-ash concrete (FAC), quarry waste concrete (QWC) and low-strength concrete (LSC) with compressive strength ranging from 21 MPa to 32.6 MPa. The depth-to-thickness ratio of the steel tube was kept as 20.5. All specimens were tested under two-point flexure loads. The yield strength of steel tubes was 345 MPa while the ultimate stress was 510 MPa.

Uy (2000) performed 5 experiments on square CFST beams filled with normal strength concrete. The strength of the concrete infill was in the range of 38 to 50 MPa while the yield strength of the steel tubes was 300 MPa. Further details of the experiments are given in Table 4.5. Probst (2010) performed one test on rectangular CFST filled with normal strength concrete having a compressive strength of 20.7 MPa. The yield strength of the steel tubes was 307 MPa.

Table 4.5: Details of the specimens used for the verification of FE model of normal strength CFST

S.No	Sample name	$M_{u\ Exp}$ (kNm)	Avg $M_{u\ Exp}$ (kNm)	$M_{u\ Num}$ (kNm)	$M_{u\ Num}/M_{u\ Exp}$	References
1	RB1-1	29.34	29.34	29	0.988	(Han, 2004)
2	RB2-1	30.16	31.67	32	1.020	
3	RB2-2	32.25				
4	RB2-3	31.69				
5	RB3-1	40.9	41.22	41	0.994	
6	RB3-2	41.54				
7	RB4-1	41.43	42.02	42.5	1.011	
8	RB4-2	42.61				
9	RB5-1	31.4	31.4	32	1.019	
10	RB5-2	31.4				
11	RB6-1	21.1	20.65	21	1.016	
12	RB6-2	20.2				
13	RB7-1	28.4	28.9	29	1.003	
14	RB7-2	29.4				
15	RB8-1	18.4	18.1	18	0.994	
16	RB8-2	17.8				
17	CB12	73.6	73.33	75	1.023	(Lu & Kennedy, 1994)
18	CB13	75.1				
19	CB15	71.3				
20	CB22	146.5	146.5	145	0.989	
21	CB31	210.7	209.67	210	1.001	
22	CB33	210.7				
23	CB35	207.6				
24	CB41	283.8	283	279	0.986	
25	CB45	282.2				
26	CB52	144.7	144.766	145	1.002	
27	CB53	146.7	27.9	27.5	0.985	(Uy, 2000)
28	CB55	142.9				
29	HS6	27.9				
30	HS12	42.4	42.4	43	1.014	
31	NS6	62.6	62.6	61	0.974	
32	NS12	103.5	103.5	104	1.004	
33	NS18	153	153	150	0.980	
35	NMC-1	10.06	10.01	10.07	1.005	(Soundararajan & Shanmugasundaram, 2008)
36	NMC-2	9.57				
37	NMC-3	10.4				
38	FAC-1	9.9	10.1233	10.07	0.994	
39	FAC-2	10.07				
40	FAC-3	10.4				

Note: $M_{u\ Num}$ is the flexural capacity of CFST beam calculated numerically, $M_{u\ Exp}$ is the flexural capacity of CFST beam obtained from test results, respectively.

4.3.1.2 Ultimate Flexure Strength of High Strength CFST Beams

The following experimental investigations reported herein were used to verify the FE model for high strength CFST beams subjected to flexure load only. The comparison between experimental and FE ultimate flexural capacity of beams is shown in Table 4.6. The experimental details of square specimens (SVA-1, SVA-2, SVB-1, SVB-2, and SB1-6-1-2) tested by Han (2006) are given in Table 4.6. The depth-to thickness ratio of square specimens ranged from 47 to 105 while the length of the specimens was in the range of 840 to 1800mm. Most of the beams were tested using two-point loading while few were tested using one-point loading. All the beams were constructed by filling with high strength concrete in steel tubes having compressive strength of 50, 60 and 80 MPa respectively whereas the modulus of elasticity of concrete was in the range of 31.9 to 42.6 GPa. For steel, two different types of steel having a yield strength of 235 and 282 MPa were used. The ultimate strength and modulus of elasticity of steel tube was about 340 MPa and 200GPa respectively.

The specimen numbered B-160-1 to B-320-2 (Table 4.6) were tested by Wang and Han (2014). Infill concrete having compressive strength of 78 MPa and modulus of elasticity of 37.2 GPa was used. All the beams having length of 4000mm (clear span of 3800mm) were tested under two-point loading conditions. Two of the tested beams were square in shape while the rest were rectangular. For all the beams, the width and thickness of the beams were kept constant. For steel tube, the yield strength, ultimate strength and modulus of elasticity were 363, 530 and 2.03×10^5 MPa respectively.

Guler et al. (2012) performed 8 experiments on square CFST beams filled with ultra-high strength concrete (compressive strength 150 MPa). The yield strength of the steel tubes was in the range of 288-266 MPa. Jiang et al. (2013) performed 4 tests on CFST filled with high strength concrete having compressive strength of 56 MPa while the yield strength of the steel tubes was 400 MPa. Further experimental details are shown in Table 4.6.

Table 4.6: Details of the specimens used for the verification of FE model of high strength CFST

S.No	Sample name	$M_{u\ Exp}$ (kNm)	Avg $_{Mu\ Exp}$ (kNm)	$M_{u\ Num}$ (kNm)	$M_{u\ Num}/M_{u\ Exp}$	References
1	SVA-1	10.83				
2	SVA-2	9.96	10.37	10.3	0.99	
3	SSCA-1	10.33				
4	SVB-1	42.3				
5	SVB-2	54.94	51.31	51.01	0.99	
6	SSCB-1	56.7				
7	SB1-1	31.9	29.70	29.6	1.00	
8	SB1-2	27.5				
9	SB2-1	29.4	29.40	29.6	1.01	(Han et al., 2006)
10	SB2-2	25.9	25.90	25	0.97	
11	SB3-1	30.2	29.80	29.6	0.99	
12	SB3-2	29.4				
13	SB4-1	37.6	40.35	39	0.97	
14	SB4-2	43.1				
15	SB5-1	37.9	37.90	39	1.03	
16	SB5-2	41.7	41.70	39.5	0.95	
17	SB6-1	49.8	48.15	48	1.00	
18	SB6-2	46.5				
19	BF2.5-1	9.92				
20	BF2.5-2	10.42	9.87	9.6	1.03	
21	BF2.5-3	9.26				
22	BF3-1	10.67				(Guler et al., 2012)
23	BF3-2	10.9	10.93	10.5	1.04	
24	BF3-3	11.21				
25	BF4-1	17.03	17.19	17.2	1.00	
26	BF4-2	17.35				
27	B09	215.5	213.95	210.2	0.98	(Gho & Liu, 2004)
28	B10	212.4				
29	B11	219.8	218.75	218.01	1.00	
						(Wang et al., 2014)
30	B12	217.7				
31	B160-1	59.3	59.40	60.23	1.01	
32	B160-2	59.5				(Jiang et al., 2013)
33	B240-1	136.8	140.85	141.67	1.01	

4.3.1.3 Moment Curvature Curves

The moment curvature curves for normal and high strength CFST beams calculated from FE model were compared with experimental results provided by Wang et al., (2014) and Lu & Kennedy (1994). The comparison for B240-2 sample tested by Wang et al., (2014) is shown in Figure 4.10. The moment curvature curve obtained from experimental results and predicted by FE model is in good agreement. The maximum difference between experimental and numerical values is only 1%.

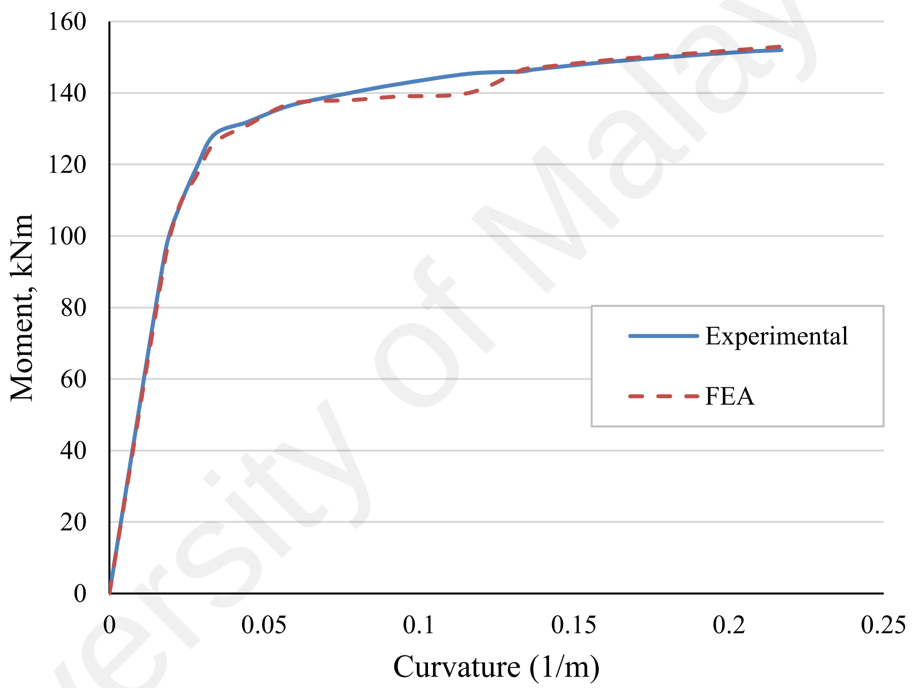

Figure 4.10: Moment curvature curve of FE model and experimental test (B240-2)

Figure 4.11 shows the comparison between the FE model and experimental moment-curvature curve for specimen CB33 tested by (Lu & Kennedy, 1994). The deflections curves obtained from FE model are almost identical to that of experimental mid-span load deflection curve. The ultimate strength predicted by FE model differs only by 2% to that of experimental value. It shows that the FE model can accurately predict the flexure load-deflection and ultimate capacities of normal and high strength CFST beams.

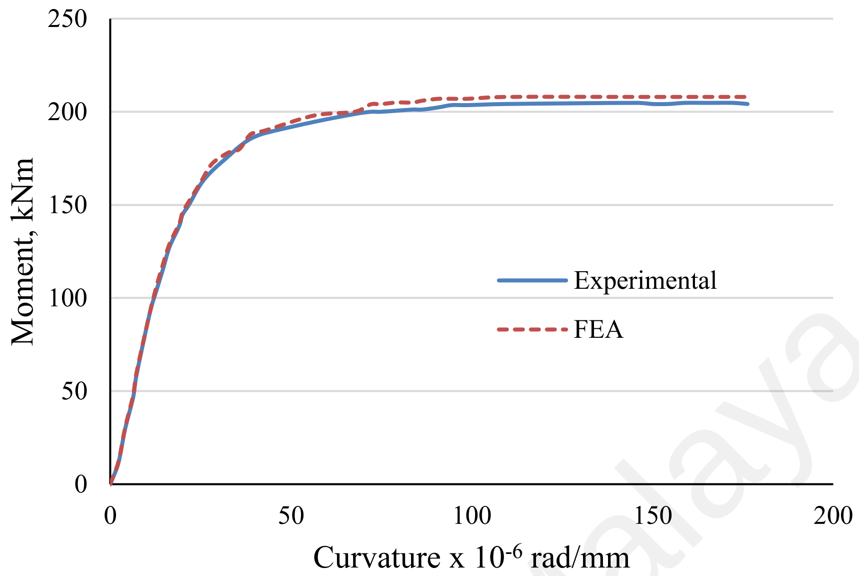

Figure 4.11: Moment curvature curve comparison of FE model and experimental test sample CB-33

The comparison of mid-span deflection between FE model and experimental specimen NMC-1 tested by Soundararajan & Shanmugasundaram (2008) is shown in Figure 4.12. The results show that FE model predicts accurately the load-deflection curve up to ultimate load. However, some deviation from the experimental load-deflection curve occurs due to the uncertainty in material properties and initial imperfections.

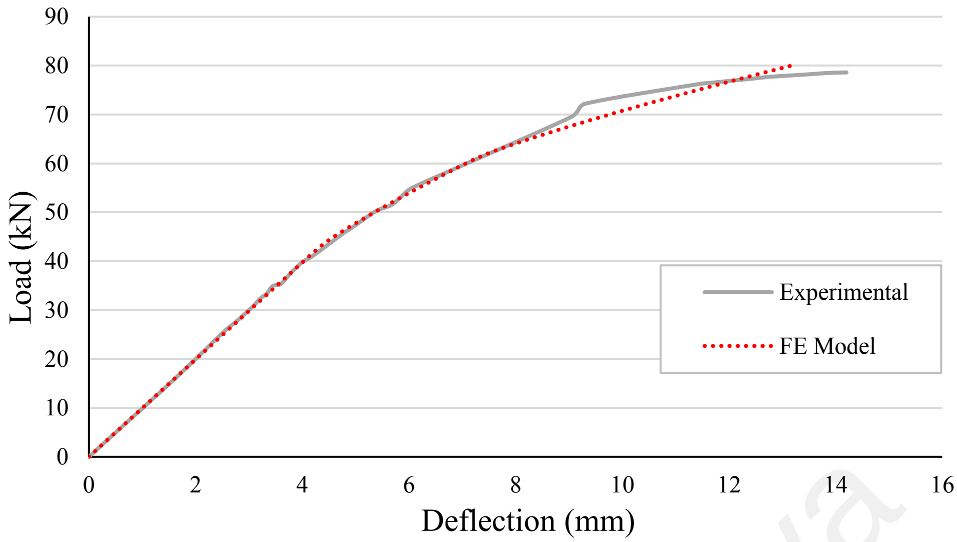

Figure 4.12: Load deflection curve comparison of experimental and FE model

4.3.2 Verification of the FE Model Experimental Results from Literature

Figure 4.13 shows the comparison between the FE model and experimental moment-curvature curve for specimen ROCFST. The moment-curvature curves obtained from FE model are almost identical to that of experimental moment-curvature curve. The ultimate strength predicted by FE model differs only by 1.5% to that of experimental value. It shows that the FE model can accurately predict the flexure moment-curvature and ultimate capacities of normal and high strength CFST beams.

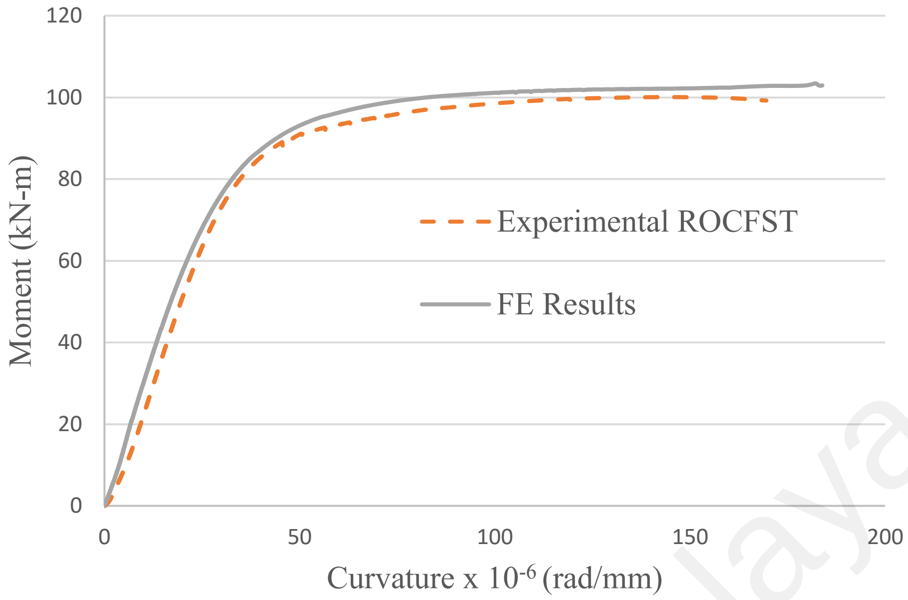

Figure 4.13 Moment-curvature curve comparison of FE model and experimental test sample ROCFST

Figure 4.14 shows the comparison between the FE model and experimental moment-curvature curve for specimen SOCFST. The ultimate strength predicted by FE model differs only by 1.8% to that of experimental value.

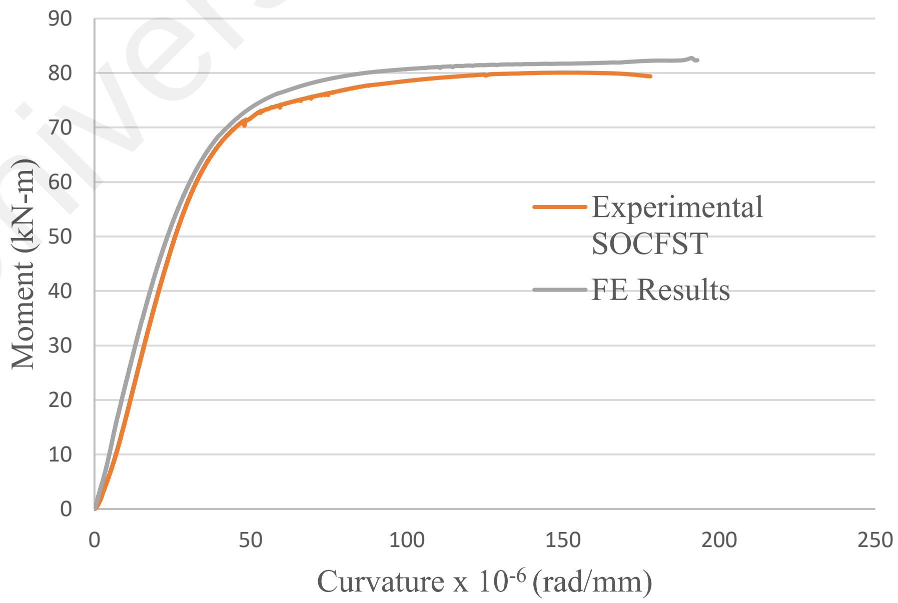

Figure 4.14: Moment-curvature curve comparison of FE model and experimental test sample SOCFST

Figure 4.15 shows the comparison between the FE model and experimental moment-displacement curve for specimen ROCFST. The ultimate strength predicted by FE model differs only by 1.5% to that of experimental value. It shows that the FE model can accurately predict the flexure moment-deflection and ultimate capacities of normal and high strength OCFST beams. As the behaviour of OCFST and NCFST beams is similar at ambient temperature, therefore in-filled concrete type is not mentioned in the parametric studies for ambient temperature in next section.

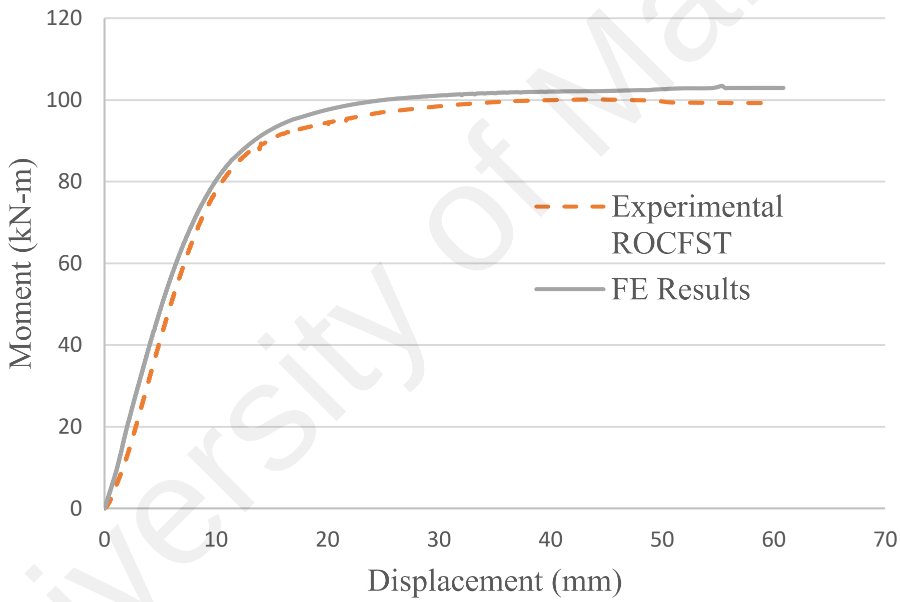

Figure 4.15:Moment-displacement curve comparison of FE model and experimental test sample ROCFST

4.4 Parametric Study for NCFST at Ambient Temperature

An extensive parametric study was performed to investigate the influences of depth-to-thickness ratio (20-200), concrete compressive strengths (2-100 MPa) and steel yield strengths (235-400 MPa) on the fundamental behaviour of CFST beams under flexure load only. To evaluate the individual effect, only one variable was considered at a time.

For parametric study, the length of the beam was kept as 1200mm. We would like to mention here that the length and the cross-sectional dimensions of steel selected for the parametric study are based on their availability in the market and recommendations of International code AISC (2005). Moreover, various researchers have used these dimensions in their experimental investigations (Han et al., 2006; Jiang et al., 2013; Wang et al., 2014; Yang & Han, 2006a; Yang & Ma, 2013). For example, in references (Yang & Ma, 2013) and (Yang & Han, 2006a), the length of specimen was 1200 mm. In (Jiang et al., 2013), the researchers used BxD as 100x200, (Han et al., 2006) used 200x200 and (Wang et al., 2014) used 160x160. Hence, the results of this parametric study can be applied to the practical structures. The details are given in the following subsections.

4.4.1 Effect of Depth to Thickness Ratio

The main objective of this parametric study was to evaluate the effects of different Depth-to-thickness ratio (D/t) of CFST beams on its structural behaviour and ultimate bending moment capacity. For this purpose, five different D/t ratios in the range of 200-20 were selected. The D/t ratio was changed by increasing the thickness of the steel tube. To represent the behaviour of square beams, the Depth-to-width (D/B) ratio of five samples was kept as 1 while for rectangular beams; the D/B ratio of the remaining 5 samples was kept as 2. The yield and tensile strengths of steel tubes were 275 MPa and 430 MPa, respectively while the modulus of elasticity was taken as 200 GPa. For in-filled concrete, the compressive strength and modulus of elasticity were 50 MPa and 29000 MPa, respectively. The detailed dimensions and designations of the FE model are presented in Table 4.7 while the rest of the parameters and boundary conditions were same as mentioned earlier in Section 3.4.

Table 4.7: Main properties for CFST models used for studying the effect of D/t ratio

Description	BxDxt (mm)	D/t	a/d	As (mm^2)	D/B	FEA (kNm)
Rectangle	100x200x1	200	2	600	2	21
	100x200x2	100	2	1200	2	39.375
	100x200x4	50	2	2400	2	76.23
	100x200x6	33.33	2	3600	2	110.5335
	100x200x10	20	2	6000	2	169.1163
Square	200x200x1	200	2	800	1	16
	200x200x2	100	2	1600	1	30
	200x200x4	50	2	3200	1	58.08
	200x200x6	33.33	2	4800	1	84.216
	200x200x10	20	2	8000	1	128.8505

The influence of D/t ratio of CFST on the flexure capacity for rectangular and square CFST beams is illustrated in Figure 4.16. By increasing D/t ratio from 20 to 200 (10 times), the ultimate bending moment capacity reduced from 169 to 21 KN-m (almost 8 times) for rectangular CFST beams. Similar observations are applicable to square CFST beams. The reduction in ultimate bending moment capacity is attributed to the fact that the beam having larger D/t ratio has a lesser area of steel. Furthermore, based on beams B/t and D/t ratios, they are categorized in different codes as compact and non-compact. The beams having higher D/t ratios are categorized as non-compact and may fail due to local buckling, which reduces the ultimate load carrying capacity of the beam. The limit ratios of wall dimension to wall thickness for which local buckling is prevented according to different codes are given in Table 4.8. It was observed from analysis that changing the D/t ratio of rectangular and square beams has no significant effect on the initial stiffness of the member. Similar conclusions were drawn by author Chen and Wang (Chen et al., 2016), after performing experiments on thin-walled walled dodecagonal section double skin CFST (Chen et al., 2016) and circular CFST (Chitawadagi & Narasimhan, 2009) under bending.

Table 4.8: Limit ratios of wall dimension to wall thickness for which local buckling is prevented

Parameters	EC 3(2005)			GB50017-2003			AISC (2010)		
f_y (MPa)	235	355	400	235	355	400	235	355	400
Hollow B/t	33	26.9	25.3	40	32.6	30.7	32.7	26.6	25.1
Hollow D/t	72	58.6	55.2	80	65.1	61.4	109.7	89.3	84.1
CFST D/t limit	52	42.4	39.9	60	48.9	46	66	53.7	50.6

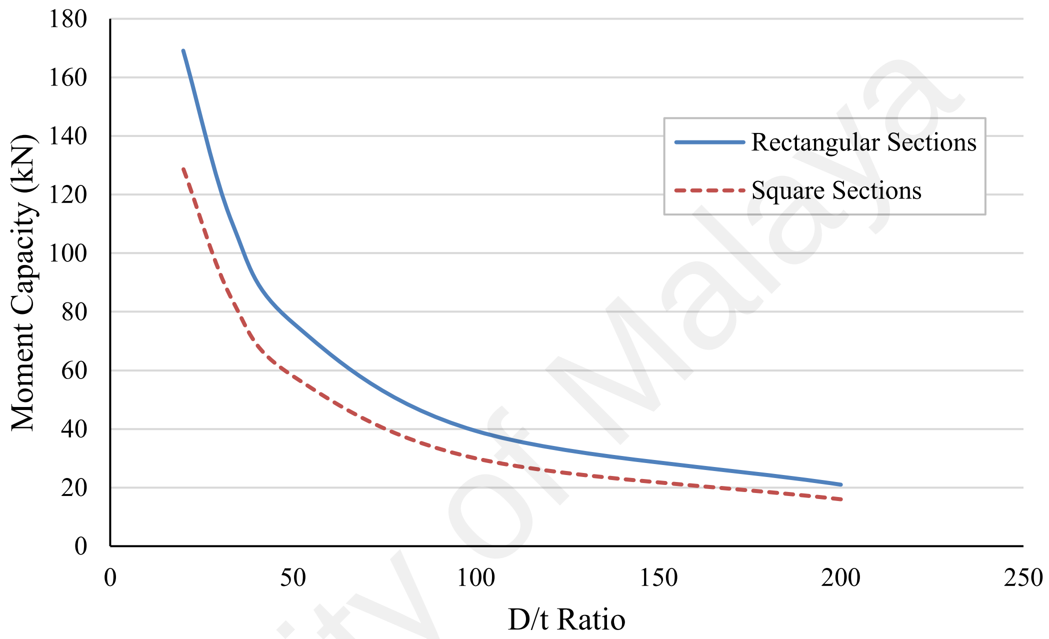

Figure 4.16: Ultimate Moment capacity of square and rectangular CFST with different D/t ratios

4.4.2 Effect of Grade of Concrete

In CFST beams, the infill concrete is divided into tensile and compressive zones and it behaves differently when compared with the infill concrete in CFST columns. The effect of compressive strength of concrete on the behaviour of CFST beams was evaluated by selecting wide range of compressive strengths of concrete (2-100 MPa). Two different steel tube wall thicknesses were selected. The yield and tensile strengths of steel tubes were 275 MPa and 430 MPa, respectively while the modulus of elasticity was taken as 200 GPa. The details of the rectangular specimens with D/t ratio of 40 and 80 are given in Table 4.9.

Table 4.9: Main properties for CFST models used for studying the effect of compressive strength

Rectangle with D/t=80						
BxDxt (mm)	D/t	a/d	D/B	f_c (MPa)	f_y (MPa)	FEA (kNm)
100x200x2.5	80	2	2	2	275	28.15475
100x200x2.5	80	2	2	4	275	26.60703
100x200x2.5	80	2	2	8	275	26.38701
100x200x2.5	80	2	2	16	275	27.97875
100x200x2.5	80	2	2	32	275	31.67841
100x200x2.5	80	2	2	50	275	35.05472
100x200x2.5	80	2	2	60	275	36.57831
100x200x2.5	80	2	2	80	275	39.03427
100x200x2.5	80	2	2	100	275	40.88124
Rectangle with D/t=40						
BxDxt (mm)	D/t	a/d	D/B	f_c (MPa)	f_y (MPa)	FEA (kNm)
100x200x5	40	2	2	2	275	67.3174
100x200x5	40	2	2	4	275	61.83775
100x200x5	40	2	2	8	275	58.18678
100x200x5	40	2	2	16	275	57.29797
100x200x5	40	2	2	32	275	60.2312
100x200x5	40	2	2	50	275	64.52531
100x200x5	40	2	2	60	275	66.83401
100x200x5	40	2	2	80	275	69.02213
100x200x5	40	2	2	100	275	71.07891

The results of load deflection curve for different concrete infilled strength are shown in Figure 4.17. For infill concrete having strength less than 8 MPa, it was not found to increase the overall strength of beam because of poor composite connection between steel and concrete. The ultimate strength capacity increases with the increase in strength of infilled concrete. The percentage increase in strength capacity per unit increase in concrete strength is different for different cross-sections and is dependent on the compactness of steel tube (Nakamura et al., 2002). According to the available literature, the minimum compressive strength of concrete required to enhance the ultimate moment capacity of CFST beams is directly proportional to (B-2t)/t ratio (Hunaiti, 1997). For D/t ratio equal to 40, when the compressive strength of concrete increased from 60 to 80 MPa and 100 MPa, the ultimate flexural strength increased by only 3% and 6% respectively. Whereas, for D/t ratio equal to 80, the flexural capacity increased up to 6% and 11% respectively. This is due to the lesser contribution of infill concrete to the bending strength of CFST as D/t ratio increases. It can be seen from Table 4.9 that with an increase in the compressive strength of concrete from 8 MPa to 100 MPa, the ultimate strength of CFST beam increased up to 40% (from 40 to 71 kN-m). This is due to composite action between steel tubes and concrete that controls the inward buckling of the steel shell. The increase in the percentage of ultimate strength of CFST beams is more in the case of thinner sections as compared to thicker sections. Moreover, the ultimate moment capacity of steel sections with higher breadth-to-depth ratios is less affected by compressive strength of infill concrete. This is due to the lesser contribution of infill concrete to the bending strength of CFST as breadth-to-depth ratio increases. However, low strength concrete can be used in the CFST beams having a mechanical device like shear connectors to enhance their flexure behaviour (Probst et al., 2010). It was also observed that the increase in the compressive strength of concrete resulted in very low improvement in the initial stiffness of the square CFST beams. Thus, it is concluded that ultimate flexural strength and ductility of CFST beams can be controlled by controlling the mechanical properties of infill concrete. Similar observations were made by a number of researchers conducting an experimental study on the behaviour of circular CFST (Chitawadagi & Narasimhan, 2009) and concrete filled double skin tubular circular deep beams (Uenaka & Kitoh, 2011) under flexural load.

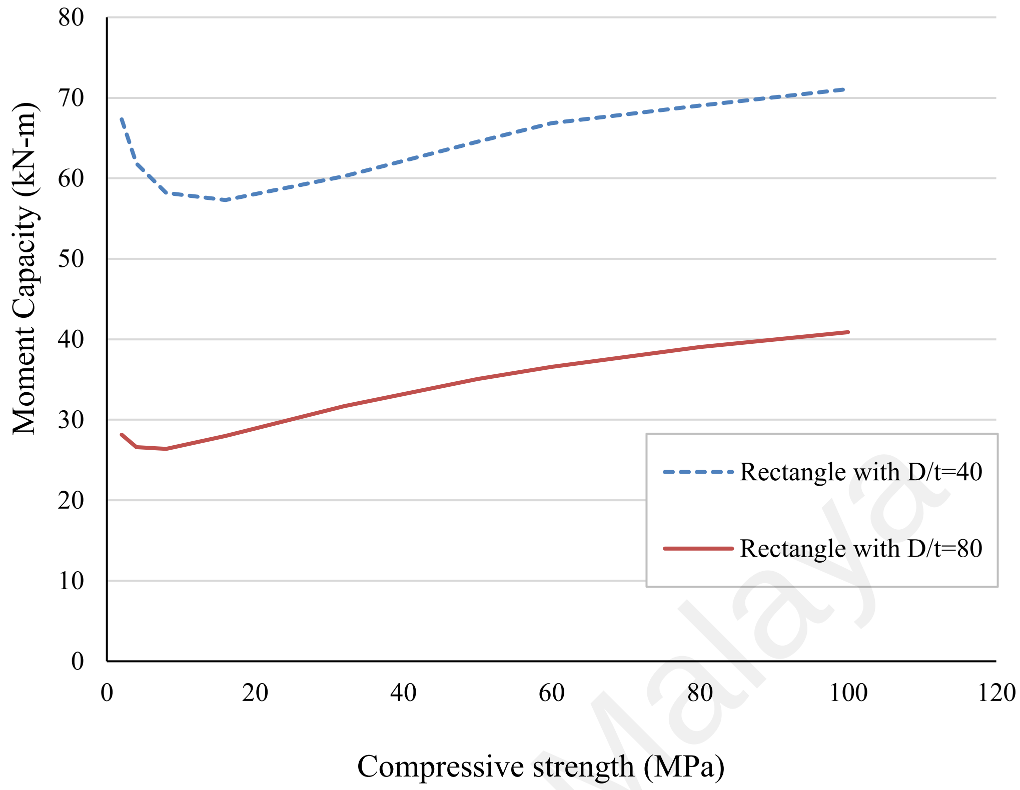

Figure 4.17: Load-deflection curve for different compressive strengths of concrete

4.4.3 Influences of Steel Yield Strengths

The square and rectangular CFST beams with different steel yield strengths and with same D/t ratio of 40 were analysed. The Young's modulus of steel was 200 GPa while the steel tubes were infilled with 50 MPa concrete having a modulus of elasticity of 32600 MPa. The loading conditions and length of the beam were same as mentioned in previous section. The rest of the parameters along with ultimate moment capacity are given in Table 4.10.

Table 4.10: Main properties for CFST models used for studying the effect of yield strength

Shape	BxDxt (mm)	f_y (MPa)	f_u (MPa)	FEA (kNm)
Rectangle	100x200x5	235	380	52.74699
	100x200x5	275	410	61.21541
	100x200x5	300	430	66.43432
	100x200x5	355	450	77.88625
	100x200x5	400	490	87.24014
Square	DxBxt (mm)	f_y (MPa)	f_u (MPa)	FEA (kNm)
	200x200x5	235	380	75.87616
	200x200x5	275	410	88.02244
	200x200x5	300	430	95.56252
	200x200x5	355	450	114.1816
	200x200x5	400	490	127.8669

Figure 4.18 illustrates the influence of steel yield strengths on the ultimate moment capacity of square and rectangular beams. The ultimate flexure strength of square CFST beams was found to increase significantly with an increase in the yield strength of steel. By increasing the yield strength of steel from 235 MPa to 300 MPa and 400 MPa, the ultimate flexure load of the square CFST beam was found to increase by 22% and 55% respectively. The rectangular CFST beams also showed similar behaviour. Similar conclusions were drawn by Duarte et al. (2016) for rubberized CFST members. We would like to mention here that during the analysis, it was observed that the yield strength of steel does not influences the initial stiffness of beams.

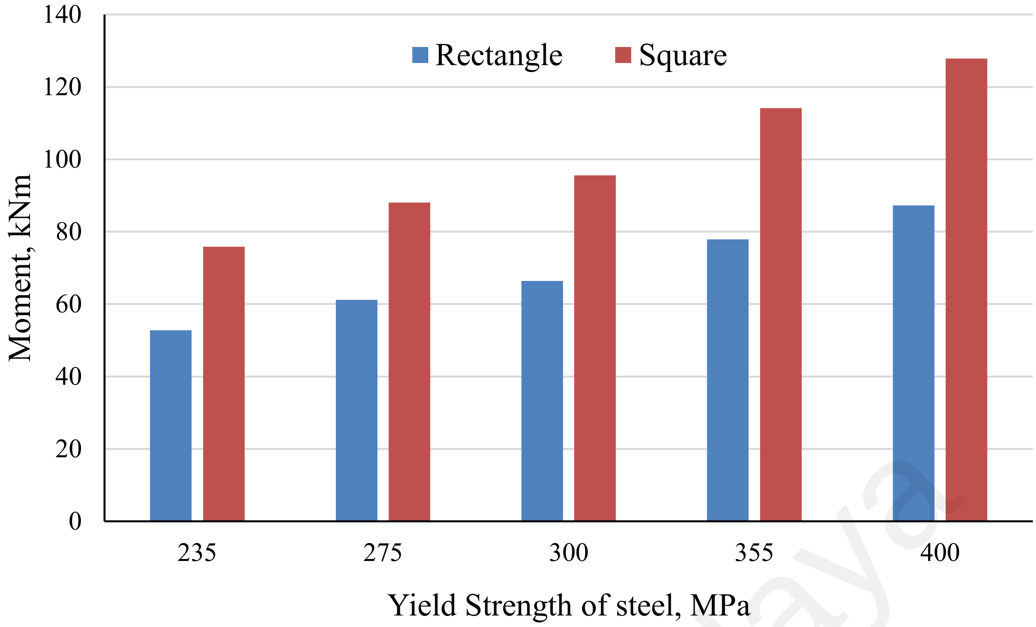

Figure 4.18: Comparison of ultimate flexural capacities of CFST members having different steel yield strength

4.4.4 Effect of D/B Ratio

The ultimate bending strength of CFST beams depends on Depth-to-width (D/B) ratio. Hence, the effect of D/B ratio on the ultimate moment/load capacity and load deflection curves of CFST beams were determined. The dimensions of the beams were selected in such a manner that the total amount of steel remains constant. For this purpose, the width and depth of steel tubes were only changed. The calculated values of D/B ratios_of the beam sections were 0.6, 0.8, 1, 1.67 and 2. The yield and tensile strengths of steel tubes were 345 MPa and 510 MPa, respectively while the modulus of elasticity was about 200 GPa. Three different compressive strengths (40 MPa, 60MPa and 80MPa) and modulus of elasticity of the in-filled concrete were selected. Further details are given in Table 4.11.

Table 4.11: Main properties for CFST models used for studying the effect of D/B ratio

BxDxt (mm)	D/t	a/d	D/B	f_y (MPa)	Mu for f_c=40 (kNm)	Mu for f_c=60 (kNm)	Mu for f_c=80 (kNm)
200x120x5	24	2	0.6	345	43.19899	44.80096	46.03551
178x142x5	28.4	2	0.8	345	50.53408	52.56008	54.08612
160x160x5	32	2	1	345	56.16774	58.54131	60.3231
120x200x5	40	2	1.67	345	67.93146	71.06645	73.50584
107x214x5	42.8	2	2	345	71.47325	74.81499	77.47927

The influence of D/B ratio of CFST steel tube on the ultimate bending moment capacity of CFST beams is shown in Figure 4.19. Irrespective of the value of compressive strength, the ultimate flexural capacity of beam increased significantly with the increase in D/B ratio. This is attributed to the fact that the beam having larger D/B ratio has a large moment of inertia and have high resistance to local and global buckling, which in turn, increased the ultimate load carrying capacity of the beam. When the D/B ratio increased from 0.6 to 2, the ultimate capacity of members is increased by more than 50%. During the analysis, it was observed that by decreasing the D/B ratio of the CFST beams, their initial stiffness increased. In some cases, the stiffness of the member increased by almost two times.

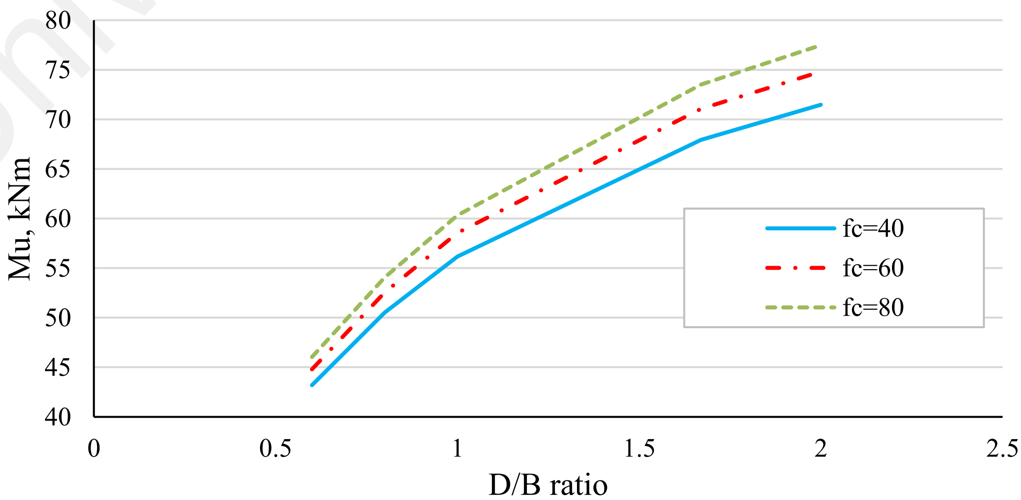

Figure 4.19: Capacity of different models having different D/B ratios and strengths

4.4.5 Effect of a/d Ratio

The behaviour of reinforced concrete deep beam is different from normal reinforced beam due to lower shear span-to-depth ratio. RC deep beams generally fail due to shear cracking as the shear crack starts from the beam web (having equal distance from loading point and support) and propagates in both directions towards loading point and support. As the cracks are caused by tensile forces and due to the small angle between stirrups and cracks, the stirrups are not effective in preventing the propagation of shear cracks. Similarly, the steel tube in CFST members' acts as a continuous stirrup to resist the shear stresses in the shear span. However, due to continuity in the steel tube, it is more effective than stirrups.

To study the effect of shear span-to-depth ratio on the performance of rectangular and square CFST beam, different shear span-to-depth ratio ranging from 1 to 8 and with the same amount of steel and D/t ratio were analysed as shown in Table 4.12. The thickness of steel tube wall was kept as 5 mm. The steel yield and ultimate strengths were 345 and 510 MPa, respectively while the modulus of elasticity was 200 GPa. For infilled concrete, the compressive strength was 60 MPa and modulus of elasticity was 32600 MPa.

Table 4.12: Details of models used to study the effect of a/d ratio

Shapes	BxDxt (mm)	D/t	a/d	D/B	f_y (MPa)	FEA (kNm)
Rectangle	100x200x5	40	1	2	345	80
	100x200x5	40	3	2	345	80
	100x200x5	40	5	2	345	80
	100x200x5	40	7	2	345	80
	100x200x5	40	8	2	345	80
Square	200x200x5	40	1	1	345	110
	200x200x5	40	3	1	345	110
	200x200x5	40	5	1	345	110
	200x200x5	40	7	1	345	110
	200x200x5	40	8	1	345	110

The load-deflection curves for rectangular cross-sections are shown in Figure 4.20. The load-deflection curve is independent of the shear span-to-depth ratio. It shows that by reducing the shear span-to-depth ratios from 1 to 8 have no significant effect on the stresses produced in the concrete and hence the same ultimate strength was obtained. As the shear force in CFST beam in the shear span is mostly resisted by steel, the stresses in concrete remain lower, hence, no shear cracks appear in the concrete. Therefore, it can be concluded that the variation of shear span-to-depth ratio has no significant effect on the performance of CFST beams.

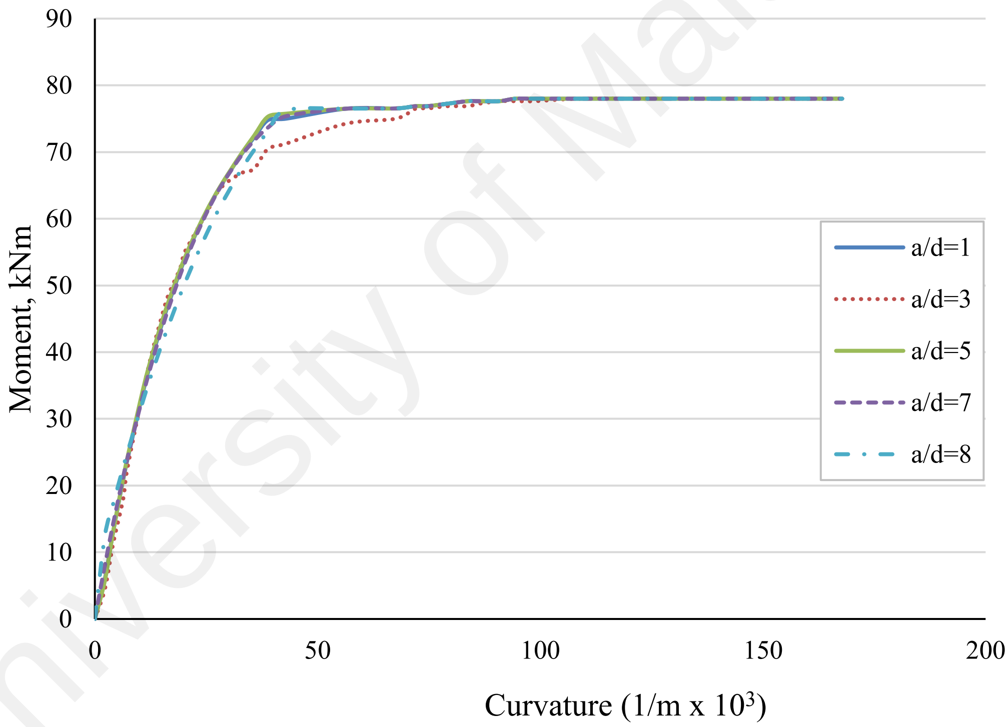

Figure 4.20: Moment curvature curve of samples having different a/d ratios

4.5 Comparison of Moment Capacities with Design Codes

The ultimate flexural load capacities of all the experimental samples used for verification as well as all FE models were compared with four different codes (EC4 (1994), AISC-LRFD (1999), GB50936-2014 (2014) and CIDECT. A summary of the range of values for which codes can be used and method for calculating important parameters are shown in Table 4.13. The procedure for calculating the flexural load bearing capacity of CFST beams is explained in the following subsections.

Table 4.13: Comparison of limitations of different codes

Code/Property	EuroCode	AISC-LRFD	CIDECT	HAN DBJ/T13-51
f'_c (MPa)	20-50	--	20-50	20-80
f_y (MPa)	460	<380	235-460	200-500
Stiffness, *K*	EsIs+0.6EcIc	EsIs+0.8EcIc	EsIs+EcIc	EsIs+0.8EcIc
D/t	52	2.26*(Es/fy)	<52*(235/fy)^1/2	60

4.5.1 Eurocode (BS EN 1994-1-1:2004)

As mentioned in Eurocode (Eurocode, 2004), the ultimate capacity of CFST columns subjected to combined bending and compression is determined from an interaction curve. An interaction curve between moment and axial compression can be obtained for a column by assuming several possible positions of neutral axis within the cross-section, and then determining the moments and internal forces from the resulting plastic stress blocks. In the absence of axial load and steel reinforcement in CFST, the equation for the moment becomes,

$$M_{pl,Rd} = f_{yd}\left(W_{pa} - W_{pan}\right) + 0.5 f_{cd}\left(W_{pc} - W_{pcn}\right) \quad \text{……………………….(4.8)}$$

$$W_{pc} = \frac{(b-2t)(h-2t)^2}{4} \quad \text{……………………………………………………….(4.9)}$$

$$h_n = \frac{A_c f_{cd} - A_{sn}(2f_{sd} - f_{cd})}{2b f_{cd} + 4t(2f_{yd} - f_{cd})} \quad \text{………..……………………………………………(4.10)}$$

$$W_{pan} = 2t h_n^2 \quad \text{……………………………………………………….(4.11)}$$

$$W_{pcn} = (b-2t)h_n^2 - W_{psn} \quad \text{……………………………………………(4.12)}$$

Where, h_n is the distance from compression region to the centre-line of the CFST cross-section, W_{pc} and W_{pa} are the plastic section modulus for concrete and steel respectively, W_{pan} and W_{pcn} are the plastic section modulus of the corresponding components within the region of $2h_n$ from the centre-line of the composite cross-section.

According to Eurocode design rules, for all the experimental and FE model samples, the mean, standard deviation and Co-efficient of Variation (COV) were found to be of 0.79, 0.08 and 0.12 respectively. The maximum value of 1 was obtained for the square sample (S-150-2.0) (Jiang et al., 2013) while the minimum value of 0.42 was also obtained for the SSCB-1 square sample (Han et al., 2006). Both maximum and minimum values are for high strength CFST having a square cross-section. Hence, to get a safe and economical design, the design rules need to be improved further.

4.5.2 AISC-LRFD-1994

The flexural strength of CFST beams and columns were calculated according to LRFD (1994) by only taking into account the steel hollow section. The Plastic moment capacity of a CFST beam was evaluated as;

$$M = Zf_y \qquad \text{...(4.13)}$$

Where, Z is the plastic section modulus and f_y is the yield strength of steel tube.

According to AISC-LRFD design rules, for all the experimental and FE model samples, the mean, standard deviation and COV were found to be 0.75, 0.08 and 0.13 respectively. The maximum and minimum values of M/Mc (0.99 and 0.54) were obtained for S-150-3.0 and BF4-1 samples, which were tested by (Jiang et al., 2013) and (Guler et al., 2012) respectively.

4.5.3 CIDECT-1995

The Ultimate moment capacity for CFST beams according to the CIDECT (Wardenier et al., 1995) can be defined as;

$$M_{u,CIDECT} = M_{ratio} \frac{D^2B-(D-2t)^2(B-2t)}{4} f_y \quad \text{...(4.14)}$$

Where, M_{ratio} is a ratio of the bearing capacity of the composite hollow section to that of the hollow section, D, t and B is the depth, thickness, and width of composite section respectively and f_y is the yield stress.

According to CIDECT design rules, for all the experimental and FE model samples, the mean, standard deviation and COV were found to be 0.85, 0.08 and 0.11 respectively. The maximum value of M/Mc was obtained for the sample SB4-1 (Han et al., 2006) and the minimum value of M/Mc was obtained for the sample BF4-1 (Guler et al., 2012).

4.5.4 GB50936 (2014)

In GB50936 (2014), the ultimate moment capacity of the CFST beam is given by;

$$M_u = \gamma_m f_{scy} W_{scm} \quad \text{...(4.15)}$$

$$f_{scy} = (1.18 + 0.85\xi) f_{ck} \quad \text{...(4.16)}$$

$$W_{scm} = \frac{B^3}{6} \quad \text{...(4.17)}$$

$$\xi = \frac{A_s f_{yk}}{A_c f_{ck}} \quad \text{...(4.18)}$$

$$\gamma_m = 1.04 + 0.48\ln(\xi + 0.1) \quad \text{...(4.19)}$$

Where, M_u is the moment capacity of the CFST beam, f_{scy} is the nominal yielding strength of the steel tube, W_{scm} is the section modulus of CFST cross-section, ξ is the constraining factor, and γ_m is the flexural strength index. However, GB50936 (2014) model is only valid for D=100-2000 mm; f_{scy}=200-500 MPa and f_{ck}=20-80 MPa and cannot be used for ultra-high strength concrete.

According to GB50936 (2014), for all the experimental and FE model samples, the mean, standard deviation and COV were found to be of 0.99, 0.08 and 0.10 respectively. This shows that GB50936 (2014) values are the best in comparison to all codes. The maximum value of M/M_c was obtained for the sample SVA-2 (Han et al., 2006) and the minimum value of M/Mc is obtained for the sample B240-2 (Wang et al., 2014).

By comparing Table 4.14 and Figure 4.21, it can be concluded that overall GB50936 (2014) model predicts better results followed by CIDECT, Eurocode, and AISC respectively. However, upon further analysis of the data, it was observed that it is not safe as it gives higher values up to 20% for some samples. The CIDECT design method is not safe to use in case of high strength square CFST samples while AISC values were lower than the rest of the codes values because it neglects the contribution of concrete. As far as Eurocode is concerned, it considers the effect of concrete to the contribution of ultimate capacity but neglects the composite action between steel tube and concrete. Upon further categorizing the data, GB50936 (2014) gives the closest as well as safe values in the case of high strength concrete filled in a rectangular steel tube. However, for low strength concrete filled steel tubes i.e., f'c<10 MPa, it over-predicts the value up to maximum of 30%. Hence, irrespective of the shape of CFST members (square or rectangular), it cannot be used for low strength concrete filled CFST. Similarly, AISC is the best to be used for high strength concrete filled steel square steel tubes but it is not good for normal strength concrete. This conclusion is not in line with reference (G. Li et al., 2017) due to the reason that the authors used high strength steel tube, however, in this research, high strength tube was not considered. Eurocode, being overall safe for normal strength CFSTs, needs to consider the combined effect of steel and concrete in calculating the ultimate bending capacity of CFST, which is more prominent in high strength rectangular CFST.

Table 4.14: Average, maximum and minimum values from different code comparison

Average of (M/Mc)				
-	Euro	AISC	CHINA	CIDECT
All Rectangular Samples	0.8	0.74	0.94	0.84
All Square Samples	0.81	0.77	1.03	0.86
Rectangular High Strength CFST	0.75	0.71	0.96	0.83
Square High Strength CFST	0.73	0.72	1.05	0.86
Rectangular Normal Strength CFST	0.82	0.76	0.92	0.85
Square Normal Strength CFST	0.89	0.82	1.01	0.87
All High strength CFST	0.74	0.72	1.03	0.85
All Low strength CFST	0.86	0.8	0.98	0.86
All samples	0.8	0.76	1	0.86
Maximum of M/Mc				
All Rectangular Samples	0.99	0.95	1.14	1.07
All Square Samples	1	0.99	1.4	1.12
Rectangular High Strength CFST	0.99	0.95	1.03	1.07
Square High Strength CFST	1	0.99	1.28	1.12
Rectangular Normal Strength CFST	0.91	0.86	1.14	0.97
Square Normal Strength CFST	0.96	0.9	1.4	1
All High strength CFST	1	0.99	1.28	1.12
All Low strength CFST	0.96	0.9	1.4	1
All samples	1	0.99	1.4	1.12
Minimum of (M/Mc)				
All Rectangular Samples	0.59	0.57	0.82	0.68
All Square Samples	0.42	0.54	0.86	0.59
Rectangular High Strength CFST	0.59	0.57	0.83	0.68
Square High Strength CFST	0.42	0.54	0.87	0.59
Rectangular Normal Strength CFST	0.72	0.64	0.82	0.72
Square Normal Strength CFST	0.78	0.73	0.86	0.77
All High strength CFST	0.42	0.54	0.83	0.59
All Low strength CFST	0.72	0.64	0.82	0.72
All samples	0.42	0.54	0.82	0.59
M=Moment calculated by FEA or obtained by tests, Mc=Moments calculated by code methods				

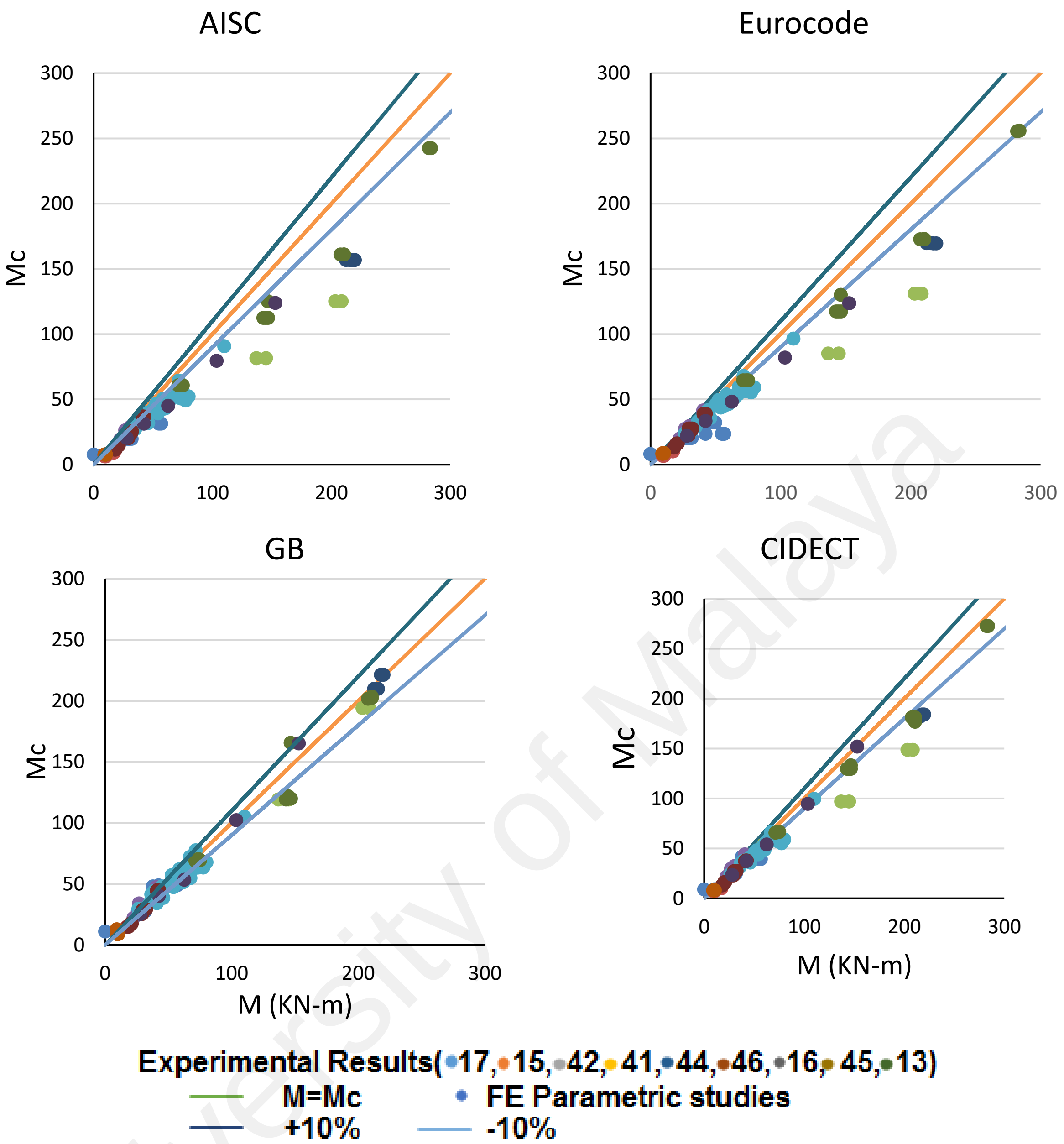

Figure 4.21: Comparison of the flexural bearing capacity

4.6 Test Results and Discussion for Elevated Temperature Testing

4.6.1 Thermal Response

4.6.1.1 Furnace Temperature vs ISO-834 Curve

The comparison of the average temperature of the furnace (T13-T16) and ISO-834 curve is shown in Figure 4.22. The furnace temperature is lower than ISO-834 curve at the start of the test. This kind of delay is common in electric furnace and was reported by several researchers (Craveiro et al., 2016; Romero et al., 2011). Furthermore, the delay was noticed to become larger for the larger furnaces (Luis Laím & João Paulo C. Rodrigues, 2016). At 15 minutes, the difference was more than 10% but less than 20%. Similar difference was reported at 15 minutes by different researchers and is considered acceptable (Laím et al., 2016; Rodrigues & Laim, 2017). The reason for evaluating the difference at 15 minutes is due to the reason that at around 15 minutes, complete furnace is heated properly and the effect of type of furnace and heating media is uninvolved (Huo et al., 2015; Sauca et al., 2016). Furthermore, the temperature of the furnace is similar irrespective of the size and shape of specimen.

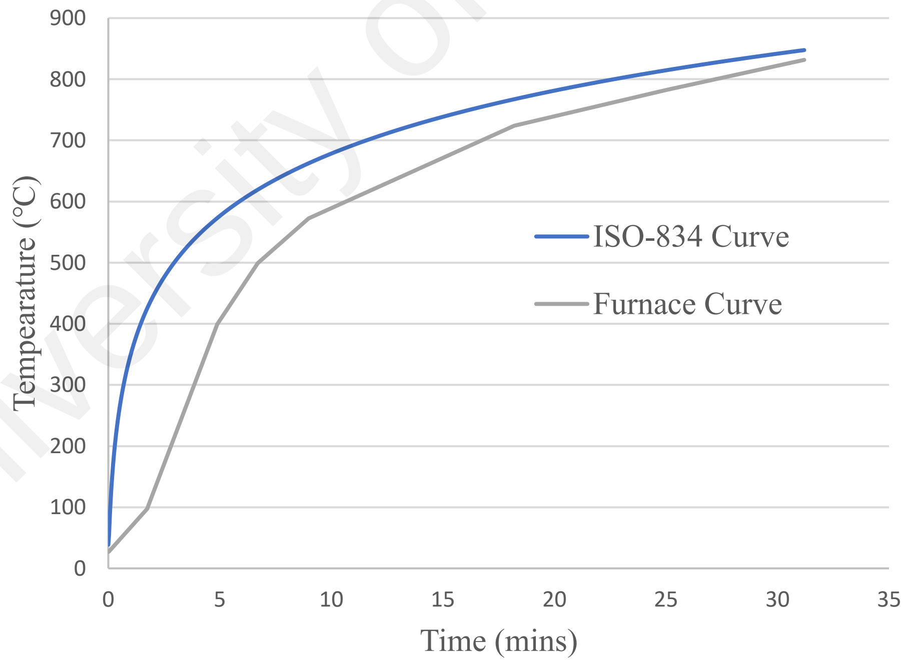

Figure 4.22: ISO-834 and furnace temperature throughout the test

4.6.1.2 General Response of Tested Specimen

The evolution of temperature in one of the tested specimen, SNCFST can be observed in Figure 4.23. T1-T9, located at the outer surface of steel tube, lie close to each other and follow the shape of the furnace curve with a certain delay. In turn, the temperature measured at concrete core (T11) is significantly lower than outer steel temperature. A decrease in heating rate of core concrete is observed between 100°C and 200°C. This decrease is observed by several researchers for CFST members (Espinos et al., 2015) and is due to the heat consumption by water evaporation. T10, closer to the support of the beam and being outside the furnace, register lowest temperature in the beginning of the test and reach to the maximum of 130°C and then stopped at maximum till end of the test. The thermal response of the rest of the specimens was similar except that the infilled concrete observes lower temperature in OCFST.

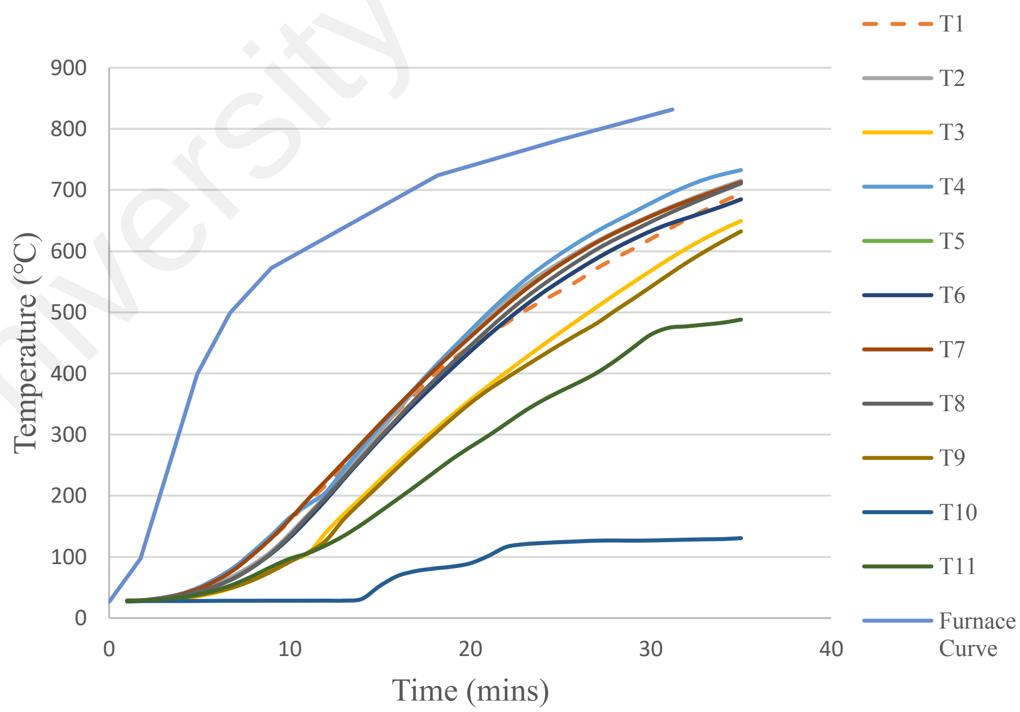

Figure 4.23: Temperature distribution in SNCFST

4.6.1.3 Effect of Type of Infilled Concrete

Figure 4.24 shows the comparison of temperature of infilled concrete of all four specimens. The temperature of the concrete in OCFST is almost 100˚C less than NCFST at 30 minutes. The main reason for this is the porous nature and low thermal conductivity of OPBC aggregate. Furthermore, OPBC is prepared at a high temperature of 1200°C. Also, for the same duration of exposure to fire, the temperature of OPBC is less than NAC as reported in literature (Jumaat et al., 2015).That's why; OCFST performs better than NCFST at elevated temperature. Figure 4.25 shows the comparison of outer steel tube temperature of square NCFST and OCFST. At 30 minutes, the difference in the temperature of steel tube of NCFST and OCFST is about 50°C. This is not always the case in case of CFST infilled with concrete having good thermal behavior. Ana Espinos et al. (2015) used geo-polymer concrete to compare the behavior of geo-polymer concrete filled steel tube columns with NCFST columns. Ana Espinos et al. (2015) concluded that due to the low thermal conductance of geo-polymer concrete the temperature of steel tube of NCFST at a given time is higher than NCFST. Thus, based on the temperature of steel tube and infilled concrete temperature, it can be concluded that OCFST performs better than NCFST in elevated temperature.

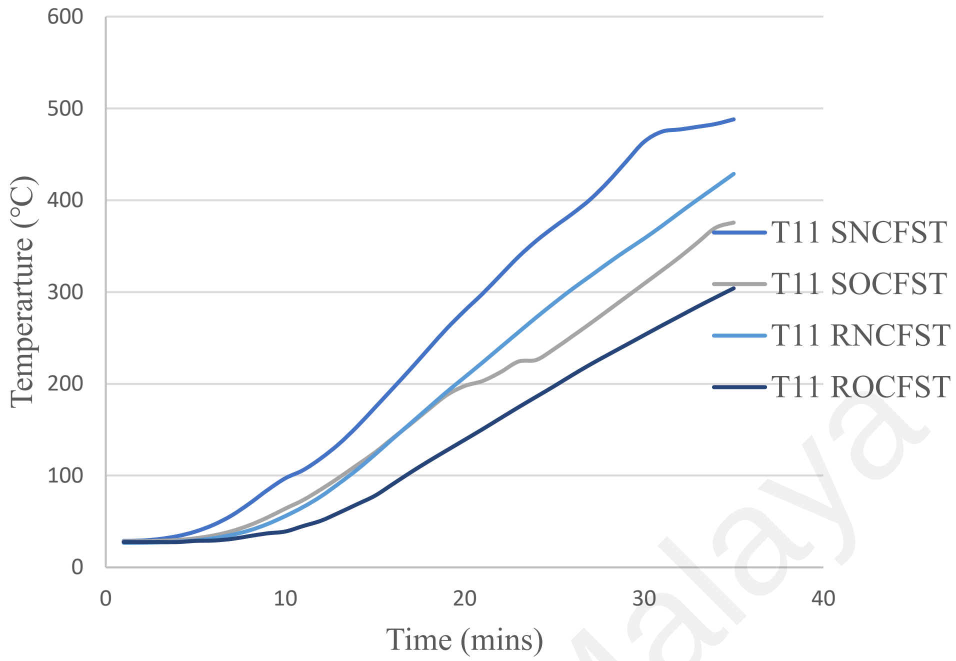

Figure 4.24: Temperature of infilled concrete of all specimens

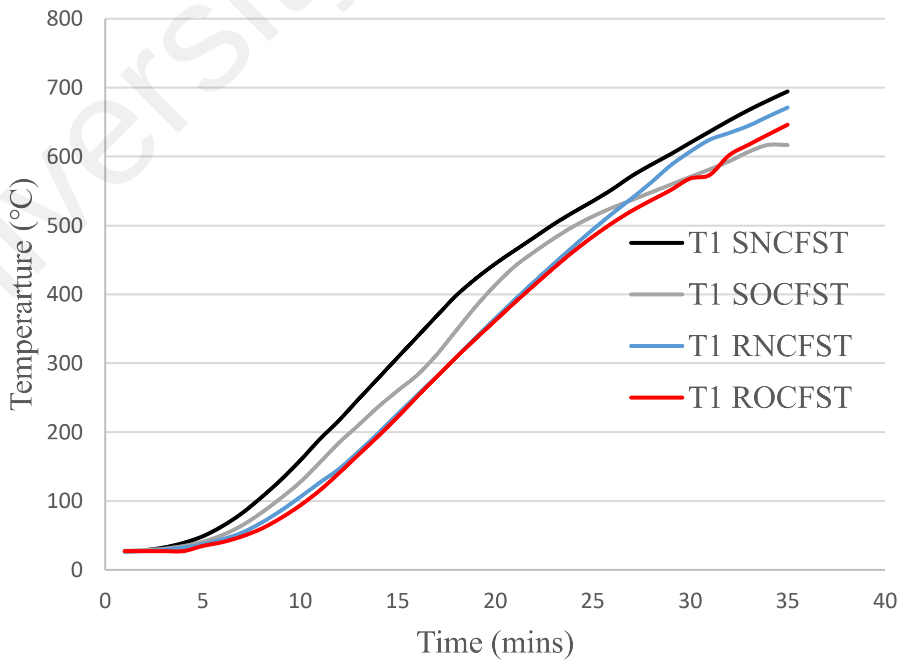

Figure 4.25: Temperature of steel tube of all the specimens

4.6.1.4 Effect of Cross-sectional Shape

Figure 4.26 shows the comparison of temperature evaluation in steel tube and infilled concrete for SOCFST and ROCFST. The rate of rise of temperature in steel is same for both square and rectangular beams whereas the rate of rise of temperature of infilled concrete in square CFST is higher than rectangular CFST. The reason for this may be the availability of larger amount of area at the end of the tube for the escape of moisture. As the end area for moisture escape in square CFST is 12% higher than rectangular beam.

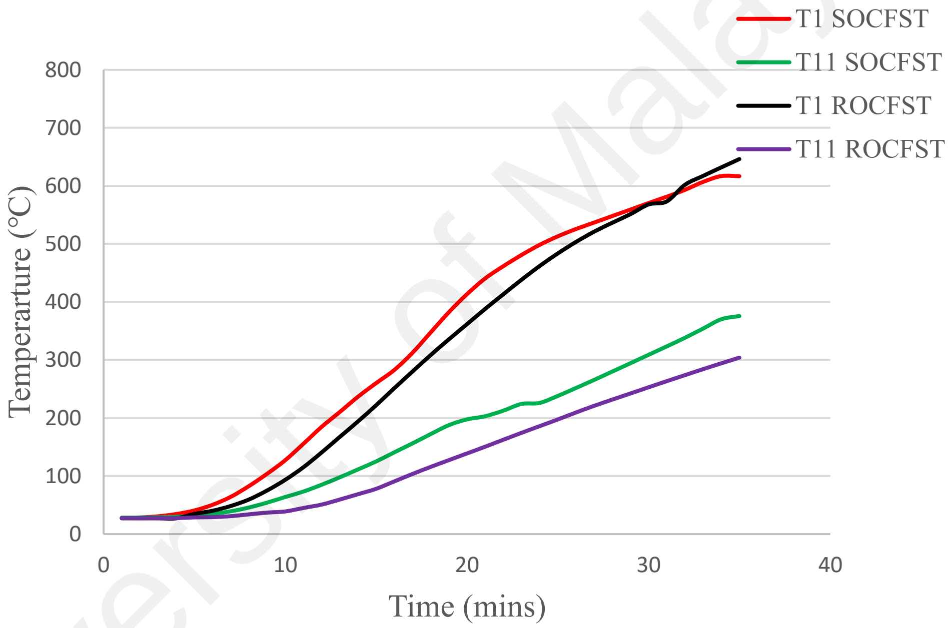

Figure 4.26: Comparison between the temperature of infilled concrete and steel tube of SOCFST and ROCFST

4.6.2 Failure Modes

Figure 4.27 shows the displacements of square and rectangular NCFST members at different time duration of the test. As the beam boundary conditions and loading was symmetrical, the deformation of the specimens was also observed to be symmetrical. The displacement increased rapidly with the increase in temperature of the member for constant load level especially between 25 mins to 30 mins. This rapid increase is due to the yielding of steel. The results of the tests performed in this study are presented in the form of displacement versus time curves, grouped in different graphs according to the infilled concrete. The deflection in rectangular cross-section is less than the square cross-section at any time interval. The reason for the better performance of rectangular cross-section is its higher moment of inertia as compared to square cross-section. It is important to mention that although the load ratio for all the specimens was kept constant i.e., 0.3, the amount of load applied on rectangular cross-sections is greater than the load applied on square cross-section as shown in Table 4.15.

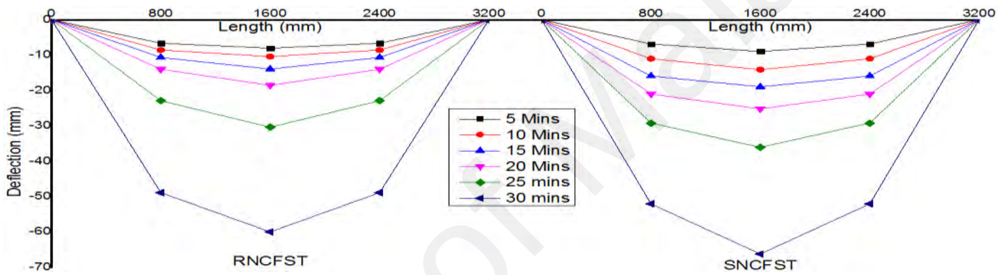

Figure 4.27: Deflection of RNCFST and SNCFST beam at different time intervals

Figure 4.28 shows the deflection of different points of the SOCFST and SNCFST at different time interval. At any instance of time, the deflection in SNCFST is much higher than SOCFST showing the superior structural behavior of SNCFST. The test was stopped before 35 minutes for NCFST samples due to excessive deflections. As mentioned before, this is due to the low temperature of infilled concrete causing the slower loss of strength due to elevated temperature. The displacement increases rapidly with an increase in temperature of the member for constant load level especially between the last 5 minutes of the test due to the yielding of steel for all the specimens.

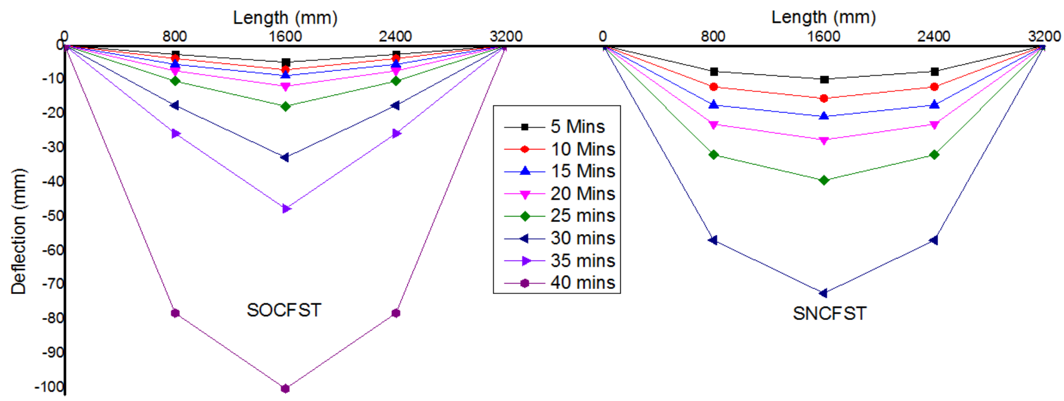

Figure 4.28: Deflection of SNCFST and SOCFST beam at different time intervals

The typical failure mode observed for all the specimens was global buckling. Figure 4.29 shows RNCFST and ROCFST after failure. The absence of local buckling shows that the hollow steel tubes were properly filled with concrete. No tensile fracture was observed on the tension flange. The evolution of mid-span deflection versus the fire exposure time was registered during the fire tests and is presented in Figure 4.30. The failure pattern showed ductile behavior, which is attributed to the ductility and shear contribution of outer steel tube. It must be noticed that due to flexural load, combined with low tensile strength of concrete, there is no plateau in these curves. The plateau in deflection versus time is commonly observed in CFST columns with high slenderness and is due to the contribution of infilled concrete (Moliner et al., 2013; Romero et al., 2011). It is important to mention at this point that majority of CFST columns when exposed to fire failed due to crushing of concrete while in this case the failure was due to the yielding of outer steel tube. According to available literature (Rush et al., 2011), the mode of failure of CFST members depends on many factors including slenderness ratio, applied load, type of load, load ratio and type of support conditions. The gap in the graphs of NCFST and OCFST increases with the passage of time. This may be due to the higher contribution of infilled concrete in OCFST. The temperature of infilled concrete in

OCFST is lower than NCFST at any instant of time as explain in section 4.6.1.3. It can be concluded that the structural response of square and rectangular beams is similar throughout the test till failure. However, the initial flexural stiffness of rectangular beams is more than square beams. Based on the initial flexural stiffness, it can be concluded that rectangular CFST performs better at elevated temperature than square CFST for members subjected to flexural loads whereas in compressive loads square sections performs better (Dai & Lam, 2012).

Figure 4.29: Failure modes of RNCFST and ROCFST

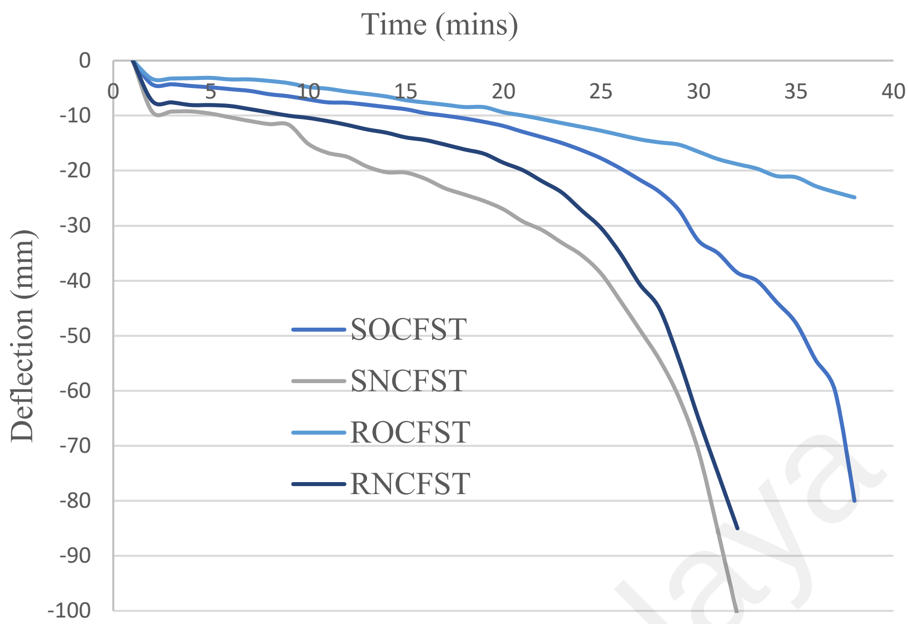

Figure 4.30: Mid-span deflection vs time of all specimens

4.6.3 Critical Temperature/ Limiting Temperature

The temperature corresponds to the deflection $L_e/50$ is taken as the critical temperature of the specimen. The definition of critical temperature is used to ease the evaluation of the fire performance of steel members (Normalisation, 1994; Franssen & Real, 2016; Tubes). This definition may also be used into the evaluation of the fire performance of CFST members. Table 4.15 shows the critical temperature measured at the middle (average of T5, T6 and T7) of the specimen. It is evident that the higher value of limiting temperature shows its tendency for higher fire resistance, showing the fact, the limiting temperature can reflect the fire behavior and resistance of the test specimens. The prediction using the limiting temperature method for fire resistance of CFST specimens is more complicated than that for the steel ones because of the non-uniform thermal distribution of the cross-section induced by the infilled concrete core (Yang et al., 2013). The critical temperature obtained from the experimental tests is also compared with the values obtained by Equation 4.20. Equation 4.20 is given in EC3 for the calculation of critical temperature of CFST columns resisting some percent of design axial load.

$$T_{cr} = 39.19\, ln\left(\frac{1}{0.9674\mu^{3.833}} - 1\right) + 482 \quad \text{……………………………………..(4.20)}$$

Where μ is the load ratio and T_{cr} in °C is the critical temperature of the specimen exposed to standard fire.

Table 4.15: Critical temperature of the tested specimens

Specimen	Applied Load, kN	Load Ratio, Hollow	T_{cr} Exp, °C	T_{cr} code hollow, °C	T_{cr} code, °C
ROCFST	38	0.3	756	584.66	663.77
RNCFST	38	0.3	722	584.66	663.77
SOCFST	30	0.3	718	604.98	663.77
SNCFST	30	0.3	685	604.98	663.77

Two values were calculated with this method of the limiting temperature corresponding to: T_{cr} code hollow and T_{cr} code. The value for hollow section is calculated because in some cases the steel tube fails before utilizing the infilled concrete. It can be concluded that the conclusions of Lu et al. (2009) is not fulfilled in case of CFST beams, where the critical temperature reached higher than the corresponding values for a hollow steel tube due to the contribution of infilled concrete. The infilled concrete delayed the heating up of the steel tube which results in higher critical temperature.

4.6.4 Critical Time

The time corresponds to critical temperature is termed as critical time. Figure 4.31 shows that critical time for ROCFST and SOCFST is more than RNCFST and SNCFST members by 10 and 7 minutes, respectively. The enhancement is more in rectangular cross-sections as compare to square cross-sections. Similarly, the critical temperature of

OCFST is greater by more 30°C than NCFST for both square and rectangular cross-section. This finding is in opposition with the conclusions drawn by (Lu et al., 2009; Moliner et al., 2013) who found that the critical temperature of CFST columns was not affected by the type of infilled concrete. The difference is due to the lower slenderness of the specimens tested in this experimental program while the slenderness of the specimens tested by (Lu et al., 2009; Moliner et al., 2013) was more, therefore making it impossible to gain advantage of the type of infilled concrete. We would like to mention here that several researchers (Laím et al., 2016; Rodrigues & Laim, 2017) investigated and compared critical temperatures of circular, square, rectangular and elliptical CFST members subjected to axial load and concluded that the critical time of elliptical CFST is highest followed by circular, rectangular and square CFST columns. It was also found that the maximum difference in critical time was less than 15%.

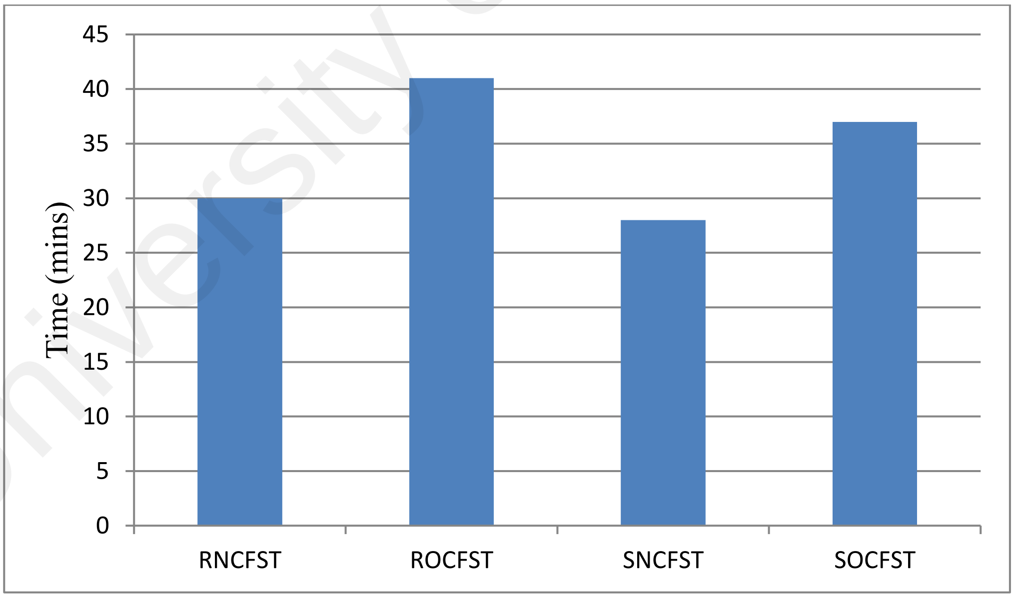

Figure 4.31: Critical time of the tested specimens

4.6.5 Fire Concrete Contribution Ratio (FCCR)

To assess the importance of filling concrete in hollow steel tube beams exposed to fire and to study the interest of using OPBC concrete compared to NMC. Fire concrete contribution ratio (FCCR) is defined as the ratio between the fire resistance rating of CFST and that of the hollow steel member, both subjected to the same amount of flexural load. (Moliner et al., 2013; Romero et al., 2011)

$$FCCR = \frac{FR_{Filled}}{FR_{Hollow}} \qquad \text{(4.21)}$$

In the above equation FR_{Filled} and FR_{Hollow} is the fire resistance time of filled CFST and hollow steel tube.

The numerator can be obtained both experimentally or numerically, but the denominator can be obtained numerically or using equations available in literature (M. Yu et al., 2014). Table 4.16 presents the FCCR obtained for the series of tested specimens, which represents the gain in the fire resistance period by using concrete-filled members instead of hollow steel members. From Table 4.16 it can be concluded that the fire resistance of a hollow steel member can be enhanced at least 1.5 to 2.5 times. Similar conclusions are found for CFST columns by Moliner et al., (2013). The FCCR values result in these cases greater than those obtained for the eccentrically loaded columns (Romero et al., 2011), with an average value of 2.30 for the eccentrically loaded columns versus a 1.92 for the beam specimens. The effect of cross-sectional shape on FRR is significant. In Table 4.16, it can be observed that for the same amount of steel and load ratio, the FRR of rectangular section is 30% higher than square cross-section for tubes filled with NMC. The FCCR of OCFST is 30% higher than NCFST. Hence, the type of infilled concrete greatly affects the FCCR despite having same compressive strength.

Based on FCCR, it can be concluded that the OCFST structural performance is better than NCFST at elevated temperature.

Table 4.16: Fire concrete contribution ratio of all tested specimens

S.No	Specimen	FRR CFST	Load Ratio, Hollow	FRR hollow	FCCR
1	ROCFST	41	0.5	16	2.56
2	RNCFST	30	0.5	16	1.88
3	SOCFST	37	0.445	20	1.85
4	SNCFST	28	0.445	20	1.40

4.7 Comparison with Previous Data

4.7.1 Strength Reduction Factors

The comparison between moment reduction factors obtained from this experimental study with the moment reduction factors given by Chung et al. (2009) is shown in Figure 4.32. It can be seen that the predictions made by Chung et al. (2009) are accurate for the exposure time of 5 minutes. Thereafter, the difference between the predicted and experimental results increased and reached up to 20% at fire exposure time of 40 minutes. Hence, formulation for strength reduction factors need to be done for flexural members. The strength reduction factors for square and rectangular members are similar with less than 5% of difference. However, in case of members exposed to flexural loads, the OCFST performed better than NCFST due to low thermal conductivity of infilled concrete. Hence, modification is recommended in the existing methods by taking into account the effect of flexural load and type of infilled concrete.

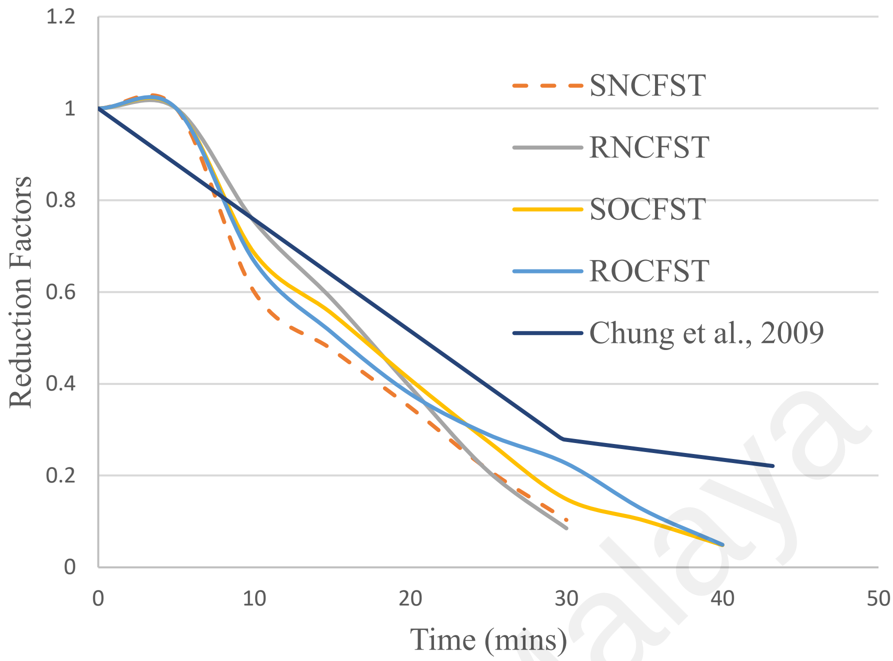

Figure 4.32: Comparison of moment reduction factors obtained from this experiment with results presented by (Chung et al., 2009)

4.7.2 Temperature of Steel Tube

As the specimen is exposed to elevated temperature, the temperature of the steel and infill concrete rises with the passage of time. For CFST columns, different equations for predicting the temperature of steel tube at certain time are available in the literature (Albero et al., 2016; Ana et al., 2013; Ibañez et al., 2016; Wan et al., 2017; Yu et al., 2014) from which five different equations were selected to predict the temperature of the outer steel tube. The equations are published in (Albero et al., 2016; Ana et al., 2013; Ibañez et al., 2016; Wan et al., 2017; Yu et al., 2014) and are given below.

$$T_s = -824.667 - 5.579R - 0.007R^2 - 0.009R\frac{A_m}{V} \mp 645.076(R)^{0.269}\left(\frac{A_m}{V}\right)^{0.017}$$

……………………………………………………………….(4.22) (Albero et al., 2016)

$$T_s = 342.1 + 10.77R - 0.044R^2 + \frac{3.922A_m}{V} - 0.025RA_m/V \quad \ldots\ldots\ldots\ldots\ldots(4.23)$$

(Ana et al.,2013)

$$T_s = \phi_{room} + [345\log(8R+1)] * [1 - 3.38R^{-0.18}] * (1 - [0.155R^{0.58} + t^{-0.1}])$$

……………………………………………………..(4.24) (Ibañez et al., 2016)

$$T_s = 1200\left(1 - \frac{1}{1+\left(\frac{R}{20.22+0.51t}\right)^{0.996+0.014t}}\right) + 20 \quad \ldots\ldots\ldots\ldots\ldots(4.25)$$ (Wan et al., 2017)

$$T_s = 1200\left(1 - \frac{1}{1+\left(\frac{R}{60(0.337+8.5d)}\right)^{0.996+14.0d}}\right) + 20 \quad \ldots\ldots\ldots(4.26)$$ (Yu et al., 2014)

In the above equations, T_s is the temperature of steel tube, R is the fire exposure time in minutes, t is thickness of steel tube in mm, $\frac{A_m}{V}$ is section factor, and d is the equivalent thickness of steel in meters.

The predicted temperature using the above equations were compared with the average temperature (Sum of temperature of T1-T9 thermo-couples/9) obtained from the experiments performed. The comparison of temperature of steel tube obtained from the equations with experimental values is shown in Figure 4.33. It can be concluded that the temperature predicted by all the equations for steel are quite accurate. Although, the equations were given for different cross-sections (ellipse, circular, square and rectangular) for CFST columns, yet they can be used for CFST beams having square and rectangular cross-sections. The equation given by (Wan et al., 2017) yielded most accurate prediction because it took into account the average temperature of steel tube along its thickness and was based on both numerical and experimental results.

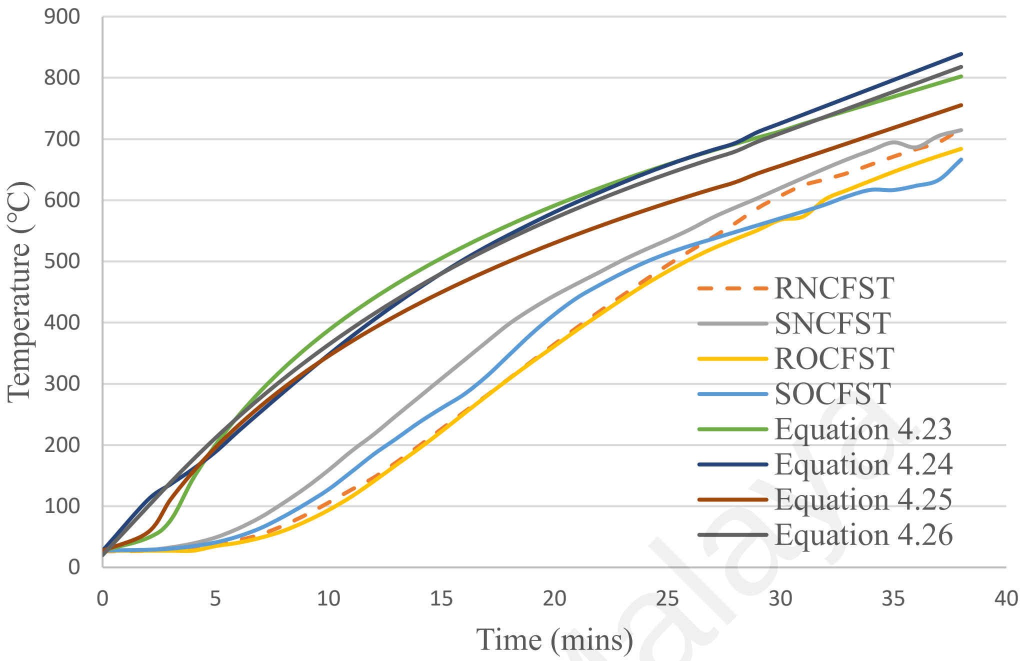

Figure 4.33: Comparison of temperature of outer steel of square CFST Beams with equations 4.23-4.26

4.7.3 Temperature of Infilled Concrete

The comparison of time-temperature curve of in-filled concrete calculated from the equations recommended by different researchers for different shapes of CFST columns (Albero et al., 2016; Ana et al., 2013; Ibañez et al., 2016; Wan et al., 2017; Yu et al., 2014) and experimental results from this research are shown in Figure 4.34. The predicted time-temperature curve obtained from equation given by Ana Espinos et al. (2013) has the difference of more than 15% when compared with the experimental time-temperature curve throughout the fire exposure time. When the time-temperature curve using equation from reference Wan et al. (2017) is compared with experimental data, it can be seen that the experimental time-temperature curve followed closely at the start of the test but lags by 100°C at the end of the test. The time-temperature values obtained from equation given by Yu et al. (2014) followed the experimental time-temperature curve closely till initial

20 minutes but lagged at the end of the test. The lagging is more prominent in square CFST as compared to rectangular CFST. Finally, the temperature predicted by Albero et al. (2016) is accurate till the end of the test for rectangular CFST but lagged by more than 15% for square CFST. Hence, modification is recommended in the existing equations by taking into account the effect of cross-section of steel tube, thickness of steel tube, type of infill concrete, type of steel and size of the furnace. The difference is more for SOCST beams due to low thermal conductivity of OPBC.

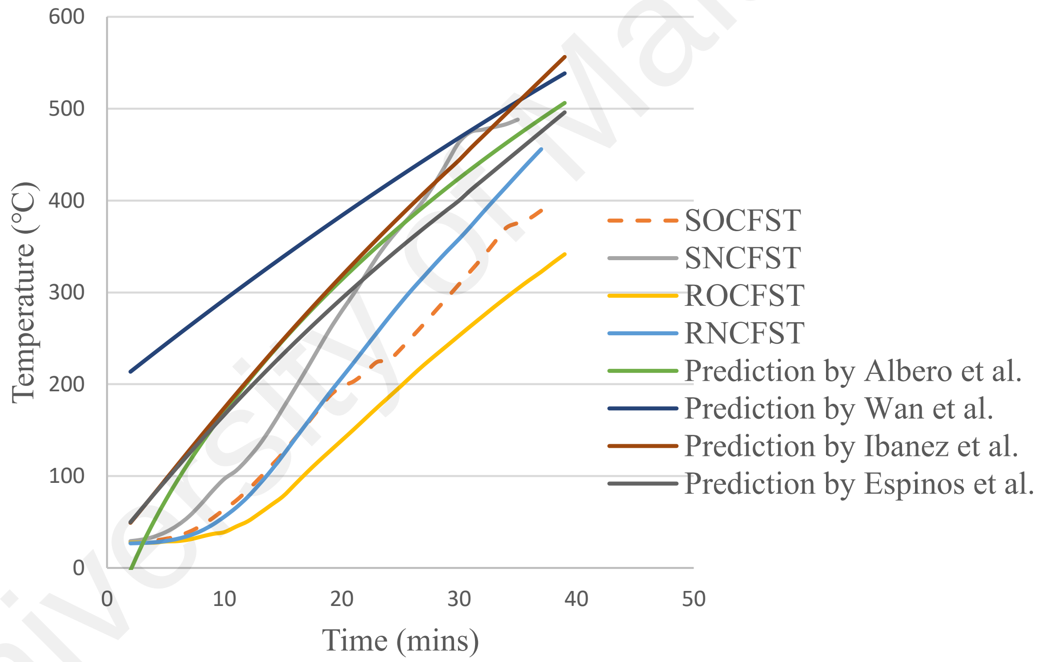

Figure 4.34: Comparison of temperature of infilled concrete of square CFST Beams with available equations

4.8 Verification of Elevated Temperature FE Model for NCFST

The experiments reported in chapter 3 were used for the verification of FE models. The temperature of steel tube and infilled concrete obtained from the experimental tests were compared with the results obtained from FE model. Figure 4.35 shows the time-temperature curve of outer steel tube of RNCFST and SNCFST obtained from experimental test and FE model. It was observed that test results and FE model shows negligible difference both for infilled concrete and outer steel tube. At the start of the test, the temperature of the infilled concrete predicted by FE model is higher than experimental values, which gets accurate at the end of the test. This may be due to the transfer of moisture towards the center, which was ignored in the FE model. At the end of test, when moisture content in concrete becomes almost zero, the predicted temperature by FE model was precise with the test results.

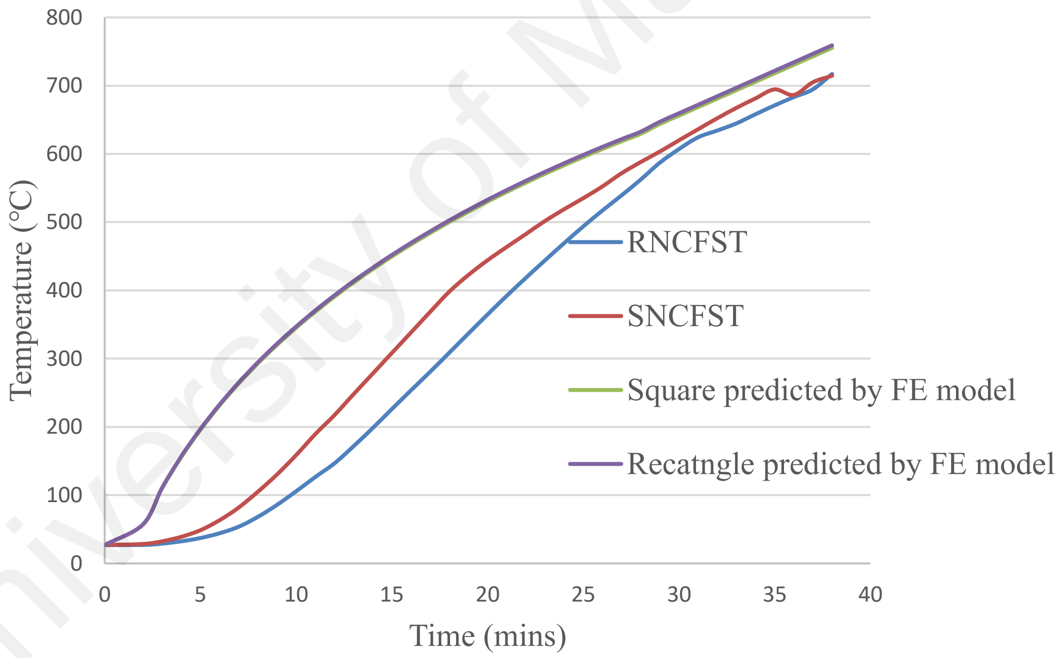

Figure 4.35: Comparison of experimental and FE model time-temperature curve for outer steel tube of NCFST specimens

The fire resistance (FR) time obtained from test results and FE model are presented in Table 4.17. The close resemblance of results between FE model and test results shows that the co-efficient of thermal expansion used for concrete, steel and steel-concrete interface are accurate and can be used in future research works. It must be noted from that the displacement predicted by FE model at the time of failure is less than the experimentally measured displacement. This may be due to the neglecting the effect of creep in the FE model as the creep is pronounced at elevated temperature (Abid et al., 2017).

Table 4.17: FR time comparison for experimental and Numerical models for NCFST

Sample Name	FR time, mins (Exp)	FR time, mins (Num)	Exp/Num
SNCFST	28	27.5	1.02
RNCFST	29.5	29.25	1.01
Mean			1.02
Standard Deviation			0.025
COV (%)			2.45

The failure criteria for CFST members subjected to only flexural load is not given in EC4. Many researchers recommended that the test should be stopped when the maximum deflection reaches to Le/50, and this point will be considered as point of failure (Han, Tao, et al., 2001). Hence, when the deflection reaches to Le/50, which was 60mm in this study, the specimen was considered failed. The ratio between the fire resistance predicted by FE model and the fire resistance obtained from experimental tests are shown in Table 4.17. The mean, standard deviation and COV for the ratio between FE model and test results for mid-span deflection and FR time are 1.02, 0.025, and 2.45%, respectively.

4.9 Verification of Elevated Temperature FE Model for OCFST

The temperature of steel tube and infilled concrete obtained from the experimental tests were compared with the results obtained from FE model. Figure 4.36 shows the time-temperature curve of steel tube of ROCFST and SOCFST obtained from experimental test and FE model. The average temperature of the steel tube was obtained from all the 9 thermocouples attached to steel surface. Figure 4.37 shows the time-temperature curve of in-filled concrete of ROCFST and SOCFST obtained from experimental test and FE model. It was observed that test results and FE model shows negligible difference both for infilled concrete and outer steel tube.

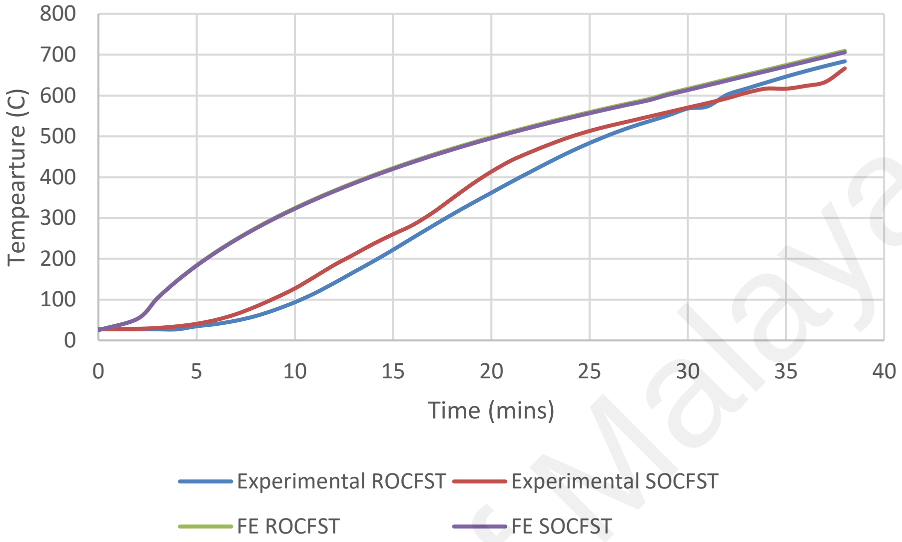

Figure 4.36: Comparison of experimental and FE model time-temperature curve for steel tube of OCFST specimens

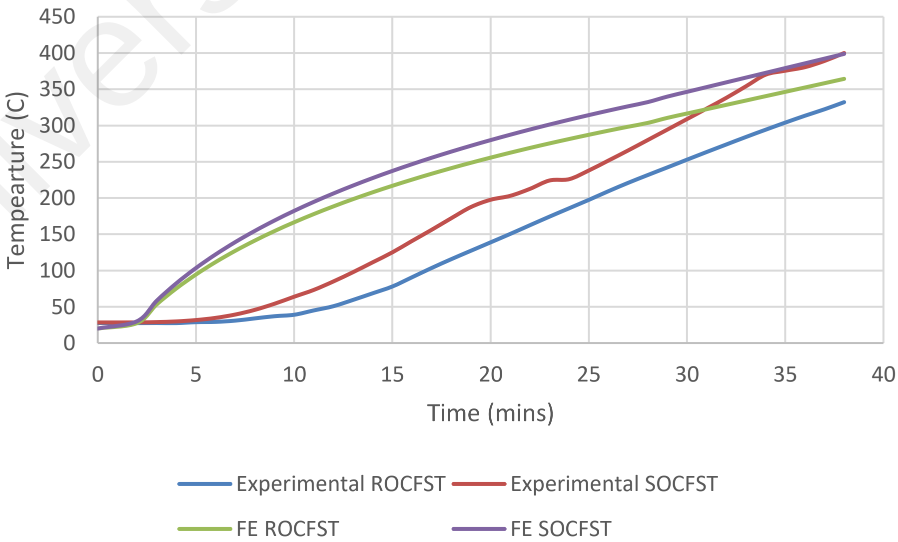

Figure 4.37:Comparison of experimental and FE model time-temperature curve for infilled concrete of OCFST specimens

The mid-span deflection obtained from FE model and the measured mid-span deflection during test are compared in Figure 4.38 for ROCFST and SOCFST. As shown in Figure 4.38, there were some minor difference between experimental and FE model results. Such kind of small differences are reported by different researchers for CFST members at room and elevated temperatures.

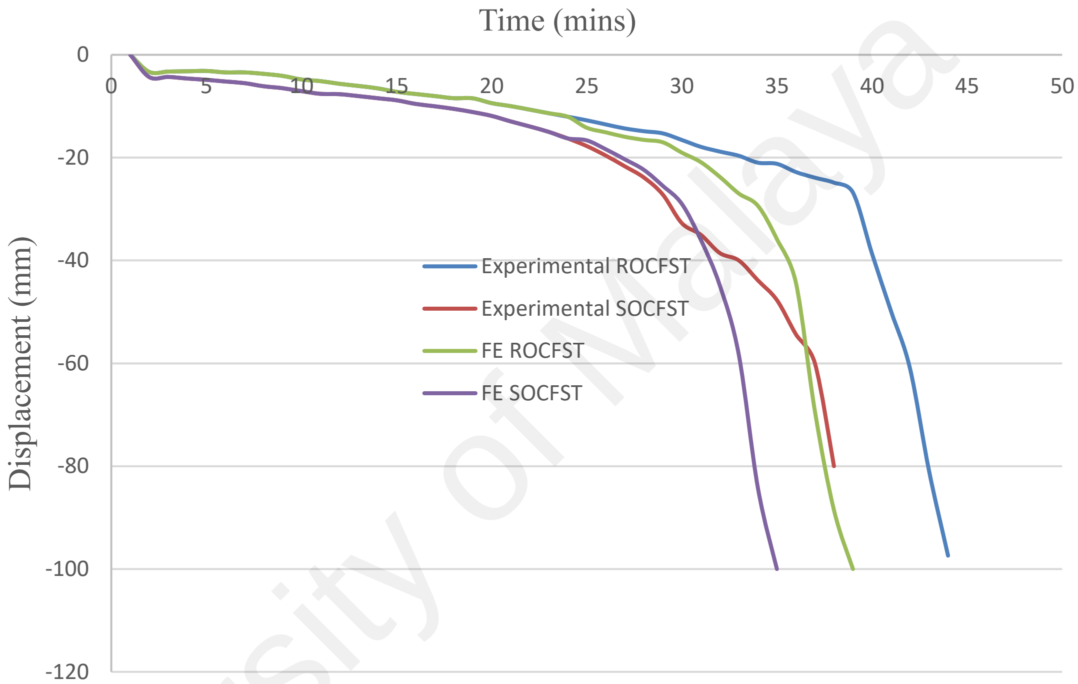

Figure 4.38:Time vs displacement curve for experimental and numerical models of OCFST specimens

4.10 Parametric Study for NCFST at Elevated Temperature

In this section, more than 40 CFST specimens were analyzed with the help of verified FE model. The dimensions and details of the analyzed specimens are given in Table 4.18. The parametric study included different strength of concrete and steel, different load ratios, different type of aggregates, different moisture content of concrete, different width-to-depth (B/D ratio) and different Depth-to-thickness ratio (D/t). The CFST beams were divided into 7 main groups. One group is used for studying the effect of specific parameters. In each group, all the parameters are kept constant except one (under study). Most of the dimensions of the beam consider in this parametric study are same, as these dimensions are most widely used in practical applications.

Table 4.18: Details of specimens used for parametric studies

Group Name	D x B x t	f_y	f_u	Fc	n	FR Time
Fc 30, n 0.3	300x150x5	235	380	30	0.3	44.7
		275	410			41.2
		300	430			35.6
		355	450			28.84
		400	490			22.35
Fc 30, n 0.6	300x150x5	235	380	30	0.6	36.8
		275	410			32.14
		300	430			25.64
		355	450			20.4
		400	490			15.824
Fc 60, n 0.3	300x150x5	235	380	60	0.3	61.2
		275	410			57.1
		300	430			50.6
		355	450			44.7
		400	490			42.228
Fc 30, n 0.3	600x300x5	235	380	30	0.3	91.6
		275	410			82.46
		300	430			73.51
		355	450			64.17
		400	490			54.96
Fc 75, n 0.3	300x150x5	235	380	75	0.3	70.15
		275	410			65.24
		300	430			59.43
		355	450			55.04
		400	490			50.57
Fc 60, n 0.3	600x300x5	235	380	60	0.3	98.4
		275	410			92.7
		300	430			85.4
		355	450			75.13
		400	490			64.02
Fc 75, n 0.3	600x300x5	235	380	75	0.3	110.74
		275	410			99.32
		300	430			88.25
		355	450			79.53
		400	490			70.25
Fc 30, n 0.45	300x150x5	235	380	30	0.45	40.87
		275	410			35.26
		300	430			29.21
		355	450			25.51
		400	490			20.435
Fc 30, n 0.3	300x300x5	235	380	30	0.3	62.58
		275	410			57.68
		300	430			49.84
		355	450			40.376
		400	490			31.29

4.10.1 Effect of Strength of Steel

The main objective of this parametric study was to evaluate the effects of different yield strengths of steel on the fire resistance time of CFST members when exposed to elevated temperature and flexural loads. For this purpose, five different yield strengths are considered. To check whether the yield strength effects the FR time similarly for different load ratios, cross-sections and concrete strengths, two different load ratios, cross-sections and concrete strengths are considered. The modulus of elasticity of steel and concrete was assumed to 200 GPa and 29 GPa, respectively. The detailed dimensions of the FE model considered for this study are shown in Table 4.18.

Figure 4.39 shows the influence of yield strength of steel on the fire resistance time of CFST members subjected to flexural load only. It can be seen in Figure 4.39 that increase in yield strength of steel causes decrease in the fire resistance time of CFST beam regardless of load ratio, compressive strength of concrete and dimensions of considered member. However, the decrease in FR time is more for bigger cross-section and lesser concrete strength. Since in bigger cross-sections and low strength infilled concrete, the steel takes majority of load, and once its losses its strength the member fails quickly. While in case of smaller cross-sections and high strength of infilled concrete, as higher amount of load is taken by concrete, hence it is less affected by the yield strength of steel. It should be kept in mind that the load taken by high strength steel of steel is more as load ratio was kept constant.

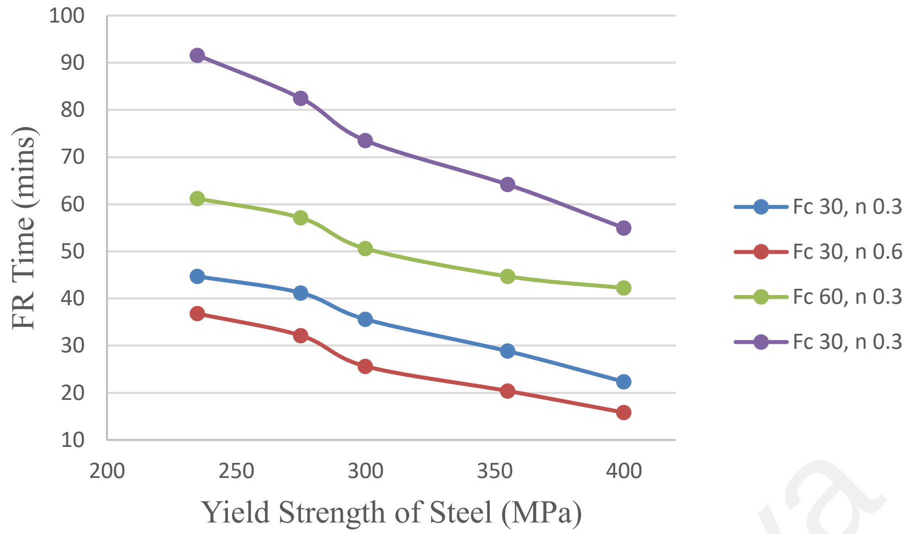

Figure 4.39: FR time values for different yield strengths of steel

4.10.2 Effect of Strength of Concrete

To study the influence of compressive strength of infilled concrete on the flexural behavior of CFST member at elevated temperature, 3 different compressive strengths of concrete are considered in this study. The modulus of Elasticity of concrete is calculated by using the equation suggested in ACI-318 (Committee, 2015). The rest of the parameters were kept constant so that the effect of compressive strength is highlighted. The detailed dimensions of the FE model considered for this study are shown in Table 4.18.

$$E = w^{1.5} \times 0.043 \times f'^{0.5}_{c} \qquad \text{(4.30)}$$

In the above equation, E is modulus of elasticity of concrete, w is unit weight of concrete and f'_c is the compressive strength of concrete.

Figure 4.40 shows the effect of compressive strength of concrete on FR time for various yield strengths of steel and different cross-sections. By increasing the compressive strength of infilled concrete, the FR time increases regardless of the size and yield strength of steel tube. The percentage increase in FR time is more for bigger cross-sections. This is due to the larger amount of concrete used in larger sections. Similar conclusions were made by researchers for concrete filled stainless steel members subjected to axial load at elevated temperature (Han et al., 2013).

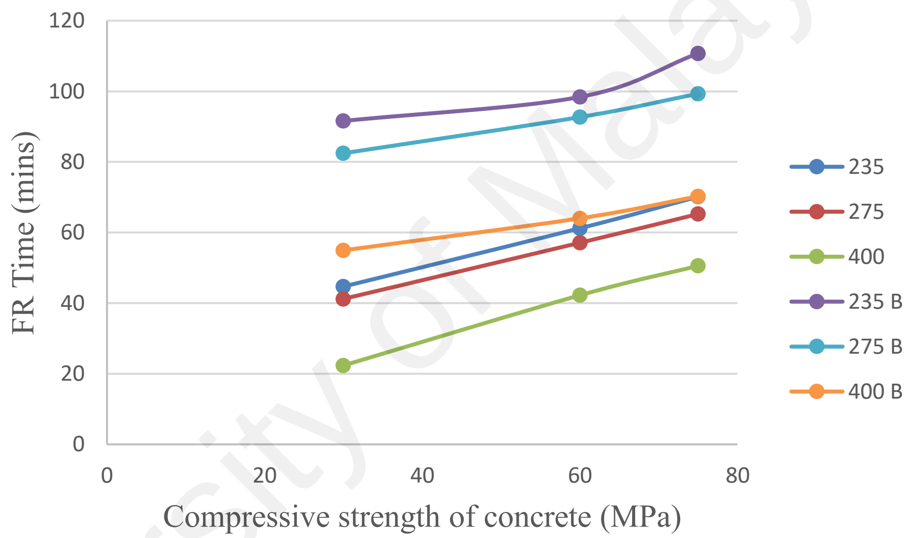

Figure 4.40: FR time of beams for different compressive strengths of concrete

4.10.3 Effect of Load Ratio

To study effect of load ratio on the elevated temperature performance of CFST members subjected to flexural members, three different load ratios were selected in this section. The properties of steel and concrete were kept same as mentioned in previous sections.

Figure 4.41 shows the relation of load ratio and fire resistance time for different yield strengths of steel. It is obvious from Figure 4.41 that with the increase in load ratio, the FR time decreases. This is due to the decrease of CFST members remaining strength with the higher load ratio. Usually, the CFST members with higher load ratio are more affected with elevated temperature. It is important to mention that during analysis it was observed that the decrease in FR time with increase in load ratio is less for smaller cross-sections as compared to bigger cross-sections due to the less amount of steel area exposed to fire. Similar kind of conclusions were made by researchers for concrete filled stainless steel tube (Han et al., 2013) and concrete filled double steel tube (Wan et al., 2017) subjected to axial load at elevated temperature.

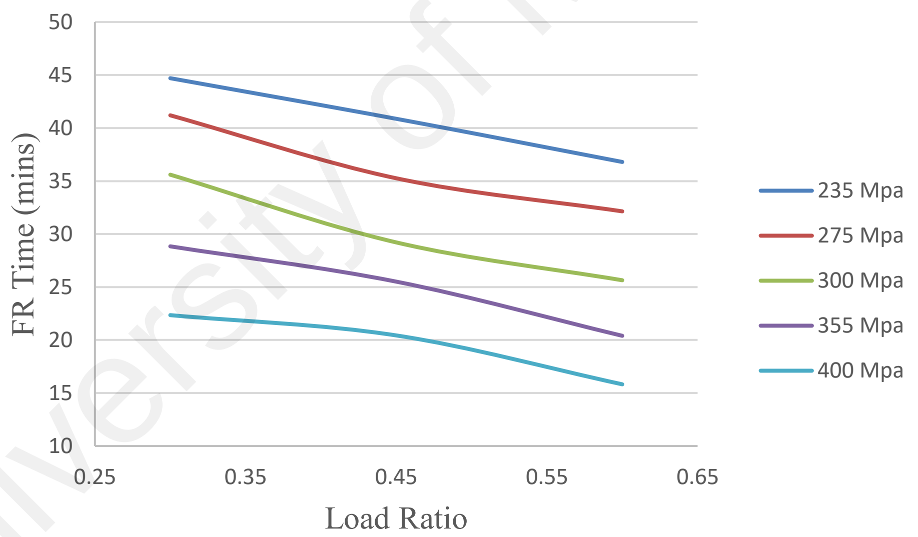

Figure 4.41: Effect of load ratio on FR time for different yield strengths of steel

4.10.4 Effect of Cross-Sectional Dimensions (B/D ratio)

The influence of cross-sectional dimension on the FR time of CFST member subjected to flexural load can be derived from the Figure 4.42. For example, for the same load ratio, compressive strength of concrete and yield stress of steel, the FR time for Section with dimension of 300 x 150 was 44.7 minutes while for 300 x 300 was 62.58 minutes showing an increase of 40%. In addition to higher FR time, the surface temperature of bigger sections will also rise slowly because of larger area of low temperature, hence leading to slower reduction in flexural capacity. This is logical since a CFST member with bigger dimensions has more infilled concrete, thus, the rise of the temperature is slower in the inner part of the member, which increases its fire endurance.

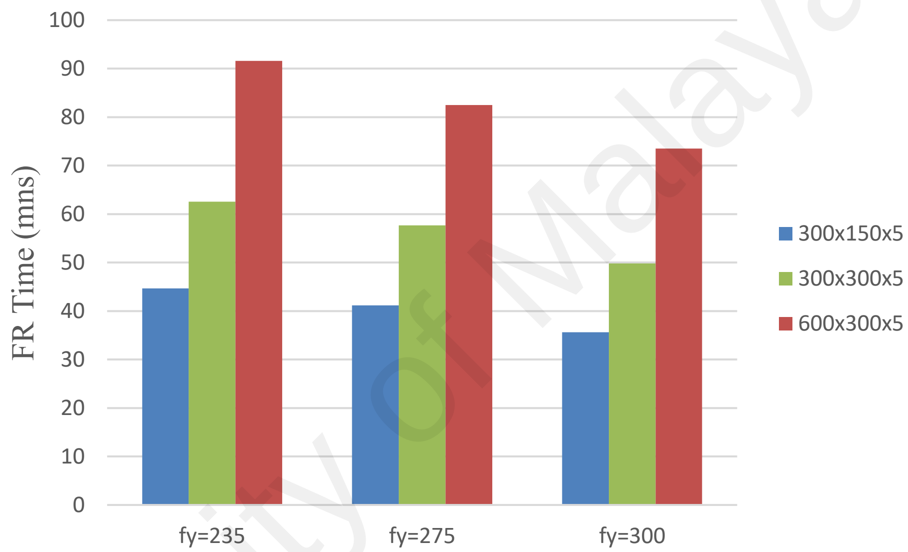

Figure 4.42: FR time for beam samples of different cross-sections

4.10.5 Effect of Steel Ratio

Steel ratio is defined as the ratio of the area of steel to the area of area of concrete of CFST member. To study the effect of steel ratio on the FR time of CFST member, 3 cross-sectional dimensions are selected. The compressive strength of concrete is assumed to be 30 MPa. The detailed dimensions of the selected sections are given in Table 4.18.

$$\alpha = \frac{A_s}{A_c} \quad \text{……………………………………………………………………….. (4.31)}$$

Figure 4.43 shows the effect of steel ratio on FR time of CFST member. It is obvious from figure that the FR time decreases with the increase in steel ratio regardless of the yield strength of steel. The FR time for steel ratio of 4.4% and 2.85% for steel of yield strength of 235 MPa was observed to be 44.5 and 90 mins, respectively. This is due to the usage of higher amount of steel in sections with higher steel ratios. As the strength degradation of steel at elevated temperature is faster than concrete core, therefore CFST member with higher steel ratio attain its FR faster when subjected to elevated temperature (Han et al., 2013).

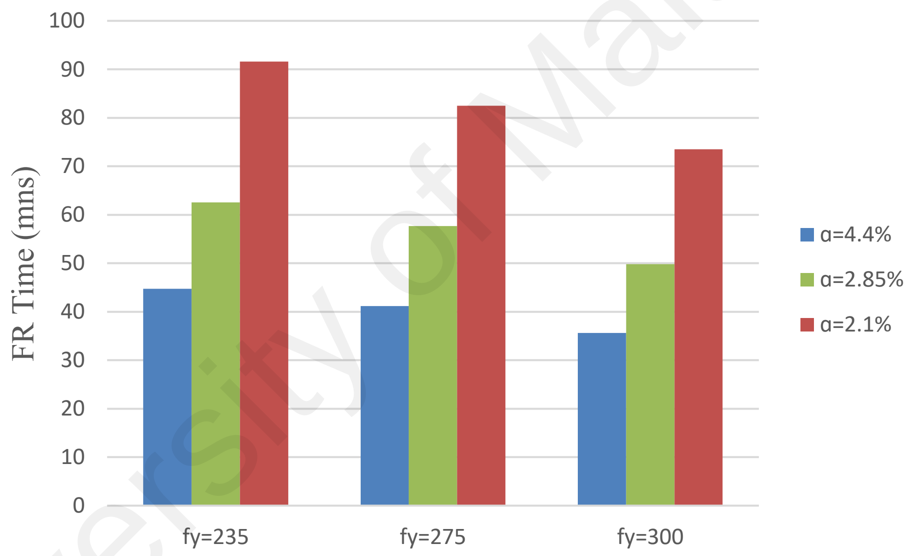

Figure 4.43: Comparison of FR time of different steel ratios with same yield strength

4.11 Parametric Study for OCFST at Elevated Temperature

In this section, more than 50 OCFST specimens were analyzed with the help of verified FE model. The dimensions and details of the analyzed specimens are given in Tables 4.19-4.22, where D, B, t, f_y and f_u represents the depth, width, thickness, yield strength and ultimate yield strength of steel section, respectively while f_c and n represent the compressive strength of concrete and load ratio, respectively.

4.11.1 Effect of yield strength of steel

Five different values of yield strengths were considered to study the behavior of OCFST for different yield strengths of steel. As changing the yield strength of steel may affect the FR time differently for different compressive strengths of concrete, load ratio and cross-sectional dimensions, therefore 20 models were analyzed. The modulus of elasticity of steel and concrete were assumed as 200 GPa and 29 GPa, respectively. The detailed dimensions of the FE model considered are shown in Table 4.19.

Table 4.19 Main properties for CFST models used for studying the effect of yield strength of steel

Group Name	D × B × t	f_y (MPa)	f_u (MPa)	f_c (MPa)	Load ratio, n	FR Time (mins)
Fy1	300x150x5	235	380	30	0.3	58.11
		275	410			53.56
		300	430			46.28
		355	450			37.492
		400	490			29.055
Fy2	300x150x5	235	380	30	0.6	47.84
		275	410			41.782
		300	430			33.332
		355	450			26.52
		400	490			20.5712
Fy3	300x150x5	235	380	60	0.3	79.56
		275	410			74.23
		300	430			65.78
		355	450			58.11
		400	490			54.8964
Fy4	300x600x5	235	380	30	0.3	119.08
		275	410			107.198
		300	430			95.563
		355	450			83.421
		400	490			71.448

Figure 4.44 shows the influence of yield strength of steel on the FR time of CFST members subjected to flexural load only. It can be seen in Figure 4.44 that increase in yield strength of steel causes decrease in the FR time of CFST beam regardless of load ratio, compressive strength of concrete and cross-sectional dimensions. By increasing the

yield strength of steel from 235 MPa to 300 MPa and 400 MPa, the FR time of Fy1 group was found to decrease by 22% and 48%, respectively. The strength degradation with increasing yield strength is similar for different load ratios. However, for Fy4 group having larger cross-section, higher load ratio and lower concrete strength, the decrease in FR time was higher. Since in larger cross-sections with low strength infilled concrete, steel takes majority of the load, and once steel losses its strength, the member fails quickly. While in case of smaller cross-sections and high strength of infilled concrete as in group Fy3, higher amount of load is taken by concrete, hence it is less affected by the yield strength of steel. It should be kept in mind that for constant load ratio, the load taken by high strength steel was more.

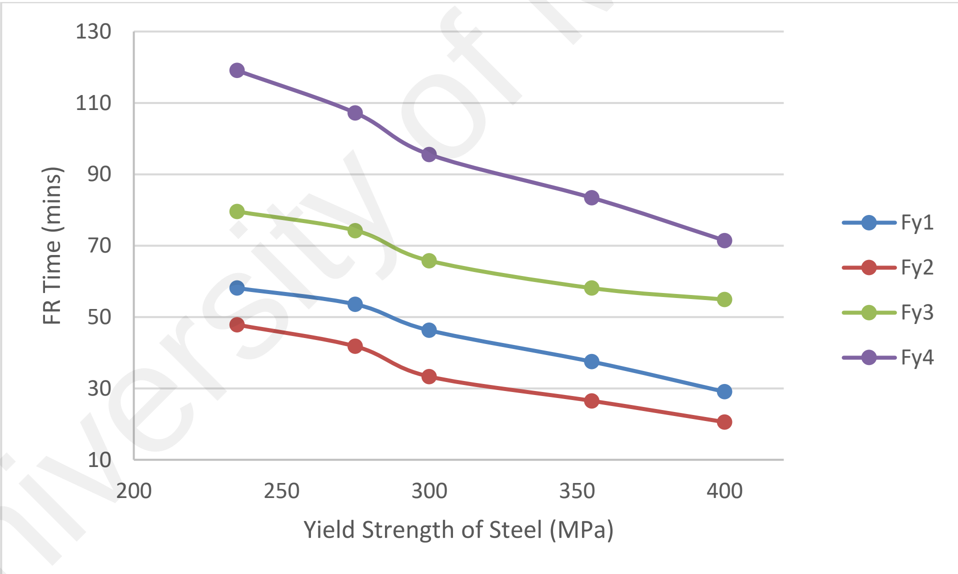

Figure 4.44 FR time values for different yield strengths of steel

4.11.2 Effect of strength of concrete

To study the influence of compressive strength of infilled concrete on the flexural behavior of OCFST member at elevated temperature, 3 different compressive strengths of concrete were considered. As varying compressive strength of concrete may affect the

FR time differently for different yield strength of concrete and cross-sectional dimensions, therefore 18 models were analyzed for this section. The modulus of elasticity of concrete was calculated by using the equations suggested in ACI-318 (2015). The rest of the parameters were kept constant so that the effect of compressive strength is highlighted. The detailed dimensions of the FE model considered are shown in Table 4.20.

Table 4.20 Details of models used to study the effect of compressive strength of concrete

Group Name	D × B × t	f_y	f_c	n	FR Time
Fc1	300x150x5	235	30	0.3	58.11
			60		79.56
			75		91.195
Fc2	300x150x5	275	30	0.3	53.56
			60		74.23
			75		84.812
Fc3	300x150x5	400	30	0.3	29.055
			60		54.8964
			75		65.741
Fc4	300x600x5	235	30	0.3	119.08
			60		127.92
			75		143.962
Fc5	300x600x5	275	30	0.3	107.198
			60		120.51
			75		129.116
Fc6	300x600x5	400	30	0.3	71.448
			60		83.226
			75		91.325

Figure 4.45 shows the effect of compressive strength of concrete on FR time for various yield strengths of steel and different cross-sections. By increasing the compressive strength of infilled concrete, the FR time increased regardless of the size and

yield strength of steel tube. By increasing the compressive strength of infilled concrete from 30 MPa to 60 MPa and 75 MPa, the FR time of Fc1 group was found to increase by 37% and 57%, respectively. In can also be seen that the percentage increase in FR time is less for larger cross-sections. For instance, by increasing the compressive strength of infilled concrete from 30 MPa to 60 MPa and 75 MPa, the FR time of Fc4 group was found to increase by only 7% and 21%, respectively.

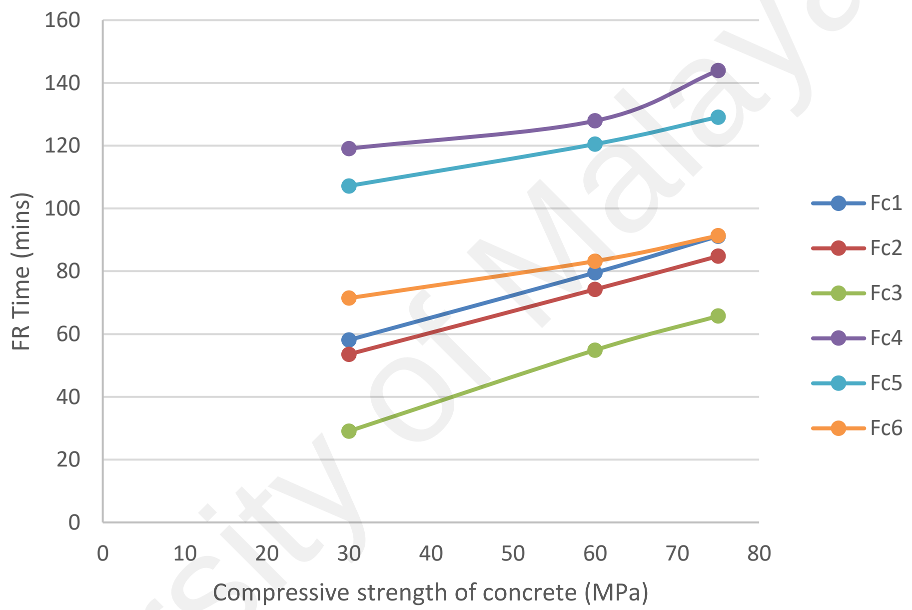

Figure 4.45 FR time of beams for different compressive strengths of concrete

4.11.3 Effect of load ratio

To study effect of load ratio on the elevated temperature performance of OCFST members subjected to flexural members, three different load ratios were selected. As varying load ratio may affect the FR time differently for different yield strength of steel, therefore 15 models were analyzed. The detailed dimensions of the FE model considered are shown in Table 4.21.

Table 4.21 Main properties for CFST models used for studying the effect of load ratio

Group Name	DxBxt	f_y	f_c	n	FR Time
LR1	300x150x5	235	30	0.3	58.11
				0.45	53.131
				0.6	47.84
LR2	300x150x5	275	30	0.3	53.56
				0.45	45.838
				0.6	41.782
LR3	300x150x5	300	30	0.3	46.28
				0.45	37.973
				0.6	33.332
LR4	300x150x5	355	30	0.3	37.492
				0.45	33.163
				0.6	26.52
LR5	300x150x5	400	30	0.3	29.055
				0.45	26.5655
				0.6	20.5712

Figure 4.46 shows the effect of load ratio on FR time for different yield strengths of steel. It is obvious from Figure 4.46 that with the increase in load ratio, the FR time decreased. By increasing the load ratio from 0.3 to 0.45 and 0.6, the FR time of LR1 group was found to decrease by 9% and 18%, respectively. The percentage decrease was similar for different yield strengths of steel. This is because, residual strength of the member is less at higher load ratios and vice versa. It is important to mention that during analysis it was observed that the decrease in FR time with increase in load ratio was less for smaller cross-sections as compared to larger cross-sections due to the lesser amount of steel area exposed to fire.

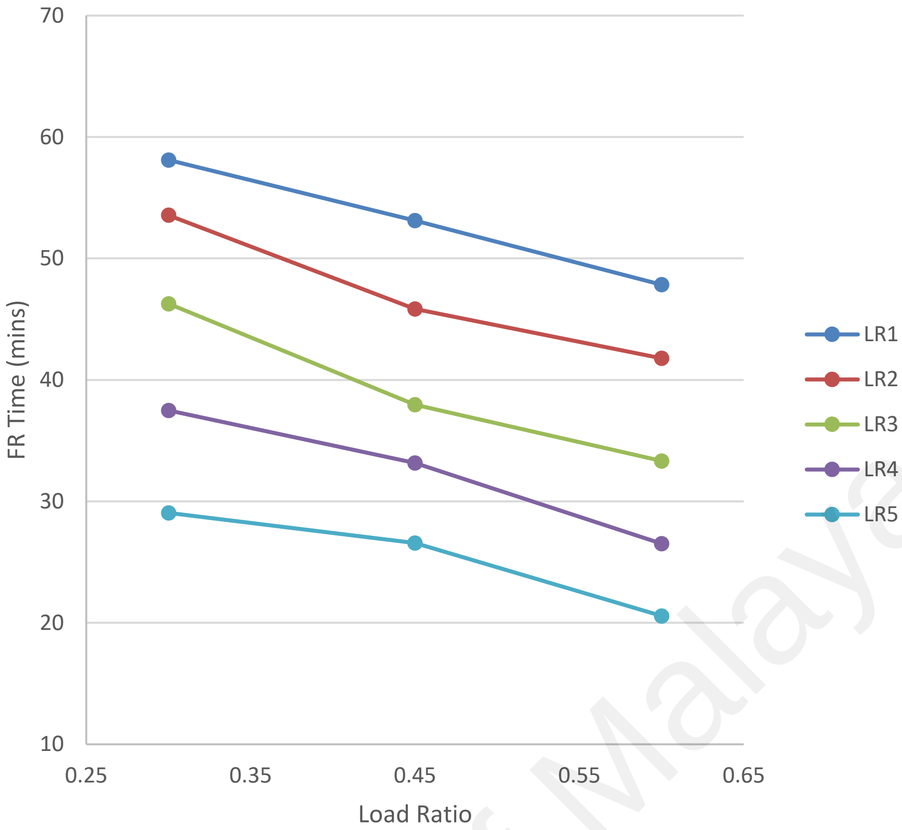

Figure 4.46 Effect of load ratio on FR time for different yield strengths of steel

4.11.4 Effect of width-to-depth ratio (B/D ratio)

The influence of B/D ratio on the FR time of CFST member subjected to flexural load is shown in Figure 4.46 and Table 4.21 respectively. For SR1 group, the FR time for cross-section having dimensions of 300 x 150 and 300 x 300 was 58.11 and 841.354 minutes respectively. This shows an increase of 40% FR time for 300x300 over 300x150. In addition to higher FR time, the surface temperature of larger cross-sections will also rise slowly hence leading to slower reduction in flexural capacity. This is logical, since a CFST member with larger cross-section dimension has more infilled concrete, thus, the rise of temperature is slower in the inner part of the member, which increases its fire endurance.

Table 4.22: Details of models used to study the effect of B/D ratio and steel ratio

Group Name	DxBxt	f_y	B/D ratio	f_c	n	Steel ratio	FR Time
SR1	300x150x5	235	2	30	0.3	4.4%	58.11
	300x300x5		1			2.85%	81.354
	600x300x5		0.5			2.1%	119.08
SR2	300x150x5	275	2	30	0.3	4.4%	53.56
	300x300x5		1			2.85%	74.984
	600x300x5		0.5			2.1%	107.198
SR3	300x150x5	300	2	30	0.3	4.4%	46.28
	300x300x5		1			2.85%	64.792
	600x300x5		0.5			2.1%	95.563

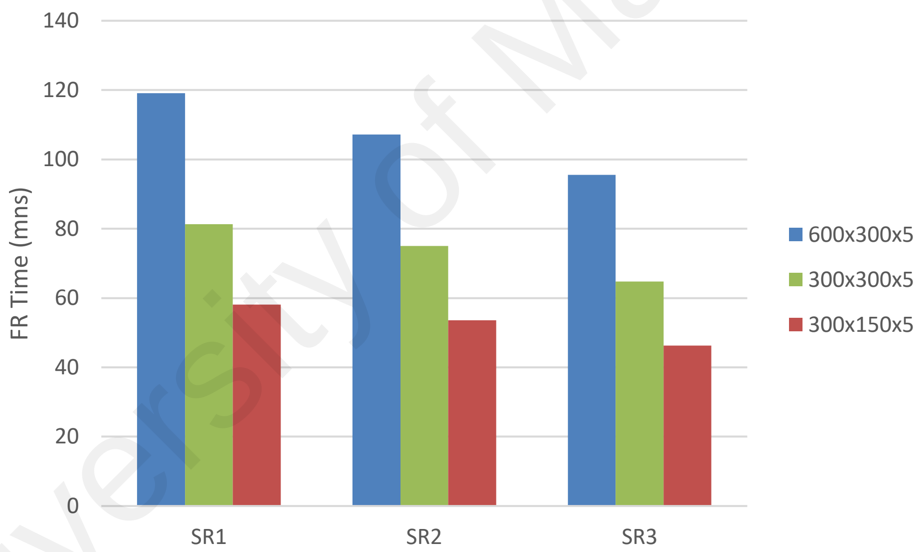

Figure 4.47: Comparison of FR time of different steel ratios and cross-sectional dimensions

4.11.5 Effect of steel ratio

Steel ratio is defined as the ratio of the area of steel to the area of concrete of CFST member. To study the effect of steel ratio on the FR time of OCFST member, 3 cross-sectional dimensions were selected. The compressive strength of concrete is assumed to be 30 MPa. The detailed dimensions of the selected sections are shown in Table 4.22.

Figure 4.47 shows the effect of steel ratio on FR time of CFST member. It is obvious from Figure 4.47 that the FR time decrease D with the increase in steel ratio regardless of the yield strength of steel. When the steel ratio increased from 2.1% to 2.85% and 4.4%, the FR time of SR2 group was found to decrease by 31% and 51%, respectively. This is due to the usage of higher amount of steel. As the strength degradation of steel at elevated temperature is faster than concrete core, therefore OCFST member with higher steel ratio attain its FR faster when subjected to elevated temperature.

CHAPTER 5: CONCLUSIONS AND RECOMMENDATIONS

5.1 Conclusions

To reduce the environmental pollution, the utilization of waste by-products in the concrete industry would be an ideal choice. Recently, the trend towards the use of agricultural waste for sustainable development has been increased around the world. The oil palm industry produces a huge amount of solid agricultural wastes including oil palm boiler clinker (OPBC). It is known that more than 90% of OPBC is used as landfilling material which causes a serious environmental problem. Hence, in this research, a new sustainable and environmentally friendly composite flexural member with conventional coarse aggregate replaced with OPBC was analyzed and its performance was compared with a conventional composite member. Based on test results, following are the conclusions

1. The behavior of hollow steel tubes filled with normal concrete (NCFST) and hollow steel tubes filled with oil palm boiler clinker concrete (OCFST) was experimentally investigated. The results showed that ductility, energy absorption, flexural stiffness and ultimate capacity of OCFST is 10-20% higher than NCFST. OCFST was 10% lighter than NCFST, with 15% higher structural efficiency.
2. The current analytical model for the prediction of the moment-curvature curve and ultimate capacity of NCFST beams can be used safely for OCFST. GB gives reasonable and closest predictions for the ultimate moment capacity of both NCFST and OCFST with an average 11% higher values as compared to EC4, AISC and CIDECT, which predicts 40% higher values.

3. The initial flexural stiffness and flexural stiffness at serviceability level predicted by all the codes are conservative except AISC for OCFST. The EC4 gives the closest value as compare to other codes.
4. All specimens fail in a ductile manner at elevated temperature. Specimens retained their integrity after testing despite of local bulge of the steel hollow section showing strong interaction of the concrete and steel in the CFST beams during the whole process of fire exposure.
5. The limiting temperature in the steel of the rectangular OCFST and square OCFST ranged from 718°C to 756°C which is more than that of rectangular NCFST and square NCFST, respectively.
6. The FCCR for OCFST was found to be 2.56 and 1.88 as compared to NCFST which is 1.55 and 1.44, respectively.
7. It was found that by changing depth-to-thickness ratio from 20 to 200 and height-to-width ratio from 0.6 to 2, the ultimate flexural capacity of rectangular CFST increased from 21 to 169 KN-m (up to 8 times) and 46 to 77 KN-m (67%), respectively.
8. The ultimate capacity also increased (41%) by changing the yield strength of steel tube from 410 to 490 MPa.
9. However, no change in the ultimate moment capacity was observed for different shear span-to-depth ratio (1,3,5,7 and 8).
10. Marginal change (up to 11%) in the ultimate capacity was observed by changing the compressive strength of infill concrete from 60 to 100 MPa.
11. GB50936 (2014) model predicts better results followed by CIDECT, Eurocode, and AISC respectively. According to GB50936 (2014), for all the experimental and FE model samples, the mean, standard deviation and COV were found to be of 0.99, 0.08 and 0.10 respectively. However, in case of low strength concrete it

over predicts the flexural capacity up to a maximum of 30%. However, for all the experimental and FE model samples, the mean, standard deviation and Co-efficient of Variation (COV) were found to be of 0.79, 0.08 and 0.12 respectively, for Eurocode.

12. EC4 considers the effect of concrete to the contribution of ultimate capacity but neglects the composite action between steel tube and concrete. AISC predicted values were lower than the rest of the predicted values because it neglects the contribution of concrete. GB method predicts the higher capacity due to considering the same effect of confinement for square and circular members. Hence, these codes need to be revised. However, in the current state, Eurocode can be used for square members, GB can be used for high-strength infilled concrete and AISC can be used for low strength infilled concrete.

5.2 Recommendations for Future

Further researches are required to encompass the different aspects of the behavior of OPBC reinforced concrete beams. Following are some recommendations for future investigations and research.

1. More research is required to study the fire performance of a NCFST and OCFST member in joints or frame structures considering the restraints from its adjacent beams and columns.
2. The use of steel fibers as reinforcement for OCFST members should also be studied and included in the proposed FE model, since their usage has increased in the last years.
3. More research is required to study the behavior of OCFST members under the combination of fire and long-term sustained loading.

4. More research and fire testing need to be done on OCFST members with different support conditions (pin, fixed and semi-rigid). Meanwhile, fire research on joints and frames with OCFST also needs to be conducted.

REFERENCES

ACI 318-14 (2014). *Building Code Requirements for Structural Concrete (ACI 318-14): An ACI Standard: Commentary on Building Code Requirements for Structural Concrete (ACI 318R-14), an ACI Report*.

AIJ, (1997). Recommendations for design and construction of concrete filled steel tubular structures. Tokyo, Japan: Architectural Institute of Japan;.

AISC, (2005). Load and resistance factor design specification for structural steel buildings. Chicago (USA): American Institute of Steel Construction.

EC4, (2005). Design of composite steel and concrete structures *structures—Part 1–2: general rules-structural fire design*. Brussels (Belgium): European Committee for Standardization, CEN; 2005.

Abdullahi, M., Al-Mattarneh, H., Abu Hassan, A., Hassan, M., & Mohammed, B. (2008). *Trial mix design methodology for Palm Oil Clinker (POC) concrete.* Paper presented at the In Proceeding of International Conference on Construction and Building Technology (ICCBT)-(45), Malaysia.

Abid, M., Hou, X., Zheng, W., & Hussain, R. R. (2017). High temperature and residual properties of reactive powder concrete–A review. *Construction and Building Materials, 147*, 339-351.

Abrams, M. S. (1971). Compressive strength of concrete at temperatures to 1600F. *Special Publication, 25*, 33-58.

Abrams, M. S. (1979). Behavior of inorganic materials in fire *Design of Buildings for Fire Safety*: ASTM International.

Adl-Zarrabi, B., Boström, L., & Wickström, U. (2006). Using the TPS method for determining the thermal properties of concrete and wood at elevated temperature. *Fire and materials, 30*(5), 359-369.

Ahmad, Hilton, M., & Noor, N. (2007). *Mechanical properties of palm oil clinker concrete.* Paper presented at the Proceedings of 1st Engineering conference on Energy and Environment (EnCon2007), Sarawak, Malaysia, UTHM repository.

Ahmad, H., Hilton, M., Mohd, S., & Mohd Noor, N. (2007). Mechanical properties of palm oil clinker concrete.

Ahmmad, R., Jumaat, M. Z., Alengaram, U. J., Bahri, S., Rehman, M. A., & Hashim, H. b. (2016). Performance evaluation of palm oil clinker as coarse aggregate in high strength lightweight concrete. *Journal of Cleaner Production, 112, Part 1*, 566-574. doi:http://dx.doi.org/10.1016/j.jclepro.2015.08.043

Al-Rawi, O., & Ghannam, S. (2011). Experimental study on light weight concrete-filled steel tubes. *Jordan Journal of Civil Engineering, 5*(4), 521-529.

Ala-Outinen, T., & Myllymäki, J. (1995). Local buckling of rhs members at elevated temperatures. *Government Research Announcements and Index*.

Albero, V., Espinos, A., Romero, M. L., Hospitaler, A., Bihina, G., & Renaud, C. (2016). Proposal of a new method in EN1994-1-2 for the fire design of concrete-filled steel tubular columns. *Engineering Structures, 128*, 237-255.

Ali, F., & O'Connor, D. (2001). Structural performance of rotationally restrained steel columns in fire. *Fire Safety Journal, 36*(7), 679-691.

Almeida, S. J., Rodrigues, J. P. C., & Neto, J. M. (2012). Behaviour of compressed cold formed steel elements at high temperatures.

Anand, N., & Arulraj, G. P. (2011). The effect of elevated temperature on concrete materials-A literature review. *International Journal of Civil & Structural Engineering, 1*(4), 928-938.

AS/NZS. (2005). Cold-Formed Steel Structures, Standards of Australia (SA) and Standards of New Zealand (SNZ). Sydney-Wellington.

Aslam, M., Shafigh, P., & Jumaat, M. Z. (2016a). Drying shrinkage behaviour of structural lightweight aggregate concrete containing blended oil palm bio-products. *Journal of Cleaner Production, 127*, 183-194.

Aslam, M., Shafigh, P., & Jumaat, M. Z. (2016b). Oil-palm by-products as lightweight aggregate in concrete mixture: a review. *Journal of Cleaner Production, 126*, 56-73.

Aslam, M., Shafigh, P., Jumaat, M. Z., & Lachemi, M. (2016). Benefits of using blended waste coarse lightweight aggregates in structural lightweight aggregate concrete. *Journal of Cleaner Production, 119*, 108-117.

Bailey, C. (1998). Computer modelling of the corner compartment fire test on the large-scale Cardington test frame. *Journal of Constructional Steel Research, 48*(1), 27-45.

Bailey, C. (2000). Effective lengths of concrete-filled steel square hollow sections in fire. *Proceedings of the Institution of Civil Engineers-Structures and Buildings, 140*(2), 169-178.

Bailey, C. (2000). The influence of the thermal expansion of beams on the structural behaviour of columns in steel-framed structures during a fire. *Engineering Structures, 22*(7), 755-768.

Bailey, C., Burgess, I., & Plank, R. (1996). The lateral-torsional buckling of unrestrained steel beams in fire. *Journal of Constructional Steel Research, 36*(2), 101-119.

Bamonte, P., & Gambarova, P. G. (2012). A study on the mechanical properties of self-compacting concrete at high temperature and after cooling. *Materials and structures, 45*(9), 1375-1387.

Bertero, V., & Polivka, M. (1972). Influence of thermal exposures on mechanical characteristics of concrete. *Special Publication, 34*, 505-531.

Bilotta, A., de Silva, D., & Nigro, E. (2016). Tests on intumescent paints for fire protection of existing steel structures. *Construction and Building Materials, 121*, 410-422. doi:http://dx.doi.org/10.1016/j.conbuildmat.2016.05.144

Borges Dinis, P., & Camotim, D. (2010). Local/distortional mode interaction in cold-formed steel lipped channel beams. *Thin-Walled Structures, 48*(10–11), 771-785.

Bronzova, M., & Garifullin, M. (2016). Fire resistance of thin-walled cold-formed steel structures. *Construction of Unique Buildings and Structures*, 61-78.

Carreira, D. J., & Chu, K.-H. (1985). *Stress-strain relationship for plain concrete in compression.* Paper presented at the Journal Proceedings.

Castillo, C. (1987). *Effect of transient high temperature on high-strength concrete.* Rice University.

Cava, D., Camotim, D., Dinis, P., & Madeo, A. (2016). Numerical investigation and direct strength design of cold-formed steel lipped channel columns experiencing local–distortional–global interaction. *Thin-Walled Structures, 105*, 231-247.

Chai, L. J., Shafigh, P., & Bin Mahmud, H. (2017). Production of high-strength lightweight concrete using waste lightweight oil-palm-boiler-clinker and limestone powder. *European Journal of Environmental and Civil Engineering*, 1-20.

Chan, D. (2009). Fire damage assessment of structural steel in a school. *Struct. Eng, 87*(19), 18-20.

Chen, J., Wang, J., Xie, F., & Jin, W.-l. (2016). Behavior of thin-walled dodecagonal section double skin concrete-filled steel tubes under bending. *Thin-Walled Structures, 98*, 293-300.

Chen, J., & Young, B. (2006). Stress–strain curves for stainless steel at elevated temperatures. *Engineering Structures, 28*(2), 229-239.

Chen, J., & Young, B. (2007). Experimental investigation of cold-formed steel material at elevated temperatures. *Thin-Walled Structures, 45*(1), 96-110.

Chen, S., Jiang, L., Usmani, A., Li, G.-Q., & Jin, C. (2015). Damage mechanisms in cementitious coatings on steel members under axial loading. *Construction and Building Materials, 90*, 18-35.

Chen, Y., Feng, R., & Wang, L. (2017). Flexural behaviour of concrete-filled stainless steel SHS and RHS tubes. *Engineering Structures, 134*, 159-171.

Cheng, F.-P., Kodur, V., & Wang, T.-C. (2004). Stress-strain curves for high strength concrete at elevated temperatures. *Journal of materials in civil engineering, 16*(1), 84-90.

Cheng, S. Y., Wu, Li, L.-Y., & Kim, B. (2014). Thermal Buckling Analysis of Axially Loaded Columns of Thin-Walled Open Section with Nonuniform Sectional Properties. *International Journal of Structural Stability and Dynamics*, 1450088.

Chitawadagi, M. V., & Narasimhan, M. C. (2009). Strength deformation behaviour of circular concrete filled steel tubes subjected to pure bending. *Journal of Constructional Steel Research, 65*(8–9), 1836-1845. doi:http://dx.doi.org/10.1016/j.jcsr.2009.04.006

Chung, K., Park, S., & Choi, S. (2009). Fire resistance of concrete filled square steel tube columns subjected to eccentric axial load. *International Journal of Steel Structures, 9*(1), 69-76.

Committee, A. (1999). *Building code requirements for structural concrete:(ACI 318-99); and commentary (ACI 318R-99)*.

Committee, A. (2015). Building Code Requirements for Structural Concrete (ACI 318-14): An ACI Standard: Commentary on Building Code Requirements for Structural Concrete (ACI 318R-14), an ACI Report: American Concrete Institute.

Correia, A. J. M., Rodrigues, J. P. C., & Gomes, F. C. (2013). A simplified calculation method for fire design of steel columns with restrained thermal elongation. *Computers & Structures, 116*, 20-34.

Craveiro, H. D., Rodrigues, J. P., & Laím, L. (2015). Baseline study on the behaviour of cold-formed steel columns subjected to fire. *Applications of Structural Fire Engineering*.

Craveiro, H. D., Rodrigues, J. P. C., & Laím, L. (1993). Cold-formed steel columns with restrained thermal elongation subjected to fire. *strain, 2005*, 2.

Craveiro, H. D., Rodrigues, J. P. C., & Laím, L. (2014). Cold-formed steel columns made with open cross-sections subjected to fire. *Thin-Walled Structures, 85*, 1-14.

Craveiro, H. D., Rodrigues, J. P. C., & Laím, L. (2016). Experimental analysis of built-up closed cold-formed steel columns with restrained thermal elongation under fire conditions. *Thin-Walled Structures, 107*, 564-579.

Cruz, C. R., & Gillen, M. (1980). Thermal expansion of Portland cement paste, mortar and concrete at high temperatures. *Fire and materials, 4*(2), 66-70.

Cusson, D., & Paultre, P. (1995). Stress-strain model for confined high-strength concrete. *Journal of structural engineering, 121*(3), 468-477.

Dai, X. H., & Lam, D. (2012). Shape effect on the behaviour of axially loaded concrete filled steel tubular stub columns at elevated temperature. *Journal of Constructional Steel Research, 73*, 117-127.

Normalisation, C. E. (1994). Eurocode 4: Design of composite steel and concrete structures. part 1-2: General rules-structural fire design. *CEN ENV*.

Dharma, R. B., & Tan, K.-H. (2007). Proposed design methods for lateral torsional buckling of unrestrained steel beams in fire. *Journal of Constructional Steel Research, 63*(8), 1066-1076.

Diederichs, U., Jumppanen, U., & Penttala, V. (1988). *Material properties of high strength concrete at elevated temperatures.* Paper presented at the Proceedings of 13th Congress of IABSE. Zurich.

Dill, F. (1960). *Structural steel after a fire.* Paper presented at the Proceedings of National Steel Construction Conference.

Ding, J., & Wang, Y. C. (2008). Realistic modelling of thermal and structural behaviour of unprotected concrete filled tubular columns in fire. *Journal of Constructional Steel Research, 64*(10), 1086-1102.

Dolamune Kankanamge, N., & Mahendran, M. (2008). Numerical Studies of Cold-formed Steel Beams Subject to Lateral-torsional Buckling at Elevated Temperatures.

Dolamune Kankanamge, N., & Mahendran, M. (2012a). Behaviour and design of cold-formed steel beams subject to lateral–torsional buckling. *Thin-Walled Structures, 51*, 25-38.

Duarte, A., Silva, B., Silvestre, N., de Brito, J., Júlio, E., & Castro, J. (2016). Finite element modelling of short steel tubes filled with rubberized concrete. *Composite Structures, 150*, 28-40.

Elchalakani, Karrech, A., Hassanein, M., & Yang, B. (2016). Plastic and yield slenderness limits for circular concrete filled tubes subjected to static pure bending. *Thin-Walled Structures, 109*, 50-64.

Elchalakani, M., Zhao, X.-L., & Grzebieta, R. (2001). Concrete-filled circular steel tubes subjected to pure bending. *Journal of Constructional Steel Research, 57*(11), 1141-1168.

Ellobody, E. (2013). A consistent nonlinear approach for analysing steel, cold-formed steel, stainless steel and composite columns at ambient and fire conditions. *Thin-Walled Structures, 68*, 1-17.

Espinos, A. (2012). *Numerical analysis of the fire resistance of circular and elliptical slender concrete filled tubular columns.* Doctoral thesis. Valencia, Spain: Universitat Politècnica de València.

Espinos, A., Gardner, L., Romero, M. L., & Hospitaler, A. (2011). Fire behaviour of concrete filled elliptical steel columns. *Thin-Walled Structures, 49*(2), 239-255.

Espinos, A., Romero, M., Serra, E., & Hospitaler, A. (2015). Experimental investigation on the fire behaviour of rectangular and elliptical slender concrete-filled tubular columns. *Thin-Walled Structures, 93*, 137-148.

Espinos, A., Romero, M. L., & Hospitaler, A. (2010). Advanced model for predicting the fire response of concrete filled tubular columns. *Journal of Constructional Steel Research, 66*(8), 1030-1046.

Espinos, A., Romero, M. L., & Hospitaler, A. (2012). Simple calculation model for evaluating the fire resistance of unreinforced concrete filled tubular columns. *Engineering Structures, 42*, 231-244.

Espinos, A., Romero, M. L., & Hospitaler, A. (2013). Fire design method for bar-reinforced circular and elliptical concrete filled tubular columns. *Engineering Structures, 56*, 384-395.

Espinos, A., Romero, M. L., Hospitaler, A., Pascual, A. M., & Albero, V. (2015). *Advanced materials for concrete-filled tubular columns and connections.* Paper presented at the Structures.

Eurocode. (1993). *1-2: 1995:"Design of steel structures: Part 1-2: General rules–Structural fire design"*.

Feng, M., Wang, Y. C., & Davies, J. M. (2003). Structural behaviour of cold-formed thin-walled short steel channel columns at elevated temperatures. Part 2: Design calculations and numerical analysis. *Thin-Walled Structures, 41*(6), 571-594.

Feng, M., Wang, Y. C., & Davies, J. M. (2004). A numerical imperfection sensitivity study of cold-formed thin-walled tubular steel columns at uniform elevated temperatures. *Thin-Walled Structures, 42*(4), 533-555.

Franssen, J.-M. (2000). Failure temperature of a system comprising a restrained column submitted to fire. *Fire Safety Journal, 34*(2), 191-207.

Franssen, J.-M., & Real, P. V. (2016). *Fire Design of Steel Structures: EC1: Actions on structures; Part 1-2: Actions on structure exposed to fire; EC3: Design of steel structures; Part 1-2: Structural fire design*: John Wiley & Sons.

Franssen, J. (2005). SAFIR: A thermal/structural program for modeling structures under fire. *Engineering Journal-American Institute of Steel Construction, 42*(3), 143.

FRDM. (2014). *Statistik Punca Kebakaran Tahun 2013*. Malaysia Retrieved from http://www.bomba.gov.my/resources/index/user_1/UploadFile/Orang%20Awam/Statistik/Perangkaan_Punca_Kebakaran_Tahun_2013.pdf.

Fu, Y., Wong, Y., Poon, C., & Tang, C. (2005). Stress-strain behaviour of high-strength concrete at elevated temperatures. *Magazine of Concrete Research, 57*(9), 535-544.

Georgieva, I., Schueremans, L., Vandewalle, L., & Pyl, L. (2012). Design of Built-Up Cold-Formed Steel Columns According to the Direct Strength Method. *Procedia Engineering, 40*, 119-124. doi:http://dx.doi.org/10.1016/j.proeng.2012.07.066

Ghafoori, E., & Motavalli, M. (2015). Lateral-torsional buckling of steel I-beams retrofitted by bonded and un-bonded CFRP laminates with different pre-stress levels: Experimental and numerical study. *Construction and Building Materials, 76*, 194-206. doi:http://dx.doi.org/10.1016/j.conbuildmat.2014.11.070

Gho, W.-M., & Liu, D. (2004). Flexural behaviour of high-strength rectangular concrete-filled steel hollow sections. *Journal of Constructional Steel Research, 60*(11), 1681-1696. doi:http://dx.doi.org/10.1016/j.jcsr.2004.03.007

Guler, S., Copur, A., & Aydogan, M. (2012). Flexural behaviour of square UHPC-filled hollow steel section beams. *Structural Engineering and Mechanics, 43*(2), 225-237.

Gunalan, S., Bandula Heva, Y., & Mahendran, M. (2014a). Design of cold-formed steel columns at elevated temperatures subject to flexural-torsional buckling. *Proceedings of the 7th European Conference on Steel and Composite Structures*.

Gunalan, S., Bandula Heva, Y., & Mahendran, M. (2015). Local buckling studies of cold-formed steel compression members at elevated temperatures. *Journal of Constructional Steel Research, 108*, 31-45.

Gunalan, S., Heva, Y. B., & Mahendran, M. (2014). Flexural–torsional buckling behaviour and design of cold-formed steel compression members at elevated temperatures. *Engineering Structures, 79*, 149-168.

Gunalan, S., & Mahendran, M. (2013a). *Improved design rules for cold-formed steel columns.* Paper presented at the Proceedings of the 10th Pacific Structural Steel Conference (PSSC 2013)–Advancements and Achievements in Structural Steel.

Gunalan, S., & Mahendran, M. (2013b). Improved design rules for fixed ended cold-formed steel columns subject to flexural–torsional buckling. *Thin-Walled Structures, 73*, 1-17.

Gunalan, S., & Mahendran, M. (2013a). Cold-formed steel columns subject to local buckling at elevated temperatures.

Gunalan, S., & Mahendran, M. (2014). Experimental and numerical studies of fire exposed lipped channel columns subject to distortional buckling. *Fire Safety Journal, 70*, 34-45.

Gunalan, S., & Mahendran, M. (2014b). Experimental investigation of post-fire mechanical properties of cold-formed steels. *Thin-Walled Structures, 84*, 241-254.

Gunalan, S., & Mahendran, M. (2014c). Distortional buckling behaviour of fire exposed cold-formed steel columns. *23rd Australasian Conference on the Mechanics of Structures and Materials (ACMSM23)*.

Gunalan, S., & Mahendran, M. (2014d). Buckling tests of fire exposed cold-formed steel columns. *Proceedings of the ICTWS 2014 7th International Conference on Thin-Walled Structures*.

Yong, K., Young-Sun, K., & Tae-Gyu, L. (2009). Mechanical properties of high-strength concrete subjected to high temperature by stressed test. *Transactions of Nonferrous Metals Society of China, 19*, s128-s133.

Haidarali, M. R., & Nethercot, D. A. (2012). Local and distortional buckling of cold-formed steel beams with edge-stiffened flanges. *Journal of Constructional Steel Research, 73*, 31-42.

Hamidian, M. R., Shafigh, P., Jumaat, M. Z., Alengaram, U. J., & Sulong, N. R. (2016). A new sustainable composite column using an agricultural solid waste as aggregate. *Journal of Cleaner Production, 129*, 282-291.

Han, L.-H. (2001). Fire performance of concrete filled steel tubular beam-columns. *Journal of Constructional Steel Research, 57*(6), 697-711.

Han, L.-H. (2004). Flexural behaviour of concrete-filled steel tubes. *Journal of Constructional Steel Research, 60*(2), 313-337.

Han, L.-H., Chen, F., Liao, F.-Y., Tao, Z., & Uy, B. (2013). Fire performance of concrete filled stainless steel tubular columns. *Engineering Structures, 56*, 165-181.

Han, L.-H., Li, W., & Bjorhovde, R. (2014). Developments and advanced applications of concrete-filled steel tubular (CFST) structures: Members. *Journal of Constructional Steel Research, 100*, 211-228.

Han, L.-H., Lu, H., Yao, G.-H., & Liao, F.-Y. (2006). Further study on the flexural behaviour of concrete-filled steel tubes. *Journal of Constructional Steel Research, 62*(6), 554-565.

Han, L.-h., Tao, Z., & Liu, W. (2001). Concrete filled steel tubular structures from theory to practice [J]. *Journal of Fuzhou University (Natural Sciences Edtion), 6*, 003.

Han, L.-H., Yao, G.-H., & Tao, Z. (2007). Performance of concrete-filled thin-walled steel tubes under pure torsion. *Thin-Walled Structures, 45*(1), 24-36.

Han, L.-H., Yao, G.-H., & Zhao, X.-L. (2005). Tests and calculations for hollow structural steel (HSS) stub columns filled with self-consolidating concrete (SCC). *Journal of Constructional Steel Research, 61*(9), 1241-1269.

Han, L.-H., Zhao, X.-L., & Tao, Z. (2001). Tests and mechanics model for concrete-filled SHS stub columns, columns and beam-columns. *Steel and Composite Structures, 1*(1), 51-74.

Han, L.-H., Zhao, X.-L., Yang, Y.-F., & Feng, J.-B. (2003). Experimental study and calculation of fire resistance of concrete-filled hollow steel columns. *Journal of structural engineering, 129*(3), 346-356.

Hancock, G. (1997). The behaviour and design of cold-formed purlins. *Steel construction, 15*(3), 2-16.

Hancock, G. J., Kwon, Y. B., & Bernard, E. S. (1994). Strength design curves for thin-walled sections undergoing distortional buckling. *Journal of Constructional Steel Research, 31*(2), 169-186.

Harada, T., Takeda, J., Yamane, S., & Furumura, F. (1972). Strength, elasticity and thermal properties of concrete subjected to elevated temperatures. *Special Publication, 34*, 377-406.

Harmathy, T. (1970). Thermal properties of concrete at elevated temperatures. *Journal of Materials*.

Harmathy, T., & Allen, L. (1973). *Thermal properties of selected masonry unit concretes.* Paper presented at the Journal Proceedings.

Heva, Y. B. (2009). Behaviour and design of cold-formed steel compression members at elevated temperatures.

Heva, Y. B., & Mahendran, M. (2013). Flexural-torsional buckling tests of cold-formed steel compression members at elevated temperatures. *Steel and Composite Structures, 14*(3), 205-227.

Hicks, S. J., Newman, G. M., Edwards, M., & Orton, A. (2005). *Design guide for SHS concrete filled columns*: Corus Tubes Structural & Conveyance Business.

Hillerborg, A., Modéer, M., & Petersson, P.-E. (1976). Analysis of crack formation and crack growth in concrete by means of fracture mechanics and finite elements. *Cement and concrete research, 6*(6), 773-781.

Hong, S., & Varma, A. H. (2009). Analytical modeling of the standard fire behavior of loaded CFT columns. *Journal of Constructional Steel Research, 65*(1), 54-69.

Hu, H., Su, F., & Elchalakani, M. (2010). Finite element analysis of CFT columns subjected to pure bending moment. *Steel and Composite Structures, 10*(5), 415-428.

Hunaiti, Y. M. (1997). Strength of composite sections with foamed and lightweight aggregate concrete. *Journal of materials in civil engineering, 9*(2), 58-61.

Huo, J., Xiao, Y., Ren, X., & Zeng, X. (2015). A new hybrid heating method used in fire test. *Experimental Thermal and Fluid Science, 62*, 52-57.

Ibañez, C., Romero, M. L., & Hospitaler, A. (2016). Effects of axial and rotational restraints on concrete-filled tubular columns under fire. *Journal of Constructional Steel Research, 125*, 114-127.

Institution, B. S. (2005). Steel, concrete and composite bridges *Part 5: code of practice for the design of composite bridges*. London (UK).

Ismail, A., Morshed, A., & Yehia, S. (2013). Ultimate Behavior of Lightweight High Strength Concrete Filled Steel Tube (LWHCFST).

Jiang, A.-y., Chen, J., & Jin, W.-l. (2013). Experimental investigation and design of thin-walled concrete-filled steel tubes subject to bending. *Thin-Walled Structures, 63*, 44-50.

Johari, A., Nyakuma, B. B., Nor, S. H. M., Mat, R., Hashim, H., Ahmad, A., . . . Abdullah, T. A. T. (2015). The challenges and prospects of palm oil based biodiesel in Malaysia. *Energy, 81*, 255-261.

John, G., Katja, D., & Martha, G. V. G. (1997). Thermal properties of commercially available high-strength concretes. *Cement, Concrete and Aggregates, 19*(1), 38-54.

Jumaat, M. Z., Alengaram, U. J., Ahmmad, R., Bahri, S., & Islam, A. S. (2015). Characteristics of palm oil clinker as replacement for oil palm shell in lightweight concrete subjected to elevated temperature. *Construction and Building Materials, 101*, 942-951.

Kanadasan, & Abdul Razak, H. (2015). Engineering and sustainability performance of self-compacting palm oil mill incinerated waste concrete. *Journal of Cleaner Production, 89*, 78-86.

Kanadasan, J., & Razak, H. (2014). Mix design for self-compacting palm oil clinker concrete based on particle packing. *Materials & Design, 56*, 9-19.

Kanadasan, J., & Razak, H. A. (2014). Mix design for self-compacting palm oil clinker concrete based on particle packing. *Materials & Design (1980-2015), 56*, 9-19.

Kankanamge, N. D. (2010). *Structural behaviour and design of cold-formed steel beams at elevated temperatures.* Queensland University of Technology, Brisbane.

Kankanamge, N. D., & Mahendran, M. (2011). Mechanical properties of cold-formed steels at elevated temperatures. *Thin-Walled Structures, 49*(1), 26-44.

Kankanamge, N. D., & Mahendran, M. (2012). Behaviour and design of cold-formed steel beams subject to lateral–torsional buckling at elevated temperatures. *Thin-Walled Structures, 61*, 213-228.

Kay, T., Kirby, B., & Preston, R. (1996). Calculation of the heating rate of an unprotected steel member in a standard fire resistance test. *Fire Safety Journal, 26*(4), 327-350.

Kesawan, S., Jatheeshan, V., & Mahendran, M. (2015). Elevated temperature mechanical properties of hollow flange channel sections. *Construction and Building Materials, 87*, 86-99.

Kesawan, S., & Mahendran, M. (2018). Post-fire mechanical properties of cold-formed steel hollow sections. *Construction and Building Materials, 161*, 26-36.

Khoury, G. (2006). Strain of heated concrete during two thermal cycles. Part 1: strain over two cycles, during first heating and at subsequent constant temperature. *Magazine of Concrete Research, 58*(6), 367-385.

Khoury, G. A., Grainger, B. N., & Sullivan, P. J. (1985). Strain of concrete during first heating to 600 C under load. *Magazine of Concrete Research, 37*(133), 195-215.

Kimura, M., Ohta, H., Kaneko, H., & Kodaira, A. (1990). Fire resistance of concrete-filled square steel tubular columns subjected to combined loads. *Elsevier Science Publishers Ltd.(UK)*, 372-379.

Kirby, B., Lapwood, D., & Thomson, G. (1986). *The reinstatement of fire damaged steel and iron framed structures*: British Steel Corporation Swinden Laboratories.

Kodur, V. (1998). Design equations for evaluating fire resistance of SFRC-filled HSS columns. *Journal of structural engineering, 124*(6), 671-677.

Kodur, V., & Arablouei, A. (2015). Effective properties of spray-applied fire-resistive material for resistance to cracking and delamination from steel structures. *Construction and Building Materials, 84*, 367-376.

Kodur, V., & Khaliq, W. (2010). Effect of temperature on thermal properties of different types of high-strength concrete. *Journal of materials in civil engineering, 23*(6), 793-801.

Kodur, V., & Sultan, M. (2003). Effect of temperature on thermal properties of high-strength concrete. *Journal of materials in civil engineering, 15*(2), 101-107.

Kodur, V. K., & MacKinnon, D. H. (2000). Design of concrete-filled hollow structural steel columns for fire endurance. *Engineering Journal-American Institute of Steel Construction, 37*(1), 13-24.

Kwon, Y. B., & Hancock, G. J. (1992). Tests of cold-formed channels with local and distortional buckling. *Journal of structural engineering, 118*(7), 1786-1803.

Laím, L., Rodrigues, J. P., & Silva, L. S. (2013). Numerical analysis of cold-formed steel beams in fire. *Proceedings of the 13th international conference and exhibition on fire and materials. San Francisco, USA*, 163-174.

Laím, L., & Rodrigues, J. P. C. (2016). Experimental and numerical study on the fire response of cold-formed steel beams with elastically restrained thermal elongation. *Journal of Structural Fire Engineering, 7*(4), 388-402.

Laím, L., & Rodrigues, J. P. C. (2016). Numerical analysis on axially-and-rotationally restrained cold-formed steel beams subjected to fire. *Thin-Walled Structures, 104*, 1-16.

Laím, L., Rodrigues, J. P. C., & Craveiro, H. D. (2015). Flexural behaviour of beams made of cold-formed steel sigma-shaped sections at ambient and fire conditions. *Thin-Walled Structures, 87*, 53-65.

Laím, L., Rodrigues, J. P. C., & Craveiro, H. D. (2016). Flexural behaviour of axially and rotationally restrained cold-formed steel beams subjected to fire. *Thin-Walled Structures, 98, Part A*, 39-47.

Laím, L., Rodrigues, J. P. C., & Silva, L. S. (2014). Experimental analysis on cold-formed steel beams subjected to fire. *Thin-Walled Structures, 74*, 104-117.

Laím, L., Rodrigues, J. P. C., & Silva, L. S. (2013a). Flexural Behaviour of Cold-Formed Steel Beams *Design, Fabrication and Economy of Metal Structures* (pp. 133-138): Springer.

Laím, L., Rodrigues, J. P. C., & Silva, L. S. d. (2013b). Experimental and numerical analysis on the structural behaviour of cold-formed steel beams. *Thin-Walled Structures, 72*, 1-13.

Lakshmi, B., & Shanmugam, N. E. (2002). Nonlinear analysis of in-filled steel-concrete composite columns. *Journal of structural engineering, 128*(7), 922-933.

Landesmann, A., & Camotim, D. (2016). Distortional failure and DSM design of cold-formed steel lipped channel beams under elevated temperatures. *Thin-Walled Structures, 98, Part A*, 75-93.

Lankard, D. R., Birkimer, D. L., Fondriest, F. F., & Snyder, M. J. (1971). Effects of moisture content on the structural properties of portland cement concrete exposed to temperatures up to 500F. *Special Publication, 25*, 59-102.

Lee, J. H. (2004). *Local buckling behaviour and design of cold-formed steel compression members at elevated temperatures.* (PhD).

Li, G., Liu, D., Yang, Z., & Zhang, C. (2017). Flexural behavior of high strength concrete filled high strength square steel tube. *Journal of Constructional Steel Research, 128*, 732-744.

Li, H.-T., & Young, B. (2017). Material properties of cold-formed high strength steel at elevated temperatures. *Thin-Walled Structures, 115*, 289-299.

Li, L.-y. (2004). Lateral–torsional buckling of cold-formed zed-purlins partial-laterally restrained by metal sheeting. *Thin-Walled Structures, 42*(7), 995-1011.

Li, L.-y., & Purkiss, J. (2005). Stress–strain constitutive equations of concrete material at elevated temperatures. *Fire Safety Journal, 40*(7), 669-686.

Liang, Q. Q., Uy, B., Bradford, M. A., & Ronagh, H. R. (2005). Strength analysis of steel–concrete composite beams in combined bending and shear. *Journal of structural engineering, 131*(10), 1593-1600.

Lie, T., & Kodur, V. (1996a). Fire resistance of steel columns filled with bar-reinforced concrete. *Journal of structural engineering, 122*(1), 30-36.

Lie, T., & Kodur, V. (1996b). Thermal and mechanical properties of steel-fibre-reinforced concrete at elevated temperatures. *Canadian Journal of Civil Engineering, 23*(2), 511-517.

Lie, T., & Stringer, D. (1994). Calculation of the fire resistance of steel hollow structural section columns filled with plain concrete. *Canadian Journal of Civil Engineering, 21*(3), 382-385.

Liew, J. R. (2004a). Buildable Design of Multi-storey and Large-span Steel Structures. *International Journal of Steel Structures, 4*(2), 53-70.

Liew, J. R. (2004b). Performance based fire safety design of structures—a multi-dimensional integration. *Advances in Structural Engineering, 7*(4), 311-333.

Lopes, N., Vila Real, P., Simoes Silva, L., & Franssen, J.-M. (2006). *Proposal to the Eurocode 3 for the lateral-torsional buckling of stainless steel I-beams in case of fire.* Paper presented at the 4th International Workshop Structures in Fire.

LRFD, A. (1994). Manual of steel construction, load and resistance factor design. *Chicago: American Institute of Steel Construction*.

Lu, H., Zhao, X.-L., & Han, L.-H. (2009). Fire behaviour of high strength self-consolidating concrete filled steel tubular stub columns. *Journal of Constructional Steel Research, 65*(10), 1995-2010.

Lu, W., Mäkeläinen, P., & Outinen, J. (2007). Numerical simulation of catenary action in cold-formed steel sheeting in fire. *Journal of Structural Mechanics, 40*(3), 28-37.

Lu, Y. Q., & Kennedy, D. L. (1994). The flexural behaviour of concrete-filled hollow structural sections. *Canadian Journal of Civil Engineering, 21*(1), 111-130.

Mahasneh, B. Z., & Gharaibeh, E. S. (2005). Enhancing filled-tube properties by using fiber polymers in filling matrix. *Journal of Applied Sciences, 5*(2), 232-235.

Malaysia, A. I. (2011). National Biomass Strategy 2020: New wealth creation for Malaysia's palm oil industry. *Agensi Inovasi Malaysia*.

Maljaars, J., Twilt, L., & Soetens, F. (2009). Flexural buckling of fire exposed aluminium columns. *Fire Safety Journal, 44*(5), 711-717.

Mander, J., Priestley, M., & Park, R. (1988). Observed stress-strain behavior of confined concrete. *Journal of structural engineering, 114*(8), 1827-1849.

Mannan, & Neglo, K. (2010). Mix design for oil-palm-boiler clinker (OPBC) concrete. *Journal of Science and Technology (Ghana), 30*(1).

Marechal, J. (1972). Thermal Conductivity and Thermal Expansion Coefficients of Concrete as a Function of Temperature and Humidty. *Special Publication, 34*, 1047-1058.

Matzumoto, Y., Fukuzawa, K., & Endo, H. (1976). *Manufacture and Behaviour of Hollow Composite Members.* Paper presented at the Final Report of 10th Congress of IABSE, Tokyo, September.

Michael, S. (2012). MALAYSIA: stagnating palm oil yields impede growth. *USDA Foreign Agricultural Service*.

Mirmomeni, M., Heidarpour, A., Zhao, X.-L., Hutchinson, C. R., Packer, J. A., & Wu, C. (2016). Fracture behaviour and microstructural evolution of structural mild steel under the multi-hazard loading of high-strain-rate load followed by elevated temperature. *Construction and Building Materials, 122*, 760-771.

Mohammed, B., Foo, W., & Abdullahi, M. (2014). Flexural strength of palm oil clinker concrete beams. *Materials & Design, 53*, 325-331.

Mohammed, B., Hossain, K., Foo, W., & Abdullahi, M. (2011). Rapid Chloride Permeability Test on Lightweight Concrete Made with Oil Palm Clinker. *Journal of Engineering Research and Applications (IJERA) ISSN. 2248, 9622*.

Mohammed, B., Hossain, K., Foo, W., & Abdullahi, M. (2013). Shear strength of palm oil clinker concrete beams. *Materials & Design, 46*, 270-276.

Moliner, V., Espinos, A., Romero, M., & Hospitaler, A. (2013). Fire behavior of eccentrically loaded slender high strength concrete-filled tubular columns. *Journal of Constructional Steel Research, 83*, 137-146.

Nadjai, A., Petrou, K., Han, S., & Ali, F. (2016). Performance of unprotected and protected cellular beams in fire conditions. *Construction and Building Materials, 105*, 579-588.

Naik, T. R., Kraus, R. N., & Kumar, R. (2010). Influence of types of coarse aggregates on the coefficient of thermal expansion of concrete. *Journal of materials in civil engineering, 23*(4), 467-472.

Nakamura, S.-i., Momiyama, Y., Hosaka, T., & Homma, K. (2002). New technologies of steel/concrete composite bridges. *Journal of Constructional Steel Research, 58*(1), 99-130.

Naus, D. (2010). *A Compilation of Elevated Temperature Concrete Material Property Data and Information for Use in Assessments of Nuclear Power Plant Reinforced Concrete Structures: Prepared by DJ Naus*: US Nuclear Regulatory Commission, Office of Nuclear Regulatory Research.

Naus, D. J. (2006). *The Effect of Elevated Temperature on Concrete Materials and Structures-a Literature Review*. Retrieved from

Neville, A. (2008). *Properties of concrete*. 14th ed., Prentice Hall, Malaysia.

Neville, A. M., & Brooks, J. J. (1987). *Concrete technology*.

Newman, G. (1999). *Cardington fire tests.* Paper presented at the 1999 North American Steel Construction Conference(NASCC).

Ng, W. P. Q., Lam, H. L., Ng, F. Y., Kamal, M., & Lim, J. H. E. (2012). Waste-to-wealth: green potential from palm biomass in Malaysia. *Journal of Cleaner Production, 34*, 57-65.

Nielsen, C. V. (2003). Experimental Investigation of Combined Thermal and Mechanical Behaviour of Danish and Swedish Concrete subject to High Temperatures. *NORDIC CONCRETE RESEARCH-PUBLICATIONS-, 30*, 1.

Omar, T., Butterworth, J., & Lowe, P. (2000). *Development of finite element model for concrete-filled steel tube members in flexure.* Paper presented at the Proc. 7th New Zealand Postgraduate Conference on Engineering and Technology, Palmerston North.

Outinen, J. (2007). *Mechanical properties of structural steels at high temperatures and after cooling down*: Helsinki University of Technology.

Outinen, J., Kaitila, O., & Mäkeläinen, P. (2001). *High-temperature Testing of Structural Steel and Modelling of Structures at Fire Temperatures: Research Report*: Helsinki University of Technology.

Outinen, J., & Mäkeläinen, P. (2004). Mechanical properties of structural steel at elevated temperatures and after cooling down. *Fire and materials, 28*(2-4), 237-251.

Pereira, C. G., Castro-Gomes, J., & de Oliveira, L. P. (2009). Influence of natural coarse aggregate size, mineralogy and water content on the permeability of structural concrete. *Construction and Building Materials, 23*(2), 602-608.

Phan, L. T. (1996). *Fire performance of high-strength concrete: A report of the state-of-the art*: US Department of Commerce, Technology Administration, National Institute of Standards and Technology, Office of Applied Economics, Building and Fire Research Laboratory.

Probst, A. D., Kang, T. H.-K., Ramseyer, C., & Kim, U. (2010). Composite flexural behavior of full-scale concrete-filled tubes without axial loads. *Journal of structural engineering, 136*(11), 1401-1412.

Qiu, W., McCann, F., Espinos, A., Romero, M., & Gardner, L. (2016). Numerical analysis and design of slender concrete-filled elliptical hollow section columns and beam-columns. *Engineering Structures*.

Qiu, W., McCann, F., Espinos, A., Romero, M. L., & Gardner, L. Numerical analysis and design of slender concrete-filled elliptical hollow section columns and beam-columns. *Engineering Structures*.

Rack, C. G. Q. S. P. (2016). , Industrial Pallet Racks and Double Deep Pallet Rack International Trade Site. Retrieved from http://www.selectivepalletracking.com/

Ranawaka, T., & Mahendran, M. (2006). *Finite element analyses of cold-formed steel columns subject to distortional buckling under simulated fire conditions.* Paper presented at the Proceedings of the International Colloquium on Stability and Ductility of Steel Structures. Instituto Superior Técnico, Lisbon, Portugal.

Ranawaka, T., & Mahendran, M. (2009a). Distortional buckling tests of cold-formed steel compression members at elevated temperatures. *Journal of Constructional Steel Research, 65*(2), 249-259.

Ranawaka, T., & Mahendran, M. (2009b). Experimental study of the mechanical properties of light gauge cold-formed steels at elevated temperatures. *Fire Safety Journal, 44*(2), 219-229.

Ranawaka, T., & Mahendran, M. (2010). Numerical modelling of light gauge cold-formed steel compression members subjected to distortional buckling at elevated temperatures. *Thin-Walled Structures, 48*(4), 334-344.

Real, P., & Franssen, J.-M. (2000). *Lateral torsional buckling of steel I-beams in case of fire—numerical modeling.* Paper presented at the Proceedings of the first international workshop on structures in fire.

Real, P. M. V., & Franssen, J.-M. (2001). Numerical Modeling of Lateral-Torsional Buckling of Steel I-Beams under Fire Conditions—Comparison with Eurocode 3. *Journal of fire protection Engineering, 11*(2), 112-128.

Real, P. V., Cazeli, R., Silva, L. S., Santiago, A., & Piloto, P. (2004). The effect of residual stresses in the lateral-torsional buckling of steel I-beams at elevated temperature. *Journal of Constructional Steel Research, 60*(3), 783-793.

Real, P. V., Lopes, N., Silva, L. S., & Franssen, J.-M. (2008). Lateral–torsional buckling of stainless steel I-beams in case of fire. *Journal of Constructional Steel Research, 64*(11), 1302-1309.

Real, P. V., Piloto, P., & Franssen, J.-M. (2003). A new proposal of a simple model for the lateral-torsional buckling of unrestrained steel I-beams in case of fire: experimental and numerical validation. *Journal of Constructional Steel Research, 59*(2), 179-199.

Richart, F. E., Brandtzaeg, A., & Brown, R. L. (1928). A study of the failure of concrete under combined compressive stresses. *University of Illinois Bulletin; v. 26, no. 12*.

Rodrigues, J. P. C., & Laim, L. (2017). Fire response of restrained composite columns made with concrete filled hollow sections under different end-support conditions. *Engineering Structures, 141*, 83-96.

Rodrigues, J. P. C., & Laím, L. (2017). Fire resistance of restrained composite columns made of concrete filled hollow sections. *Journal of Constructional Steel Research, 133*, 65-76.

Romero, M. L., Moliner, V., Espinos, A., Ibañez, C., & Hospitaler, A. (2011). Fire behavior of axially loaded slender high strength concrete-filled tubular columns. *Journal of Constructional Steel Research, 67*(12), 1953-1965.

Rush, D., Bisby, L., Melandinos, A., & Lane, B. (2011). Fire resistance design of unprotected concrete filled steel hollow sections: meta-analysis of available furnace test data. *Fire Safety Science, 10*, 1549-1562.

Saatcioglu, M., & Razvi, S. R. (1992). Strength and ductility of confined concrete. *Journal of structural engineering, 118*(6), 1590-1607.

Saito, H., & Saito, H. (1990). Fire resistance of concrete-filled square steel tubular columns under deformation to simulate the elongation of steel beams. *Journal of Structural and Construction Engineering, Transaction of AIJ*(458), 163-169.

Sakumoto, Y., Okada, T., Yoshida, M., & Tasaka, S. (1994). Fire resistance of concrete-filled, fire-resistant steel-tube columns. *Journal of materials in civil engineering, 6*(2), 169-184.

Sarshar, R., & Khoury, G. (1993). Material and environmental factors influencing the compressive strength of unsealed cement paste and concrete at high temperatures. *Magazine of Concrete Research, 45*(162), 51-61.

Sauca, A., Gernay, T., Robert, F., Tondini, N., & Franssen, J.-M. (2016). *Stability in hybrid fire testing.* Paper presented at the Proceedings of the 9th International Conference on Structures in Fire.

Schafer, B. (2002). Local, distortional, and Euler buckling of thin-walled columns. *Journal of structural engineering, 128*(3), 289-299.

Schneider, U. (1976). Behaviour of concrete under thermal steady state and non-steady state conditions. *Fire and materials, 1*(3), 103-115.

Schneider, U., Diederichs, U., & Ehm, C. (1982). Effect of temperature on steel and concrete for PCRV's. *Nuclear Engineering and Design, 67*(2), 245-258.

Schneider, U., & Kassel, G. (1985). *Properties of materials at high temperatures: concrete*: Gesamthochschul-Bibliothek.

Scott, B., Park, R., & Priestley, M. (1982). Stress-strain behavior of concrete confined by overlapping hoops at low and high strain rates. *ACI journal, 79*(1), 13-27.

Shedquarters. (2009). STRUCTURAL PRODUCTS. Retrieved from http://www.shedquarters.net.au/products.php

Shi, X., Tan, T.-H., Tan, K.-H., & Guo, Z. (2002). Concrete constitutive relationships under different stress-temperature paths. *Journal of structural engineering, 128*(12), 1511-1518.

Shin, K.-Y., Kim, S.-B., Kim, J.-H., Chung, M., & Jung, P.-S. (2002). Thermo-physical properties and transient heat transfer of concrete at elevated temperatures. *Nuclear Engineering and Design, 212*(1), 233-241.

Sinaie, S., Heidarpour, A., & Zhao, X. L. (2014). Mechanical properties of cyclically-damaged structural mild steel at elevated temperatures. *Construction and Building Materials, 52*, 465-472.

Song, T.-Y., Han, L.-H., & Yu, H.-X. (2010). Concrete filled steel tube stub columns under combined temperature and loading. *Journal of Constructional Steel Research, 66*(3), 369-384.

Soundararajan, A., & Shanmugasundaram, K. (2008). Flexural behaviour of concrete-filled steel hollow sections beams. *Journal of Civil Engineering and Management, 14*(2), 107-114.

Standard, I. (1999). 834: Fire resistance tests-Elements of building construction. *International Organization for Standardization, Geneva*.

Stone, T. A., & LaBoube, R. A. (2005). Behavior of cold-formed steel built-up I-sections. *Thin-Walled Structures, 43*(12), 1805-1817.

Sundarraja, M., & Prabhu, G. G. (2011). Finite element modelling of CFRP jacketed CFST members under flexural loading. *Thin-Walled Structures, 49*(12), 1483-1491.

Sundarraja, M. C., & Ganesh Prabhu, G. (2011). Finite element modelling of CFRP jacketed CFST members under flexural loading. *Thin-Walled Structures, 49*(12), 1483-1491.

Takeuchi, M., Hiramoto, M., Kumagai, N., Yamazaki, N., Kodaira, A., & Sugiyama, K. (1993). *Material properties of concrete and steel bars at elevated temperatures.* Paper presented at the Transactions of the 12. international conference on Structural Mechanics in Reactor Technology (SMiRT). Volume H: Concrete and concrete structures.

Tang, Y.-C., Li, L.-J., Feng, W.-X., Liu, F., & Liao, B. (2017). Seismic performance of recycled aggregate concrete–filled steel tube columns. *Journal of Constructional Steel Research, 133*, 112-124.

Tao, Z., Uy, B., Han, L.-H., & Wang, Z.-B. (2009). Analysis and design of concrete-filled stiffened thin-walled steel tubular columns under axial compression. *Thin-Walled Structures, 47*(12), 1544-1556.

Tide, R. H. (1998). Integrity of structural steel after exposure to fire. *Engineering Journal-American Institute of Steel Construction, 35*, 26-38.

Tubes, B. S. Pipes.(1990).“. *Design for SHS fire resistance to BS5950: Part, 8*.

Twilt, L., Hass, R., Klingsch, W., Edwards, M., & Dutta, D. (1994). *Design guide for structural hollow section columns exposed to fire*.

Uenaka, K., & Kitoh, H. (2011). Mechanical behavior of concrete filled double skin tubular circular deep beams. *Thin-Walled Structures, 49*(2), 256-263.

Uy, B. (2000). Strength of concrete filled steel box columns incorporating local buckling. *Journal of structural engineering, 126*(3), 341-352.

Uygunoğlu, T., & Topçu, İ. B. (2009). Thermal expansion of self-consolidating normal and lightweight aggregate concrete at elevated temperature. *Construction and Building Materials, 23*(9), 3063-3069.

Valente, J. C., & Neves, I. C. (1999). Fire resistance of steel columns with elastically restrained axial elongation and bending. *Journal of Constructional Steel Research, 52*(3), 319-331.

van den Berg, G., & Bredenkamp, P. (1994). *The lateral torsional buckling strength of cold-formed stainless steel beams.* Paper presented at the Twelfth international specialty conference on cold-formed steel structures.

Vila Real, P. M., & Franssen, J.-M. (1999). Lateral buckling of steel I beams under fire conditions-Comparison between the EUROCODE 3 and the SAFIR code. *Relatório interno*(99/02).

Wan, C.-Y., Zha, X.-X., & Dassekpo, J.-B. M. (2017). Analysis of axially loaded concrete filled circular hollow double steel tubular columns exposed to fire. *Fire Safety Journal, 88*, 1-12.

Wang, K., & Young, B. (2013). Fire resistance of concrete-filled high strength steel tubular columns. *Thin-Walled Structures, 71*, 46-56.

Wang, W.-H., Han, L.-H., Li, W., & Jia, Y.-H. (2014). Behavior of concrete-filled steel tubular stub columns and beams using dune sand as part of fine aggregate. *Construction and Building Materials, 51*, 352-363.

Wang, Y. (1999). The effects of structural continuity on the fire resistance of concrete filled columns in non-sway frames. *Journal of Constructional Steel Research, 50*(2), 177-197.

Wang, Y. (2000). A simple method for calculating the fire resistance of concrete-filled CHS columns. *Journal of Constructional Steel Research, 54*(3), 365-386.

Wang, Y., & Moore, D. (1994). *The effect of frame continuity on the critical temperature of steel columns.* Paper presented at the Third Kenrensky Conference on Flobal Trends in Structural Engineering, Singapore.

Wardenier, J., Dutta, D., & Yeomans, N. (1995). *Design guide for structural hollow sections in mechanical applications*: Verlag TÜV Rheinland.

Wastney, C. (2002). *Performance of unprotected steel and composite steel frames exposed to fire*. Retrieved from

Webb, J., & Peyton, J. (1990). *Composite concrete filled steel tube columns.* Paper presented at the Second National Structural Engineering Conference 1990: Preprints of Papers.

Weigler, H., Fischer, R., & Kesler, C. (1972). *Influence of high temperatures on strength and deformations of concrete*. Retrieved from

Weller, A. (1992). Broadgate phase 8: Fire, 22 June 1990. *Summary report of damage and repair, Building Research Establishment PD, 21*, 92.

Xing, Z., Beaucour, A.-L., Hebert, R., Noumowe, A., & Ledesert, B. (2011). Influence of the nature of aggregates on the behaviour of concrete subjected to elevated temperature. *Cement and concrete research, 41*(4), 392-402.

Xiong, M.-X., Xiong, D.-X., & Liew, J. R. (2017). Flexural performance of concrete filled tubes with high tensile steel and ultra-high strength concrete. *Journal of Constructional Steel Research, 132*, 191-202.

Yang, B., Xiong, G., Ding, K., Nie, S., Zhang, W., Hu, Y., & Dai, G. (2015). Experimental and Numerical Studies on Lateral-Torsional Buckling of GJ Structural Steel Beams Under a Concentrated Loading Condition. *International Journal of Structural Stability and Dynamics*, 1640004.

Yang, H., Lam, D., & Gardner, L. (2008). Testing and analysis of concrete-filled elliptical hollow sections. *Engineering Structures, 30*(12), 3771-3781.

Yang, H., Liu, F., Zhang, S., & Lv, X. (2013). Experimental investigation of concrete-filled square hollow section columns subjected to non-uniform exposure. *Engineering Structures, 48*, 292-312.

Yang, Y.-F., & Han, L.-H. (2006a). Compressive and flexural behaviour of recycled aggregate concrete filled steel tubes (RACFST) under short-term loadings. *Steel and Composite Structures, 6*(3), 257.

Yang, Y.-F., & Han, L.-H. (2006b). Experimental behaviour of recycled aggregate concrete filled steel tubular columns. *Journal of Constructional Steel Research, 62*(12), 1310-1324.

Yang, Y.-F., & Ma, G.-L. (2013). Experimental behaviour of recycled aggregate concrete filled stainless steel tube stub columns and beams. *Thin-Walled Structures, 66*, 62-75.

Yin, Y., & Wang, Y. (2003). Numerical simulations of the effects of non-uniform temperature distributions on lateral torsional buckling resistance of steel I-beams. *Journal of Constructional Steel Research, 59*(8), 1009-1033.

Yu, C., & Schafer, B. W. (2006). Distortional buckling tests on cold-formed steel beams. *Journal of structural engineering, 132*(4), 515-528.

Yu, M., Zha, X., Ye, J., & Wang, B. (2014). A unified method for calculating fire resistance of solid and hollow concrete-filled steel tube columns based on average temperature. *Engineering Structures, 71*, 12-22.

Zakaria, M. (1986). Strength Properties of Oil Palm Clinker Concrete. *Jurnal Teknologi UTM, 8*(1), 28-37.

Zhao, X.-L., Han, L.-H., & Lu, H. (2010). *Concrete-filled tubular members and connections*: Spon Press London.

LIST OF PUBLICATIONS AND PAPERS PRESENTED

A. ISI Indexed Journals

No	Title	Authors	Name of the Journals	Status
1	FE modelling of the flexural behavior of square and rectangular steel tubes filled with normal and high strength concrete	Muhammad Faisal Javed, Nor Hafizah Ramli, Shazim Ali Memon, Sardar Kashif, Niaz Bahadur khan	Thin Walled Structures (Q1)	Published
2	Recent research on cold-formed steel beams and columns subjected to elevated temperature: A review	Muhammad Faisal Javed, Nor Hafizah Ramli, Shazim Ali Memon, Muhammad Jameel	Construction and Building Materials (Q1)	Published
3	Flexural behaviour of steel hollow sections filled with concrete that contains OPBC as coarse aggregate	Muhammad Faisal Javed, Nor Hafizah Ramli, Shazim Ali Memon, Sardar Kashif, Niaz Bahadur khan	Journal of Constructional Steel Research (Q1)	Published
4	Innovative oil palm waste concrete filled steel tube beams exposed to fire	Muhammad Faisal Javed, Nor Hafizah Ramli, Shazim Ali Memon, Sardar Kashif, Niaz Bahadur khan	Journal of Cleaner Production (Q1)	Minor revisions Received

B. Papers Presented in International Conferences

No	Title	Authors	Name of the Conferences	Places	Status
1	Finite element analysis on the structural behaviour of square CFST beams	Muhammad Faisal Javed, Nor Hafizah Ramli, Kashif-Ur-Rehman	International Technical Postgraduate Conference, 2017	Kuala Lumpur, Malaysia	Published
2	Finite element analysis of the flexural behavior of square CFST beams at ambient and elevated temperature	Muhammad Faisal Javed, Nor Hafizah Ramli Sulong, Kashif-Ur-Rehman, Niaz B Khan	12^{th} International Conference on Advances in Steel-Concrete Composite Structures	Valencia, Spain	Published